AD-A133 676 RESEARCH ON ADAPTIVE ANTENNA TECHNIQUES V(U) STANFORD 1/2
UNIV CA INFORMATION SYSTEMS LAB K M DUVALL ET AL.
SEP 83 N00019-82-C-0189

UNCLASSIFIED F/G 17/4 NL

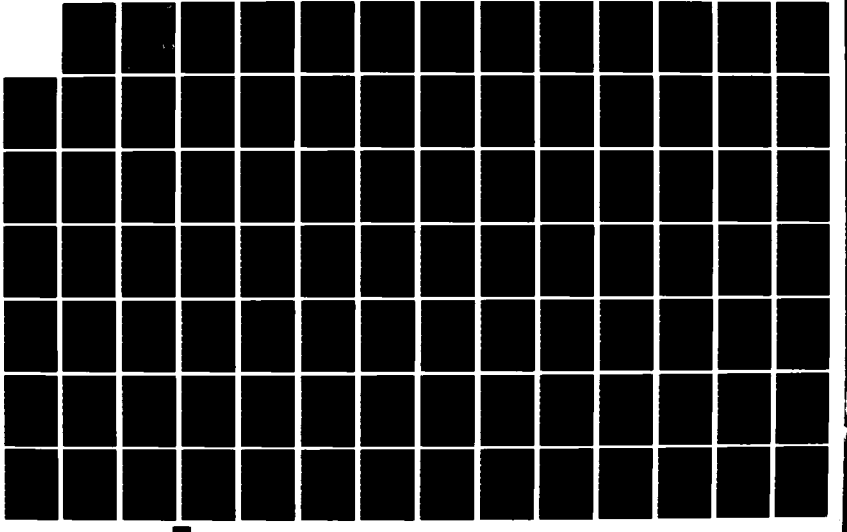

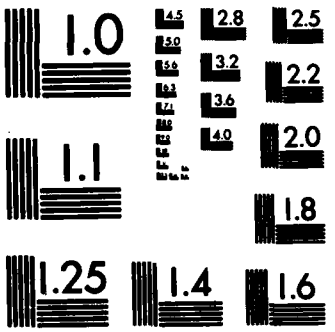

MICROCOPY RESOLUTION TEST CHART
NATIONAL BUREAU OF STANDARDS-1963-A

RESEARCH ON ADAPTIVE ANTENNA TECHNIQUES V

FINAL REPORT

by

Kenneth M. Duvall
Bernard Widrow

September 1983

Information Systems Laboratory
Department of Electrical Engineering
Stanford University
Stanford, CA 94305

This research was supported by the
Naval Air Systems Command of the Department of Defense
Under Contract N00019-82-C-0189

The views and conclusions contained in this document
are those of the authors and should not be interpreted as
necessarily representing the official policies, either expressed or implied
of the Naval Air Systems Command or the U. S. Government.

ABSTRACT

Adaptive antennas provide an important means of enhancing signal-to-noise ratio in the adverse electromagnetic environments that sometimes arise due to jamming or interference. For that reason, adaptive antennas are increasingly finding application in high performance radar and communications systems. In many of these systems the adaptive subsystem must exhibit robust performance in the face of multipath or rapidly changing interference.

Unfortunately, the adaptive beamformers now in use do not perform well in certain environments. It has been known for some time that correlated-signal conditions (e.g., due to multipath) can lead to partial or total cancellation of the desired signal within an adaptive beamformer. More recently it has been recognized that signal cancellation can arise during high-speed adaptation even though 1) the desired signal and interfering signals are uncorrelated and 2) the look-direction response is rigidly controlled. The initial sections of this report examine the signal-cancellation mechanism, with emphasis on the more difficult uncorrelated-signal case. Simulation results are presented that illustrate the cancellation effect, and an analysis is given for a simple environment consisting of the desired signal and one jammer.

The remaining sections of the report describe a technique for avoiding signal cancellation. The adaptation problem is reformulated to permit jammer nulling and signal recovery under conditions that ordinarily result in signal cancellation.

The reformulated problem suggests a new adaptive structure comprised of a master beamformer in which adaptation is conducted in a synthetic, signal-free environment and a slaved beamformer in which the actual array-element signals are processed. The new structure, which is termed a composite beamformer, is compared to Frost's hard-constrained adaptive beamformer. Particular attention is given to relative performance in cancellation environments, to conditions under which optimal behavior is approached, to convergence speed, and to weight behavior near convergence.

TABLE OF CONTENTS

LIST OF FIGURES

I. INTRODUCTION

The past two decades have witnessed the emergence of the adaptive antenna as an important element in countermeasures-resistant radar and communications systems. The application that has inspired most of the development effort is jammer nulling; adaptive antennas can eliminate a substantial fraction of the incident jammer power while admitting some desired signal (or signals) with useful gain. A key aspect of this selective treatment of jammers and desired signals is that it is accomplished without extensive a priori knowledge of the jammer environment. Instead, the locations of jammers are "learned" by some adaptive algorithm, and nulls are automatically steered to and maintained on the jammers.

One of the fundamental issues in adaptive antennas has been signal preservation. It has been clear from the beginning that the nulling behavior which is of such great value in eliminating jammers is a two-edged sword that also threatens the desired signal. Proper control is absolutely essential to avoid signal loss in the adaptive beamformer (ABF). The original sidelobe-canceller scheme of Howells and Applebaum [1,2] exploited the differing signal-to-jammer ratios in a directive primary antenna and an omnidirectional auxiliary antenna to avoid seriously attenuating desired radar signals. Widrow [3], operating with somewhat different signal and antenna assumptions, took the tack of introducing pilot signals to control beamformer response in specified look directions. Griffiths [4] devised a different soft-constraint technique that involved statistical

characterization of the desired signals rather than the actual surrogate signals required by the pilot-signal scheme. Frost [5,6] developed a constrained least-mean-square (LMS) algorithm that assured exact conformance with some prespecified look-direction response. More recently, Griffiths and Jim [7,8] contributed a structure called the "generalized sidelobe canceller," which provided an alternative method of realizing hard constraints. Some further development and generalization of soft-constraint methods has also taken place within the past few years; Chestek [9] brought together much of the earlier work on soft-constrained methods by combining soft linear constraints with a mean-square-error criterion in his soft-constrained LMS algorithm.

A unifying factor in the work just outlined is the focus on the response of the antenna to desired signals. This approach involves a tacit assumption that the problem decomposes in a tractable way, i.e., that desired signals and jammers can be treated independently. The assumption can be justified in many cases, but, as will be demonstrated, there are some rather simple signal/jammer scenarios where difficulty arises. When a failure occurs, the usual constraint methods do not adequately protect the desired signal. Instead, the signal is partially or totally destroyed in the adaptive beamformer by residual jammer signals. This phenomenon is termed signal cancellation.

The remainder of this report is devoted to a further discussion of signal cancellation and to the description of a method for avoiding it. The next chapter

provides insight into the signal cancellation phenomenon by explaining how it was recognized and by showing the effect in two simple cases. Chapter III introduces a composite beamformer that defeats signal cancellation and demonstrates the performance improvement that it provides. Chapter IV elaborates upon the characteristics of the composite beamformer by describing convergence behavior, illustrating performance under additional signal conditions, and examining the issues of convergence rate and weight behavior near convergence. Finally, Chapter V summarizes the status of the work on signal cancellation and lists some topics that deserve further research.

II. SIGNAL CANCELLATION IN HARD-CONSTRAINED BEAMFORMERS

Jamming or interference generally involves the addition of spurious components to the desired or target signal. These spurious components can decrease intelligibility or cause decoding errors, sometimes to the extent of denying communication or surveillance altogether. Adaptive antennas are useful in suppressing the "additive" jamming effect, but can be responsible for introducing a "subtractive" jamming effect. Subtractive jamming amounts to the cancellation of desired signal components and, like ordinary jamming, can disrupt communications. The purpose of this chapter is to provide insight into the nature of this signal cancellation phenomenon.

The cancellation phenomenon will be examined in the context of adaptive beamformers that use versions of the LMS algorithm. It will be seen, however, that cancellation arises not from any special properties of the adaptation method, but due to nonzero correlation between the signal and jamming waveforms during the data window being considered by the adaptive algorithm. Similar cancellation effects will take place with any least-squares algorithm that might be used to adjust the beamformer weights at a comparable rate.

The chapter has been divided into several sections. The first section furnishes a brief historical perspective on signal cancellation. The second section provides a review of the properties of Frost's hard-constrained algorithm and

establishes notation that will be useful throughout the report. The third section discusses the effects of signal cancellation on a wideband signal and illustrates the destruction of signal components that can occur. The final two sections consider cancellation in the narrowband case. Appendix A contains a supporting analysis for the final section.

A. Background

It has been realized for some time that signal cancellation can occur even in hard-constrained beamformers when correlation exists between the desired signal and some other signal impinging upon the array. (See, for example, [6] by Frost.) This was a disquieting fact, because this is precisely the condition that can arise naturally as a result of multipath or can be induced artificially through repeater jamming. It appears, however, that this troublesome case was more or less set aside* while work continued on other aspects of adaptive antennas.

As adaptive-antenna work went forward in other areas during the mid-seventies, developments relevant to signal cancellation were taking place in another branch of adaptive systems. Experimental work in adaptive noise cancellation had disclosed filtering phenomena that fell outside the purview of Wiener filter theory. Glover [10,11,12] analyzed this non-Wiener behavior and

*Some work directed specifically toward adaptive elimination of multipath interference at HF was described in November 1981 by Hansen and Loughlin [19]. Their method makes use of a modulated pilot signal that is added to the communication signal at the transmitter. Pilot bandwidth must be adequate to provide discrimination between the various modes arriving at the receiver. This approach is limited to those situations where the transmitter is accessible and bandwidth allocations are not restrictive.

showed that, for the case involving sinusoidal reference inputs, the adaptive noise canceller can be regarded as a stable notch filter. Shensa [13,14] was later successful in treating a somewhat more general class of input signals.

Widrow was able to extrapolate from the work being done on adaptive noise cancellers and draw some disturbing new conclusions concerning signal cancellation in adaptive beamformers. Widrow realized that correlation (in the usual long-term sense) was a sufficient, but *not necessary,* condition for the destructive effects of signal cancellation. If high adaptation speeds are employed, signal cancellation can be induced by a broad class of jammer signals, and close replication of the desired signal (e.g., through repeater jamming) is not necessarily required. Since high adaptation rates are being sought so that good jammer nulling performance can be obtained in dynamic countermeasures environments, the conditions that support signal cancellation may be routinely present. Recognition of this state of affairs added considerable incentive to study signal cancellation. Simulation work was begun at Stanford in 1980 to confirm the effects predicted by Widrow and to support the search for methods of avoiding signal cancellation. Portions of this work have been reported in References 15 and 16. Other workers [17,18] have observed signal cancellation in actual adaptive-antenna systems.

B. Frost's Constrained LMS Algorithm

The application of his constrained LMS algorithm to adaptive arrays has been described in some detail by Frost [5,6]. Some of the key results will be restated in this section to provide the background and notation for discussions that follow.

The adaptive array problem to be considered is pictured in Figure 1. A uniform linear array of K elements is connected to an adaptive beamformer that consists of K tapped-delay-line filters, each with J taps and J adjustable weights. The sampled tap voltages and the weights are indexed in the columnar scheme shown in the figure and are identified in vector notation as

$$X^T(j) \triangleq [x_1(j),\ x_2(j),\ \ldots,\ x_{KJ}(j)] \tag{2-1}$$

$$W^T(j) \triangleq [w_1(j),\ w_2(j),\ \ldots,\ w_{KJ}(j)] \quad , \tag{2-2}$$

where j is the sample number. The filter outputs are summed to form the beamformer output:

$$y(j) = W^T(j)X(j) = X^T(j)W(j) \quad . \tag{2-3}$$

In addition to being the useful output signal from the system, the beamformer output serves as the error signal that is fed back for use in the weight adaptation process. The goal of adaptation is to minimize the output contribution of noise sources (such as the jammer indicated in the figure), subject

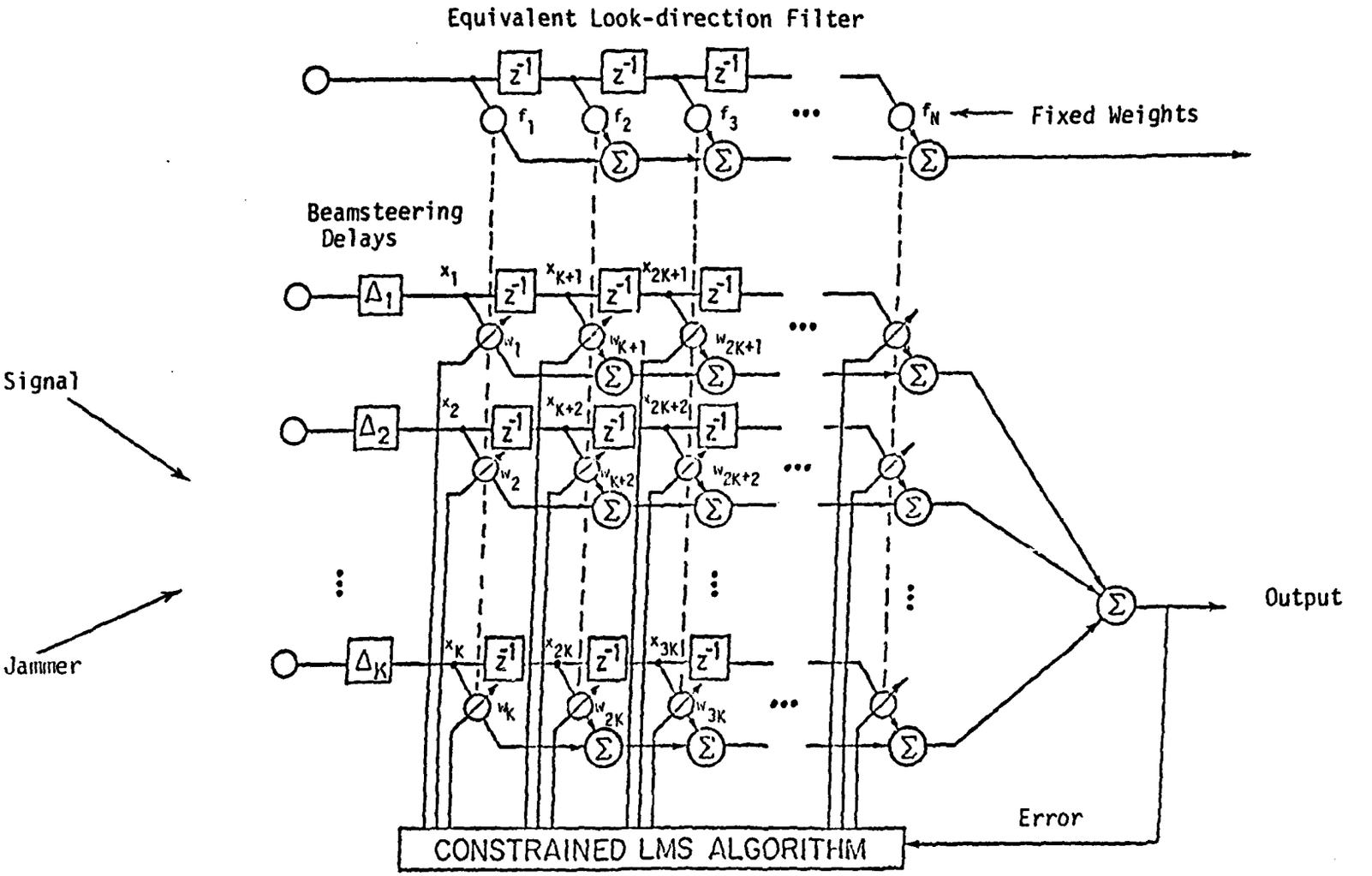

Figure 1. Block Diagram of the Frost Adaptive Beamformer

to a set of constraints that provide rigid control over the array response in the direction from which desired signals are expected.

It is assumed that the desired signal and the interference are uncorrelated. The incident signal vector may be decomposed according to

$$X(j) = S(j) + N(j) \tag{2-4}$$

by letting $S(j)$ represent the vector of desired signals at the beamformer taps and $N(j)$ represent the aggregate contribution of the various noise sources. If the autocorrelations of the quantities of Eq. 2-4 are defined by

$$R_{XX} \triangleq E[X(j)\, X^T(j)] \tag{2-5}$$

$$R_{SS} \triangleq E[S(j)\, S^T(j)] \tag{2-6}$$

$$R_{NN} \triangleq E[N(j)\, N^T(j)] \quad , \tag{2-7}$$

then the assumed lack of correlation between the desired signal and the noise is expressed by

$$R_{XX} = R_{SS} + R_{NN} \quad . \tag{2-8}$$

This correlation condition must hold if the look-direction constraints are to afford protection for the desired signal.

The constraint method depends upon knowing the arrival direction of the desired signal. The array is assumed to be steered (either mechanically or

electrically) toward the known look direction. Under this assumption, the desired signal components are identical at the inputs to the beamformer filters and along any column of taps in the beamformer. An equivalent look-direction processor can therefore be formed by summing the weights in each beamformer column to arrive at the J-tap filter shown at the top of Figure 1. The equivalent look-direction filter provides the key to an algorithm that minimizes noise contributions at the output without influencing the response to the desired signal. Specifically, the weights may be freely adjusted to minimize the noise output provided the column sums in the beamformer remain equal to the preselected weights in the equivalent look-direction processor. In order to state the minimization problem succinctly, it is helpful to express the look-direction impulse response in vector form and to define a constraint matrix. The look-direction-response vector is formed from the weights in the equivalent look-direction filter:

$$\underline{f} \triangleq [f_1, f_2, \ldots, f_J] \quad . \tag{2-9}$$

The constraint matrix C is composed of columns of the form

$$c_i = \begin{bmatrix} 0 \\ \vdots \\ 0 \end{bmatrix} \left.\vphantom{\begin{matrix} 0 \\ \vdots \\ 0 \end{matrix}}\right\} 1^{st} \text{group of } K \text{ elements}$$
$$\begin{matrix} \vdots \\ 0 \end{matrix} \left.\vphantom{\begin{matrix} 0 \\ \vdots \\ 0 \end{matrix}}\right\} (i-1)^{st} \text{group of } K \text{ elements}$$
$$\begin{matrix} 1 \\ \vdots \\ 1 \end{matrix} \left.\vphantom{\begin{matrix} 0 \\ \vdots \\ 0 \end{matrix}}\right\} i^{th} \text{group of } K \text{ elements}$$
$$\begin{matrix} 0 \\ \vdots \\ 0 \end{matrix} \left.\vphantom{\begin{matrix} 0 \\ \vdots \\ 0 \end{matrix}}\right\} (i+1)^{st} \text{group of } K \text{ elements}$$
$$\begin{matrix} \vdots \\ 0 \end{matrix} \left.\vphantom{\begin{matrix} 0 \\ \vdots \\ 0 \end{matrix}}\right\} J^{th} \text{group of } K \text{ elements} \qquad (2\text{-}10)$$

That is,

$$C \triangleq [c_1,\ c_2,\ \ldots,\ c_i,\ \ldots,\ c_J] \quad . \qquad (2\text{-}11)$$

The matrix C is a $KJ \times J$ matrix that conveys the beamformer structural information needed to implement the constraints.

With the notation developed to this point, the constrained-LMS problem may be stated:

$$\underset{W}{\text{Minimize}}\ E[y^2(j)] = E[W^T X(j) X^T(j) W] = W^T R_{XX} W \quad (2\text{-}12)$$

$$\text{subject to } C^T W = \mathcal{L} \quad .$$

Frost developed both closed-form and adaptive solutions for the constrained-LMS problem. The method of Lagrange multipliers was used to arrive at the optimal solution in terms of the signal statistics and the constraints:

$$W^* = R_{XX}^{-1} C [C^T R_{XX}^{-1} C]^{-1} \mathcal{L} \quad . \quad (2\text{-}13)$$

This solution assumes that the signal statistics are known (or have been estimated) and imposes a heavy computational burden if the matrix inversions must be repeatedly performed to track a dynamic environment.

The adaptive algorithm generates an asymptotically optimal solution to the constrained-LMS problem and requires much less computation per weight-update cycle than the closed-form solution. The update scheme is most easily understood from the individual weight recursions:

$$w_1(j+1) = w_1(j) - \mu y(j) x_1(j) - \frac{1}{K} \sum_{i=1}^{K} [w_i(j) - \mu y(j) x_i(j)] + \frac{f_1}{K}$$

$$\vdots$$

$$w_K(j+1) = w_K(j) - \mu y(j) x_K(j) - \frac{1}{K} \sum_{i=1}^{K} [w_i(j) - \mu y(j) x_i(j)] + \frac{f_1}{K}$$

$$w_{K+1}(j+1) = w_{K+1}(j) - \mu y(j) x_{K+1}(j) - \frac{1}{K} \sum_{i=K+1}^{2K} [w_i(j) - \mu y(j) x_i(j)] + \frac{f_2}{K}$$

$$\vdots$$

$$w_{2K}(j+1) = w_{2K}(j) - \mu y(j) x_{2K}(j) - \frac{1}{K} \sum_{i=1}^{K} [w_i(j) - \mu y(j) x_i(j)] + \frac{f_2}{K}$$

$$\vdots$$

$$w_{KJ}(j+1) = w_{KJ}(j) - \mu y(j) x_{KJ}(j) - \frac{1}{K} \sum_{(J-1)K+1}^{KJ} [w_i(j) - \mu y(j) x_i(j)] + \frac{f_J}{K} . \quad (2\text{-}14)$$

The right-hand side of each recursion involves the current weight value plus several update terms. The first update term depends upon the current error and the signal at the weight in question. The adaptation constant μ is used to scale this term; μ is set* to yield stable system operation and to provide an appropriate adaptation rate. The second update term is the average correction over a column of weights, and the third update term is a fractional allocation of the appropriate weight in the equivalent look-directional filter. Taken together, the three update terms drive the weights toward the values that minimize output power subject to the specified linear constraints. It is easy to verify the efficacy of the constraint method by summing the updated weights over any column of the beamformer and noting that the constraint is always satisfied.

The constrained-LMS algorithm may be written in matrix form to provide a more compact description. It is helpful to introduce a KJ-dimensional initial weight vector F, where

*Factors governing the choice of μ are discussed in References 5, 6, and 10.

$$F \triangleq C(C^T C)^{-1} \mathcal{L} \quad , \tag{2-15}$$

and a $KJ \times KJ$ projection operator P, where

$$P \triangleq I - C(C^T C)^{-1} C^T \quad , \tag{2-16}$$

With this added notation, the constrained-LMS algorithm may be stated as:

$$\begin{aligned} W(0) &= F \\ W(j+1) &= P[W(j) - \mu y(j) X(j)] + F \quad . \end{aligned} \tag{2-17}$$

It will also be useful to note the time constants exhibited by the hard-constrained algorithm. Frost showed that the matrix $P\, R_{XX} P$ determines the rate of convergence of the mean weight vector toward the optimal weight vector W^*. Specifically, convergence of the mean weight vector along the i^{th} eigenvector of $P\, R_{XX} P$ occurs with a time constant given by

$$\tau_i = \frac{1}{ln(1-\mu\sigma_i)} \cong \frac{1}{\mu\sigma_i} \quad , \tag{2-18}$$

where σ_i is the eigenvalue associated with the i^{th} eigenvector and where updating at the sample rate (as opposed to, say, every tenth sample) is assumed.

C. Signal Cancellation in the Wideband Case

The effects of signal cancellation in a hard-constrained ABF can be readily demonstrated by simulating* the simple adaptive-antenna problem diagrammed in Figure 2. The selected adaptive antenna was a two-element Frost ABF with

*An overview of the simulation methods used in this research is given in Appendix E.

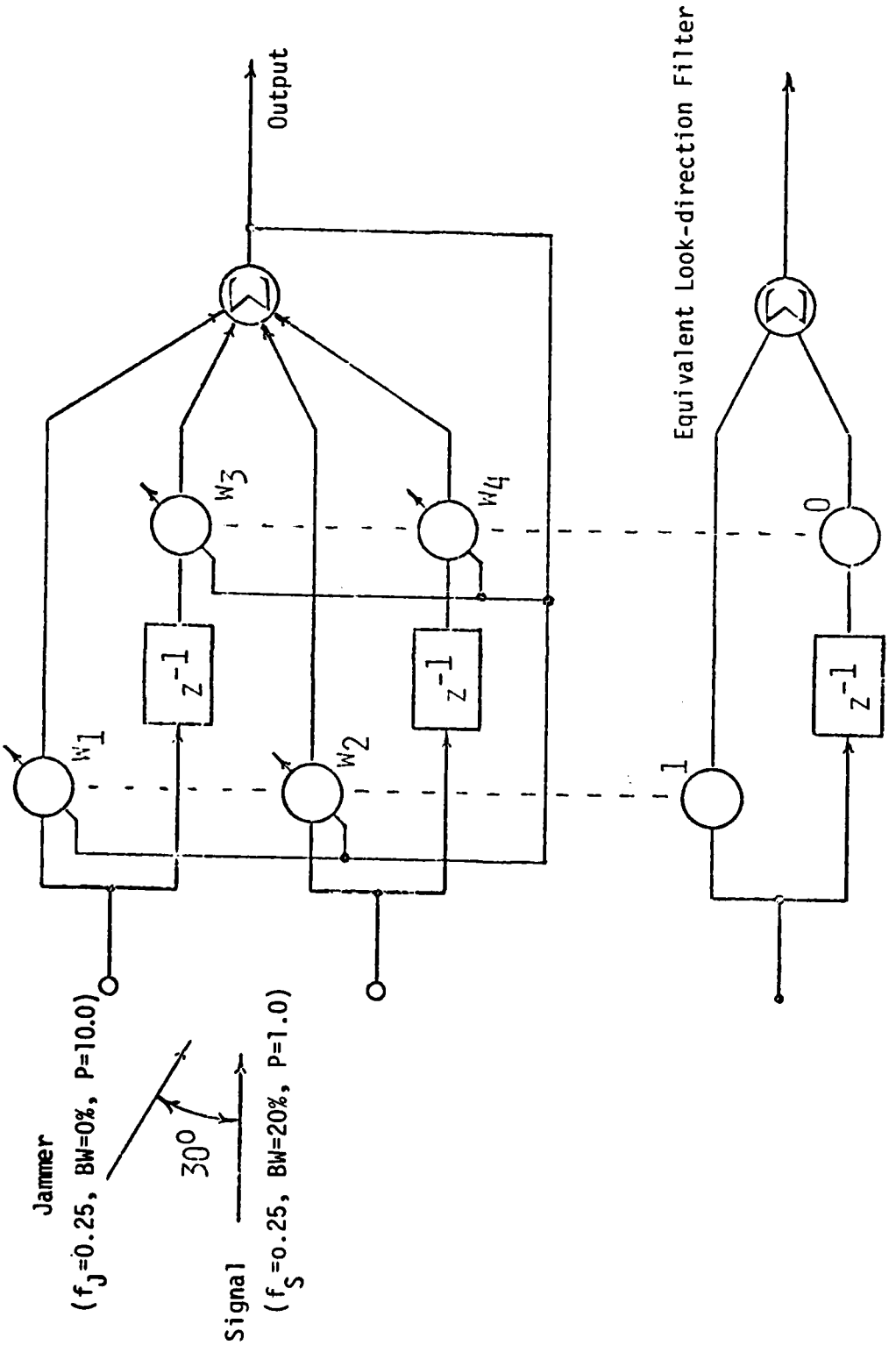

Figure 2. A Four-weight Frost ABF with a Wideband Signal and a Sinusoidal Jammer

two weights per element. A wideband desired signal S with power P_S equal to one was incident from broadside, while a narrow-band jammer J with power P_J equal to 10 was incident from an angle of 30°. The ABF was constrained to provide unity gain and a flat frequency response in the look direction by setting the constraint-vector elements f_1 and f_2 to 1 and 0, respectively. ABF weights were updated using the constrained LMS algorithm, which in this particular case may be written from (2-14) as

$$\begin{aligned}
w_1(j+1) &= \frac{1}{2}[w_1(j) - \mu y(j)x_1(j)] - \frac{1}{2}[w_2(j) - \mu y(j)x_2(j)] + \frac{f_1}{2} \\
w_2(j+1) &= \frac{1}{2}[w_2(j) - \mu y(j)x_2(j)] - \frac{1}{2}[w_1(j) - \mu y(j)x_1(j)] + \frac{f_1}{2} \\
w_3(j+1) &= \frac{1}{2}[w_3(j) - \mu y(j)x_3(j)] - \frac{1}{2}[w_4(j) - \mu y(j)x_4(j)] + \frac{f_2}{2} \\
w_4(j+1) &= \frac{1}{2}[w_4(j) - \mu y(j)x_4(j)] - \frac{1}{2}[w_3(j) - \mu y(j)x_3(j)] + \frac{f_2}{2} \quad .
\end{aligned} \tag{2-19}$$

In these equations μ is the constant that controls the rate of adaptation; μ was set to 1×10^{-2} in this simulation.

Figure 3 shows some measurements made after a sufficient number of adaptations to allow transient phenomena to die away. Part a) of the figure shows the antenna pattern at the jammer frequency of 0.25 f_{samp} and confirms that a null has been placed on the jammer. Part b) is a plot of the frequency response in the jammer direction; this plot also shows a deep null at the jammer frequency. The third plot simply confirms that the specified response in the look direction has been attained. Taken together, the three plots seem to indicate

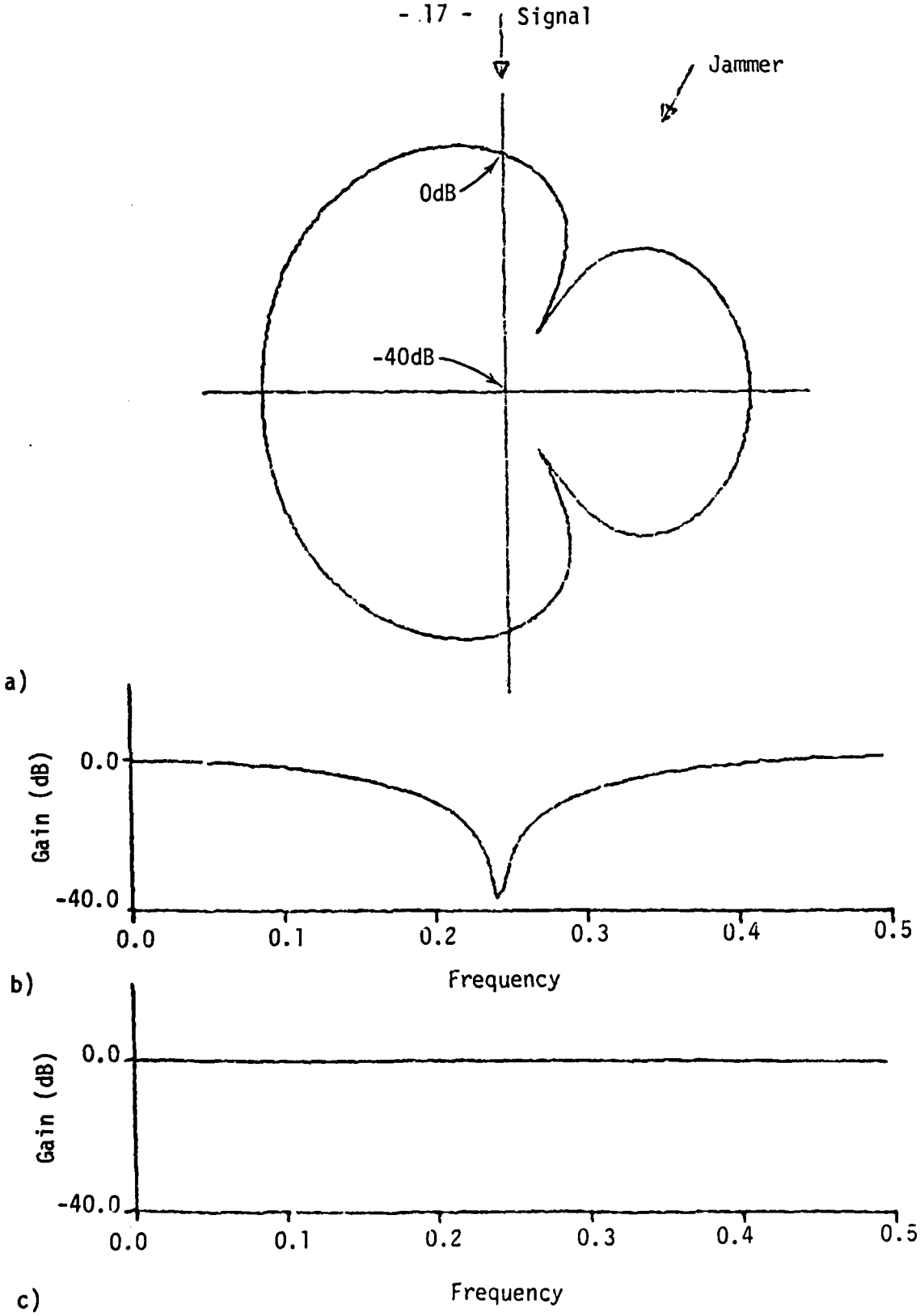

Figure 3. Postconvergence Plots for the Four-element Frost ABF
a) Beampattern
b) Jammer-direction Frequency Response
c) Signal-direction Frequency Response

that all is well and that the intended objectives of signal recovery and jammer rejection have been attained.

The favorable picture provided by the antenna plots of Figure 3 darkens considerably when the desired signal and the ABF output are compared. Figure 4 is a plot of ensemble-averaged spectra of the desired signal, the jammer signal, and the ABF output. It is clear that, despite very rigid control of the look-direction response and good jammer rejection, the desired signal has not been recovered intact. Instead the signal has experienced frequency-dependent distortion. Signal components on the skirts of the signal remain unaffected, but components in the vicinity of the jammer frequency have been totally or partially destroyed in the ABF.

The extent of signal cancellation for a given antenna structure and signal environment is governed by the rate of adaptation, i.e., by the adaptation parameter μ. The simulation just described was repeated for several different values of μ; output spectra for the series of experiments are assembled in Figure 5. Parts a and b of the figure involve lower adaptation rates than the rate used to produce the results in Figure 4 and reveal lesser amounts of signal destruction. In fact, cancellation is almost undetectable in Part a. Part c repeats the results shown in Figure 4. Part d involves a large μ (a value near the instability point) and shows the near-total signal destruction that can occur in an extreme case. It is apparent from Figure 5 that cancellation occurs over a considerable range of adaptation parameter selections and that the destructive effects can be quite

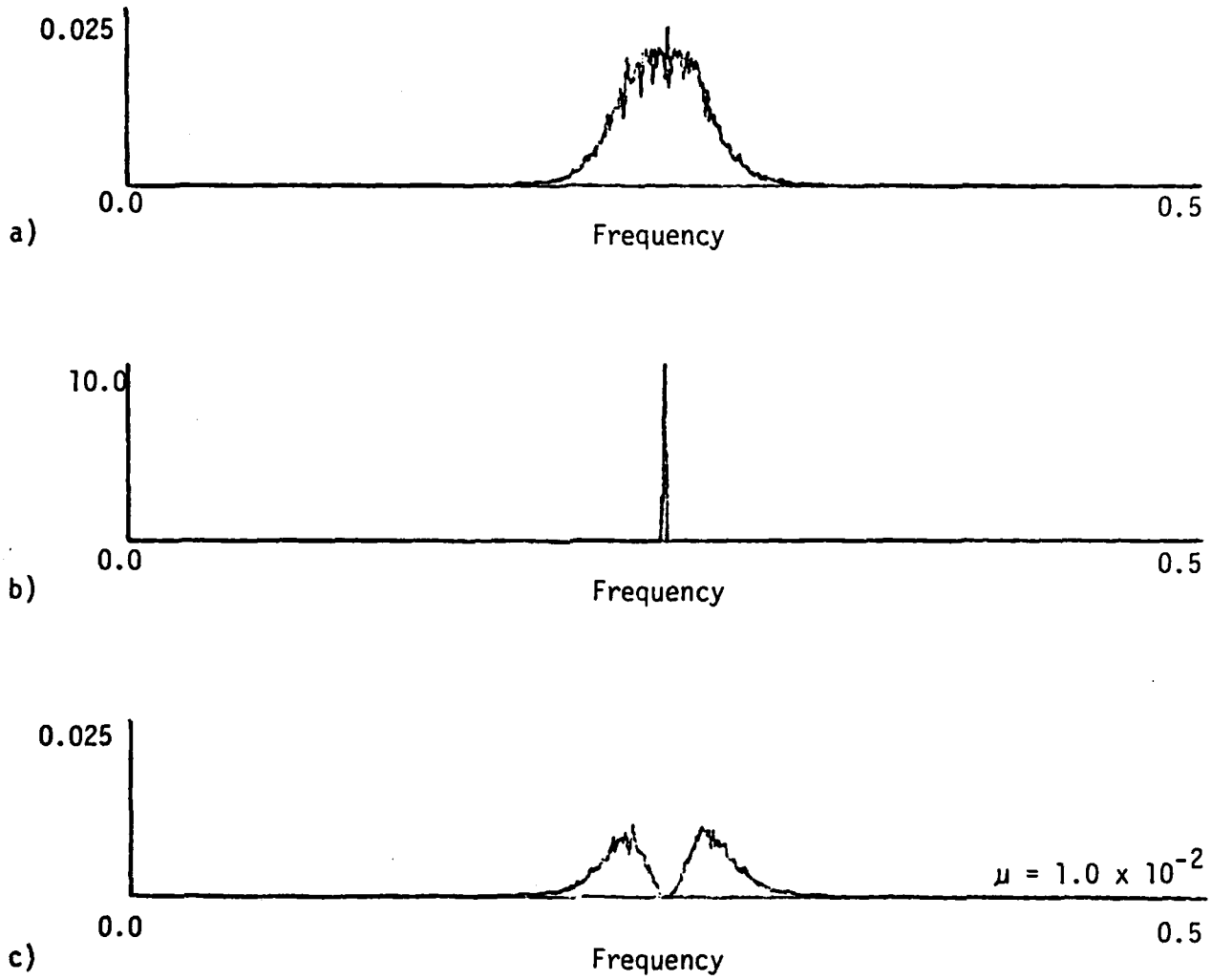

Figure 4. Input and Output Spectra for the Four-weight Frost ABF

a) Signal
b) Jammer
c) ABF Output

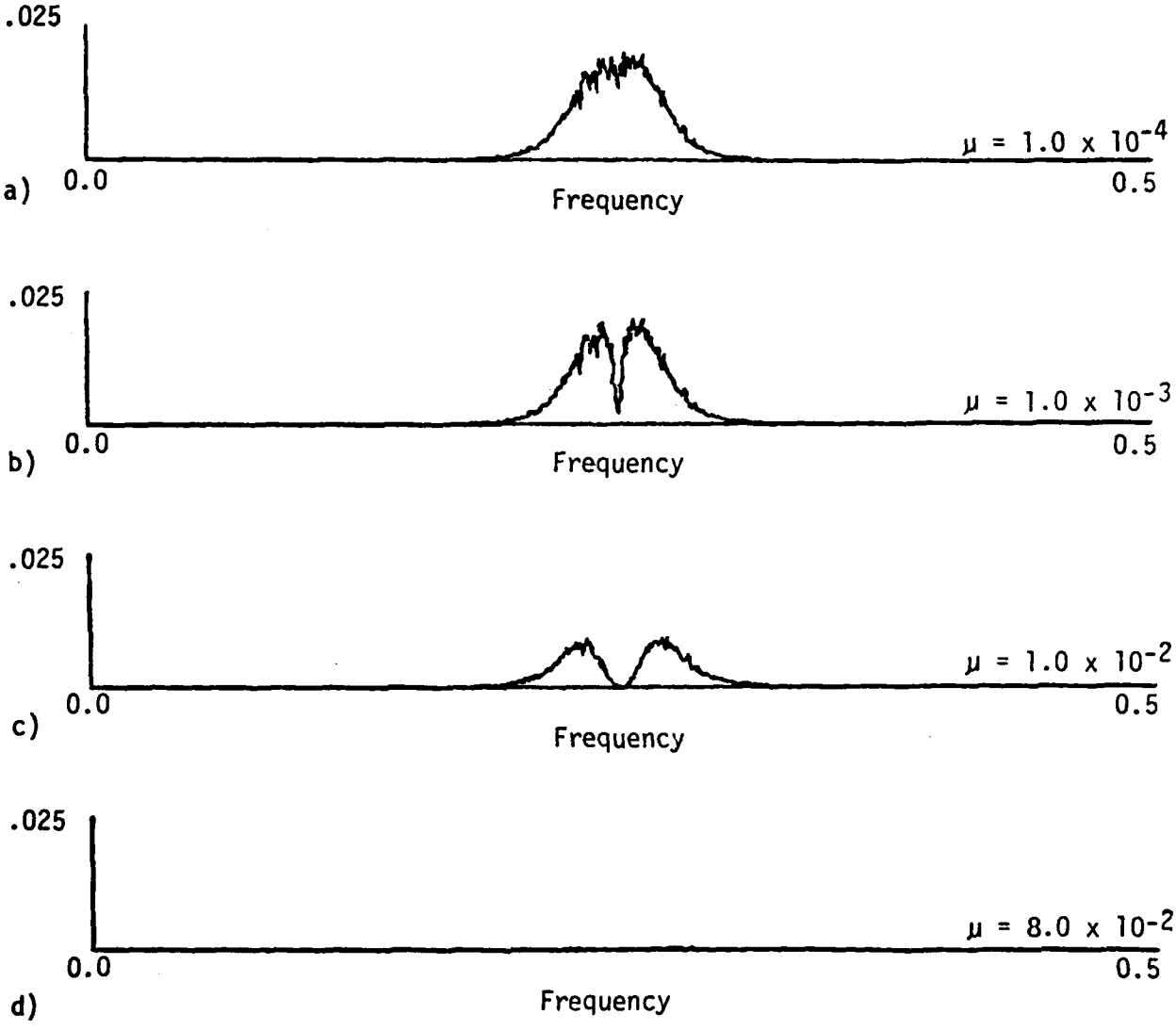

Figure 5. Output Power Spectra of the Four-weight Frost ABF for Various Adaptation Constants

important when high adaptation rates are sought. It is also clear that, although cancellation effects may be made negligible by choosing a sufficiently small μ, orders of magnitude in convergence rate must be sacrificed to maintain signal quality. At these low adaptation rates the ability to track a dynamic environment will be greatly reduced.

D. Signal Cancellation in the Narrowband Case

A wideband signal was useful in the examples of the previous section because the broad spectrum clearly showed the extent of cancellation effects. This section will concentrate on developing a more detailed picture of the cancellation phenomenon by considering the internal operation of a beamformer while cancellation is occurring. A narrowband signal as well as a narrowband jammer will be used to facilitate the analysis of beamformer behavior.

A particularly simple beamformer structure and signal/jammer scenario were sought to provide a test case for the study of cancellation effects in the Frost ABF. The selected problem is illustrated in Figure 6, which shows a sinusoidal desired signal S (frequency $f_S = 0.25$) incident on a two-element array from broadside and a sinusoidal jammer J (frequency $f_J = 0.26$) incident from 45°. Element spacing was a half wavelength at the signal frequency. The antenna elements were tied to a four-weight Frost ABF that was steered to broadside and constrained to provide unit gain and flat frequency response in the look direction. (The constraints were $f_1 = 1$ and $f_2 = 0$, as indicated in the equivalent look-

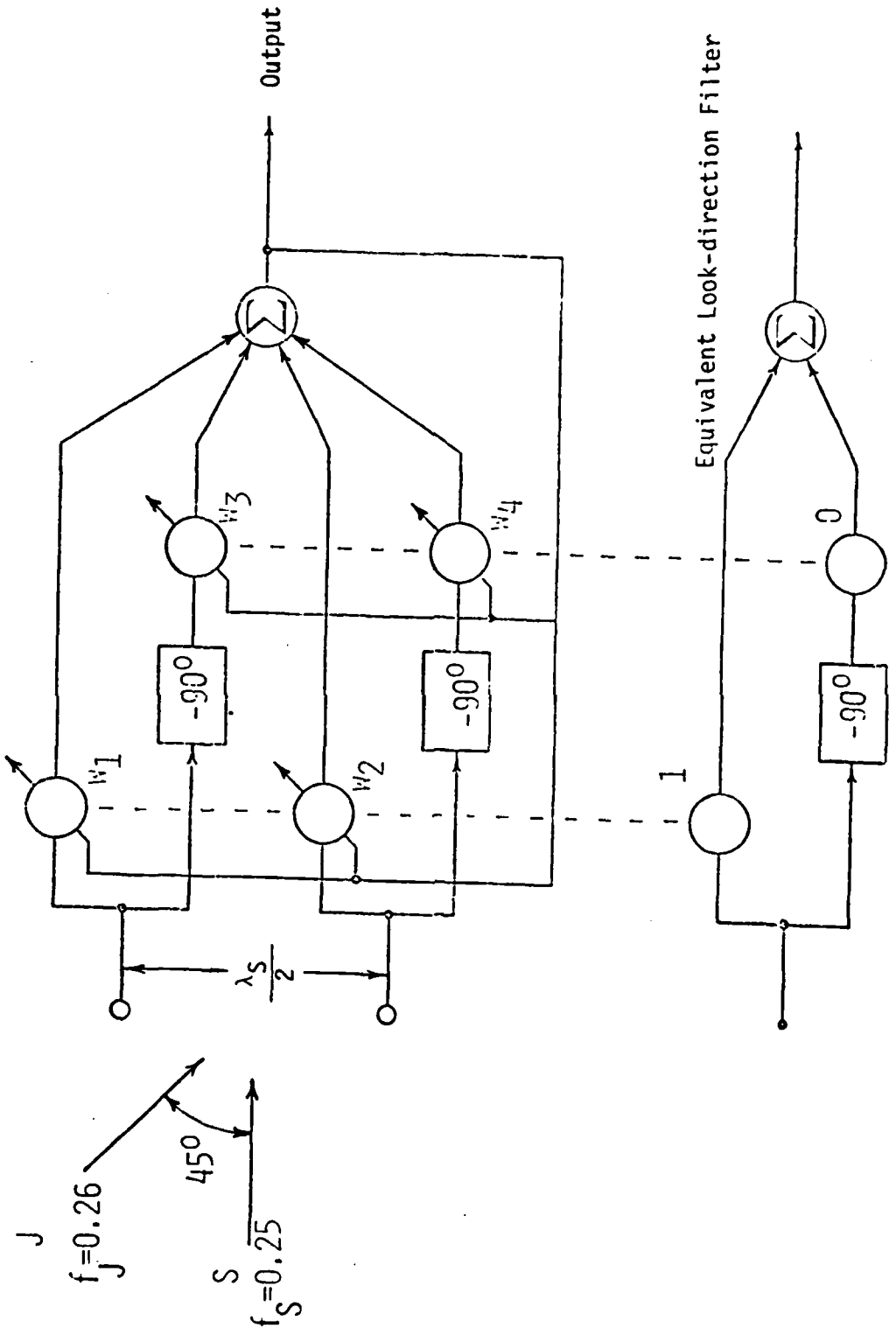

Figure 6. Four-weight Frost ABF with Sinusoidal Signal and Jammer

direction filter.) The weights were updated using the constrained LMS algorithm given in Equations (2-19).

Just enough degrees of freedom were provided in this test case to allow the objectives of signal reception and jammer rejection to be realized. Constant gain in the signal direction was assured by the hard constraints of the Frost algorithm:

$$\begin{cases} w_1 + w_2 = 1 \\ w_3 + w_4 = 0 \end{cases} \quad . \tag{2-20}$$

The constraints consumed two of the four available degrees of freedom; the remaining two degrees of freedom were adequate for eliminating the jammer.

The requirements for eliminating jammer energy can be readily derived for the simple case at hand. The array output attributable to the jammer is given by

$$y_J(t) = e^{j\omega_J t}[w_1 - jw_3] + e^{j(\omega_J t - \phi_{ee})}[w_2 - jw_4] \quad , \tag{2-21}$$

where ϕ_{ee} is the element-to-element phase shift for the jammer signal. The element-to-element phase shift may be computed from the array geometry and the signal and jammer parameters:

$$\phi_{ee} = \frac{2\pi \left(\frac{\lambda_S}{2}\right) \sin 45^\circ}{\lambda_J} = \frac{2\pi \left(\frac{\lambda_S}{2}\right) \sin 45^\circ}{\lambda_S \left(\frac{.25}{.26}\right)} = 2.31 \text{ radians} \quad . \tag{2-22}$$

Inserting the value for ϕ_{ee}, expanding, and equating real and imaginary parts to

zero yields

$$\begin{cases} w_1 - .6739\, w_2 - .7388\, w_4 = 0 \\ -.7388\, w_2 - w_3 + .6739\, w_4 = 0 \end{cases} \quad (2\text{-}23)$$

The equations 2-20 arising from the constraints and the equations just given may be solved simultaneously to arrive at the ideal weight values for signal reception and jammer nulling. The desired weights are:

$$\begin{cases} w_1 = 0.50 \\ w_2 = 0.50 \\ w_3 = -0.22 \\ w_4 = 0.22 \end{cases} \quad (2\text{-}24)$$

These are the Wiener weight values that will be approached as the adaptation constant μ is decreased to small values and adaptation proceeds very slowly. Ideal beamformer operation (i.e., perfect signal reception and jammer nulling) is obtained with these weights. In practice, however, dynamic signal environments may make high adaptation speeds necessary, and weight values may be far from the Wiener ideal. It is of interest to examine weight behavior under these more demanding circumstances.

Figure 7 shows the weight dynamics over a period of 256 adaptation cycles for the test case outlined above and $\mu = 0.1$. The epoch shown is after initial transients have died away; the non-Wiener behavior exhibited here will continue indefinitely. Each weight can be seen to oscillate about the desired Wiener weights; i.e., the average values of the weights are the Wiener weights. The oscillation frequency of 0.01 f_{samp} is the difference frequency between the desired

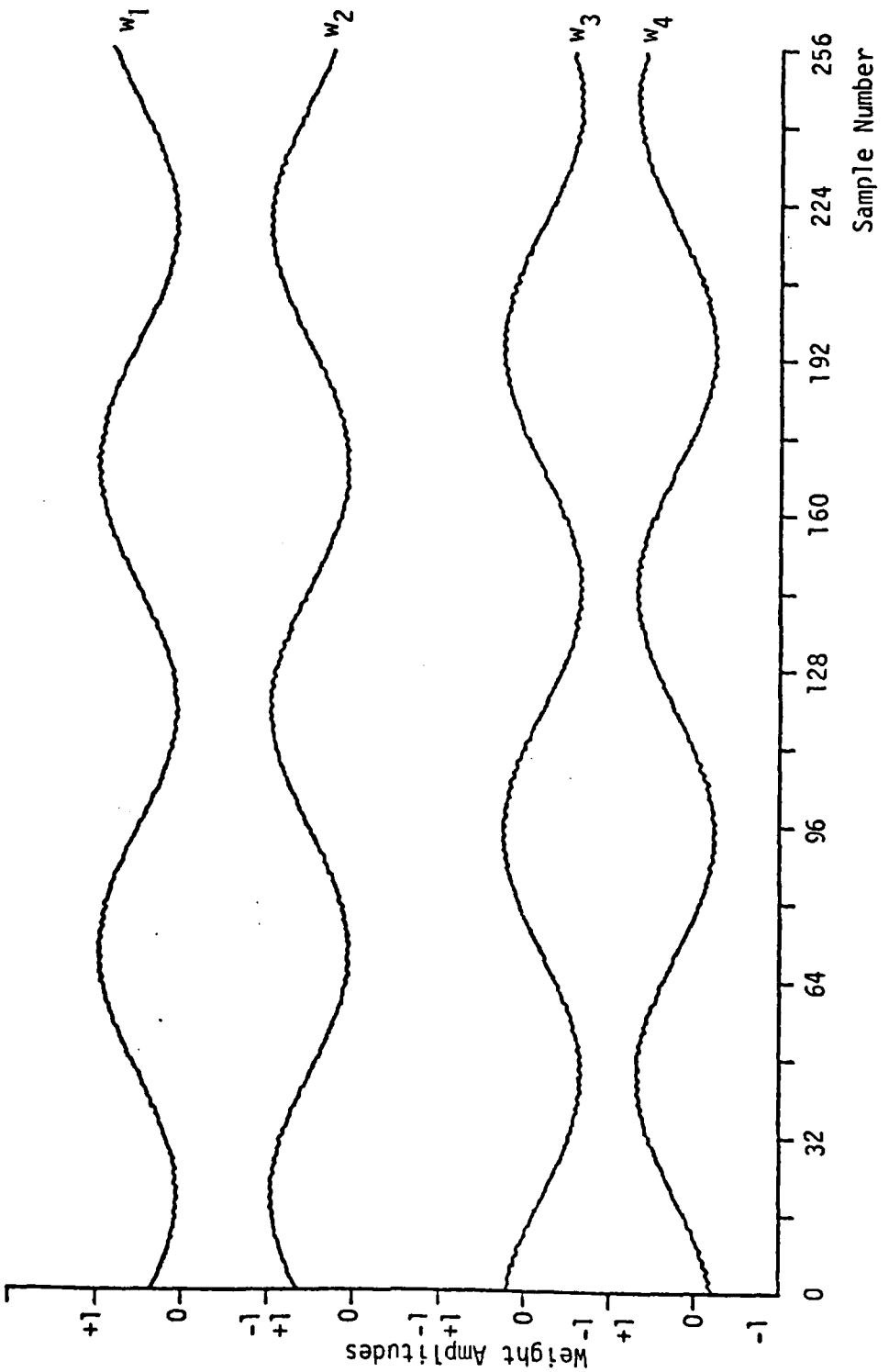

Figure 7. Weight Dynamics in the Frost ABF.

signal at 0.25 f_{samp} and the jammer signal at 0.26 f_{samp}. This is the same weight behavior noted by Glover [11,12] in a related noise-cancelling problem.

Figure 8 documents the behavior of the weights when the simulation experiment is altered by abruptly switching off the signal at the time indicated. The oscillatory behavior of the weights ceases, and, after a brief transient period, the weights reach and hold the optimal values that were calculated earlier. It thus appears that signal energy is needed to support the non-Wiener behavior that has been observed. The precise role of the signal in the adaptive system may be better understood by examining the interactions of the desired and jammer signals and the dynamic weights.

From Figure 7 it is clear that during signal presence each of the weights is of the form

$$w_i = C_i + A_i \sin(\omega_\Delta t + \phi_i) \quad , \tag{2-25}$$

where C_i is a constant giving the mean weight value, $\omega_\Delta = (2\pi)(0.01\ f_{samp})$ is the radian difference frequency, and A_i and ϕ_i are constants expressing the amplitude and phase of the sinusoidal component of the weight. Arbitrarily selecting w_1 as the phase reference and measuring the remaining constants yields the following expressions for the weights:

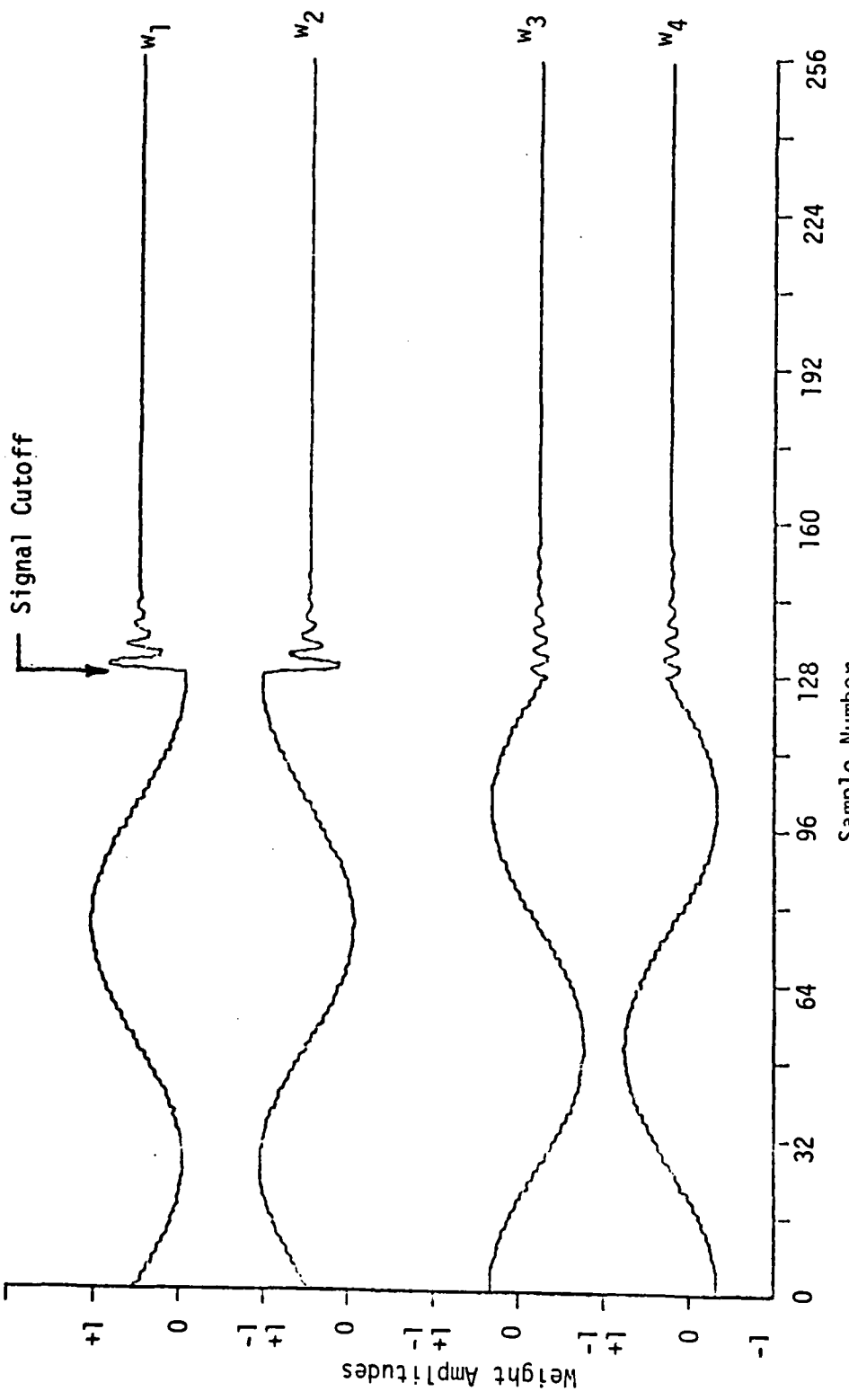

Figure 8. Signal Influence on Weight Dynamics

$$\begin{cases} w_1 = 0.50 + 0.46 & \sin(\omega_\Delta t - \phi_o) \\ w_2 = 0.50 + 0.46 & \sin(\omega_\Delta t - \phi_o - \pi) \\ w_3 = -0.22 + 0.46 & \sin(\omega_\Delta t - \phi_o - \pi/2) \\ w_4 = 0.22 + 0.46 & \sin(\omega_\Delta t - \phi_o - 3\pi/2) \end{cases} \quad (2\text{-}26)$$

Note that the oscillations of weights w_1 and w_2 are 180° out of phase so that the hard constraint for these two weights is always satisfied. Similarly, weights w_3 and w_4 are antiphased and satisfy the constraint at all times.

For purposes of analysis the beamformer of Figure 6 may be redrawn to reflect the observed nature of the weight behavior. Figure 9 shows a revised structure in which each weight has been replaced by the parallel combination of a fixed gain and a mixer. The fixed gains are set to the Wiener weights as required by the observed average values of the weights. The mixers have introduced into them a set of sinusoidal voltages with radian frequency equal to ω_Δ, as required by the observations regarding the oscillatory component of the weights. The relative phases of the mixer input voltages are shown in the phasor diagram inset into the upper right of the figure.

It is evident from Figure 9 that the oscillatory behavior of the weights creates a considerably more complicated signal set in the adaptive beamformer than would be the case with constant weights. The fixed gain associated with each weight contributes one component at the signal frequency and a second component at the jammer frequency. The mixer, however, yields sum and difference components for both the signal and the jammer. The net contribution

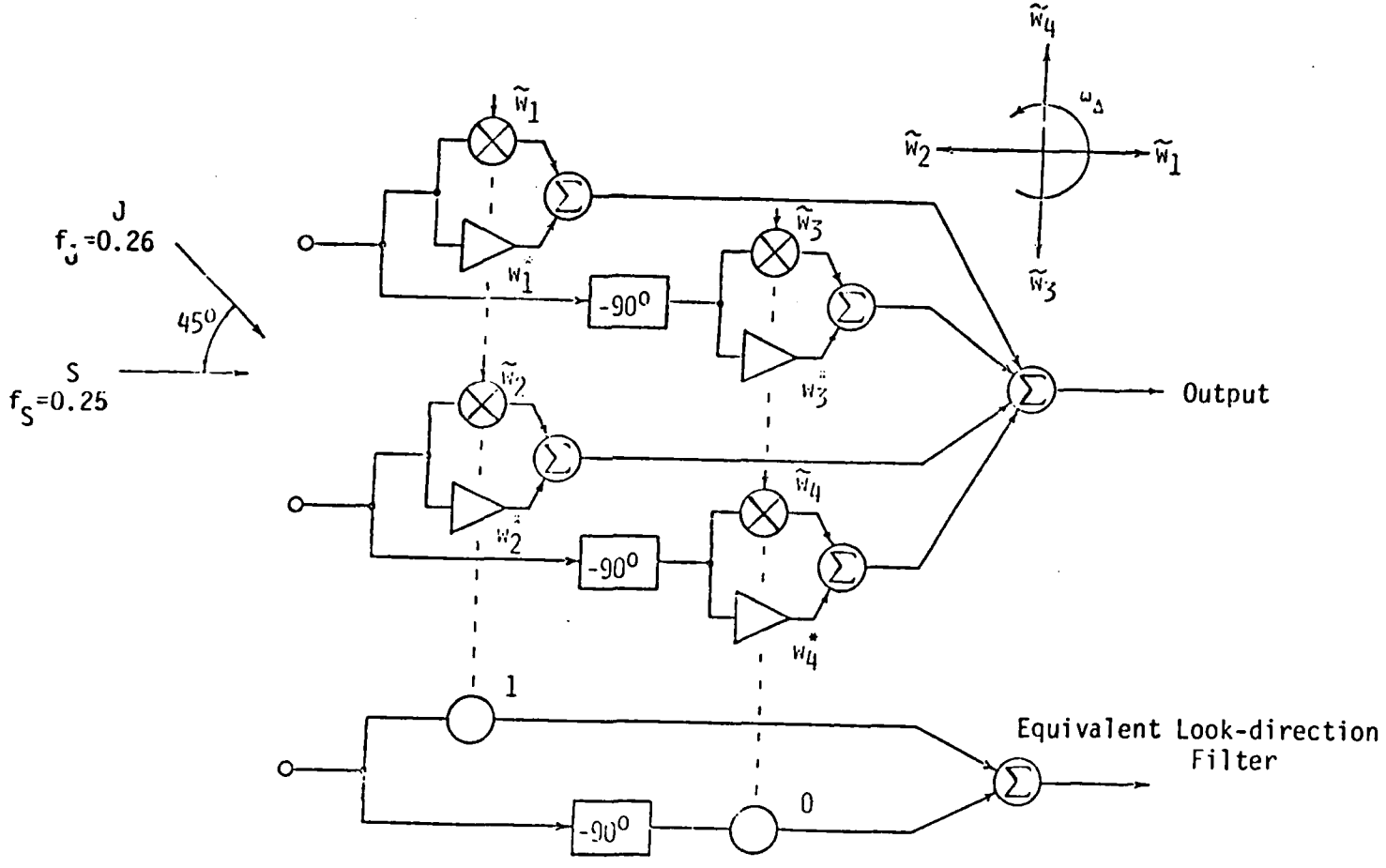

Figure 9. Frost ABF with Weights Decomposed into Static and Dynamic Components

from each weight is six components at four different frequencies; the signal set entering the final summing junction in Figure 9 consists of 24 different components. A detailed examination of these components is necessary to understand signal cancellation in even this simple case.

Fortunately, the apparent complexity of the 24-signal set is greater than its actual complexity. First, it should be recalled that the Wiener weights are known in this case to provide perfect signal reception and perfect jammer nulling. It follows that the eight components attributable to the fixed gains combine to simply yield a single component equal to the desired signal as seen at either array element. Second, it should be noted that in both beamformer columns (i.e. at weights w_1 and w_2 and at weights w_3 and w_4) the desired signal is cophased while the weights are antiphased. All eight terms arising from mixer action on the desired signal therefore sum to zero in the output summing junction. It should be noted that components generated from the desired signal by weight dynamics will always cancel in a properly steered Frost ABF due to the phase relationships enforced by array steering and the hard constraints.

At this point the only components that have not been examined are those generated by mixer action on the jammer signals. The output signal may be written as

$$
\begin{aligned}
y(t) \;=\; & \cos \omega_S t \\
& + \; [\cos \omega_J t][A \sin(\omega_\Delta t - \phi_0)] \\
& + \; [\cos(\omega_J t - \phi_{ee})]\,[A \sin(\omega_\Delta t - \phi_0 - \pi)] \\
& + \; [\sin \omega_J t]\,[A \sin(\omega_\Delta t - \phi_0 - \pi/2)] \\
& + \; [\sin(\omega_J t - \phi_{ee})]\,[A \sin(\omega_\Delta t - \phi_0 - 3\pi/2)] \quad , \qquad \text{(2-27)}
\end{aligned}
$$

where A is the amplitude of the weight oscillations. Expanding the products of signals and weights yields

$$
\begin{aligned}
y(t) \;=\; & \cos \omega_S t \\
& + \; \frac{A}{2} \sin[(\omega_\Delta + \omega_J)t - \phi_0] + \frac{A}{2} \sin[(-\omega_S)t - \phi_0] \\
& + \; \frac{A}{2} \sin[(\omega_\Delta + \omega_J)t - \phi_0 - \phi_{ee} - \pi] + \frac{A}{2} \sin[(-\omega_S)t - \phi_0 + \phi_{ee} - \pi] \\
& - \; \frac{A}{2} \sin[(\omega_\Delta + \omega_J)t - \phi_0] + \frac{A}{2} \sin[(-\omega_S)t - \phi_0] \\
& - \frac{A}{2} \sin[(\omega_\Delta + \omega_J)t - \phi_0 - \phi_{ee} - \pi] + \frac{A}{2} \sin[(-\omega_S)t - \phi_0 + \phi_{ee} - \pi] \quad .
\end{aligned}
$$

(2-28)

Further simplifications are obvious at this point. Cancellation eliminates all the terms at the radian frequency $(\omega_\Delta + \omega_J)$. Additionally, terms at $-\omega_S$ can be combined and then reexpressed using the relationship

$$\sin(-\theta) \;=\; -\sin(\theta) \quad . \qquad \text{(2-29)}$$

These steps plus inserting the measured value of A yield

$$y(t) \;=\; 1.0 \cos \omega_S t - 0.46 \sin(\omega_S t + \phi_o) - 0.46 \sin(\omega_S t + \phi_o - \phi_{ee} + \pi) \quad . \qquad \text{(2-30)}$$

The above expression for $y(t)$ indicates the interesting nature of the beamformer output in the case at hand. Weight dynamics have generated a

number of components at various frequencies, but weight phases are such that all components except those at the signal frequency sum to zero within the beamformer. The net result of the weight dynamics is a pair of synthesized components at the signal frequency that, when added to the actual signal, serve to drive the beamformer output power below the desired level.

Figure 10 is a phasor diagram that shows the three output signal components and their sum. The output signal amplitude is 0.64, not 1.00 as desired; output power is approximately 3.9 dB below the desired level. The signal has been partially cancelled by non-Wiener behavior in the weights even though the Frost constraint is perfectly sustained in the look direction. Faster adaptation would cause even more signal loss.

E. An Equivalent Adaptive-Noise-Cancelling Problem

The problem set forth in Figure 6 can be treated as an adaptive-noise-cancelling problem if it is imagined that the desired and jammer signals are available separately. The equivalent problem structure is illustrated in Figure 11. The desired signal may be taken straight through to the summing junction since the hard constraints specify unity gain and a flat frequency response. The jamming signal is brought to the summing junction through an adaptive filter that emulates the jammer-direction gain of the Frost beamformer. An in-phase gain G_I and a quadrature gain G_Q are able in this special case to give complete control over both the amplitude and phase of the jammer contribution.

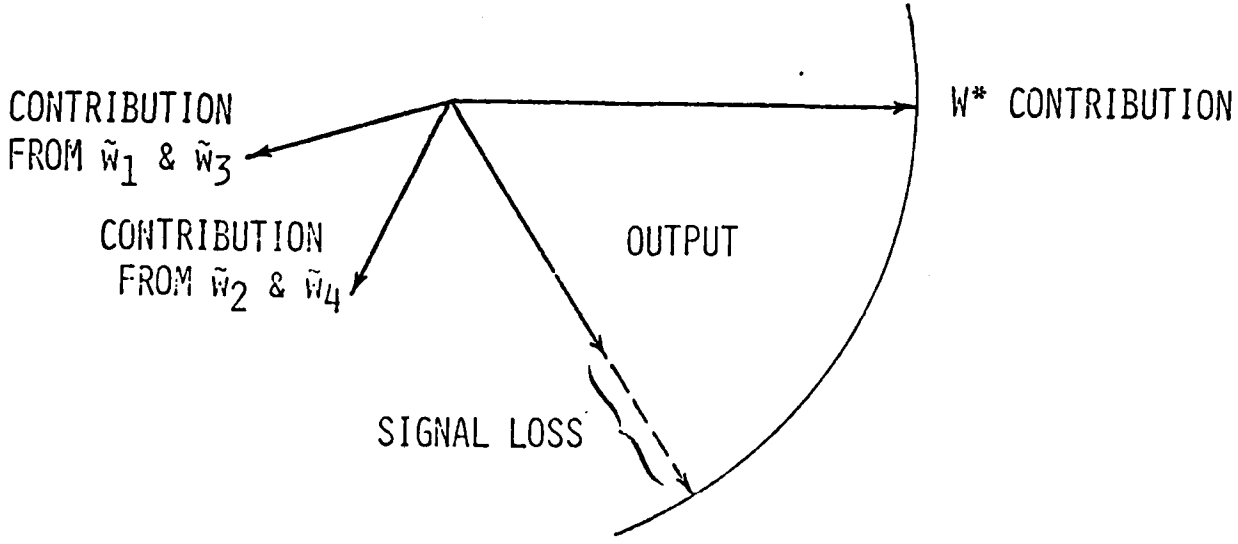

Figure 10. Phasor Diagram for Signal-frequency Components

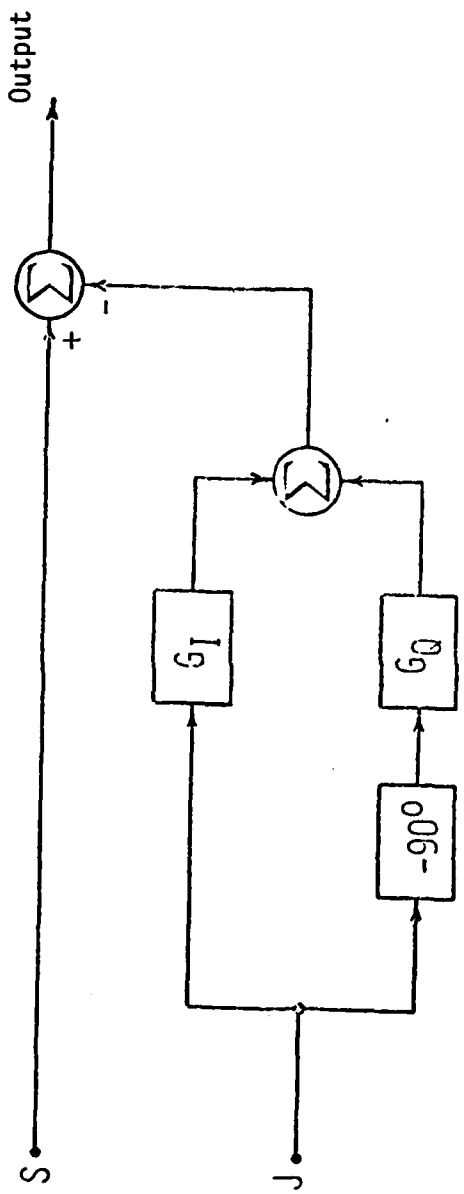

Figure 11. Equivalent Two-channel Structure for the Frost ABF

Expressions relating G_I and G_Q to the ABF weights w_1, w_2, w_3, and w_4 are needed to complete the specification of the equivalent problem. The required expressions may be derived from the equation for the jammer output from the ABF:

$$y_J(t) = w_1 \cos \omega_J t + w_2 \cos(\omega_J t - \phi_{ee}) + w_3 \sin \omega_J t + w_4 \sin(\omega_J t - \phi_{ee}) \quad . \tag{2-31}$$

where ϕ_{ee} is the element-to-element phase delay for the jammer signal. After making use of trigonometric identities and regrouping terms, the equation becomes

$$\begin{aligned} y_J(t) = {} & [w_1 + (\cos \phi_{ee}) w_2 - (\sin \phi_{ee}) w_4] \cos \omega_J t \\ & + [(\sin \phi_{ee}) w_2 + w_3 + (\cos \phi_{ee}) w_4] \sin \omega_J t \quad . \end{aligned} \tag{2-32}$$

Comparison of this equation with the structure of Figure 11 yields the relationships

$$\begin{aligned} G_I &= -[w_1 + (\cos \phi_{ee}) w_2 - (\sin \phi_{ee}) w_4] \\ G_Q &= -[(\sin \phi_{ee}) w_2 + w_3 + (\cos \phi_{ee}) w_4] \quad . \end{aligned} \tag{2-33}$$

The equivalent system involving G_I and G_Q allows a considerably simpler characterization of the weight dynamics associated with signal cancellation than would have been possible in the four-dimensional weight space of the original problem. In particular, the reduced dimensionality simplifies comparisons of the dynamic solution obtained during cancellation with the Wiener solution that is approached at low adaptation rates.

The Wiener solution in terms of G_I and G_Q may be determined by inspection for the ANC structure:

$$\begin{cases} G_I^* = 0 \\ G_Q^* = 0 \end{cases} \quad . \tag{2-34}$$

Thus it is seen that, in the two-space defined by plotting G_I along the x axis and G_Q along the y axis, the origin represents the solution that gives perfect signal recovery and perfect jammer rejection.

Figure 12 is a plot that shows the loci of several dynamic solutions in the $G_I - G_Q$ plane. Each solution is obtained by repeating the narrowband simulation of the previous section for the indicated value of μ and computing G_I and G_Q from the weights $\{w_i\}$. At μ=.001, the solution locus is a tiny circle that blurs into a dot at the origin, i.e., the solution almost exactly duplicates the Wiener solution. Signal cancellation is negligible in this case. As μ is increased, the solution loci expand to form circles * about the origin, and the amount of signal cancellation is increased. Cancellation exceeds 90 percent at the point where stability considerations forbid further increases in μ.

It is worthwhile to note the range of μ over which departure from the Wiener solution is visible in Figure 12. At $\mu = 0.001$ the deviation from the Wiener solution is barely perceptible. Instability does not occur until μ reaches

*Some departure from a circular locus is evident for $\mu = 0.1$. The effect is due to second-order weight oscillations at the sum frequency, i.e., at $f_S + f_J$. Glover reported similar effects in [11].

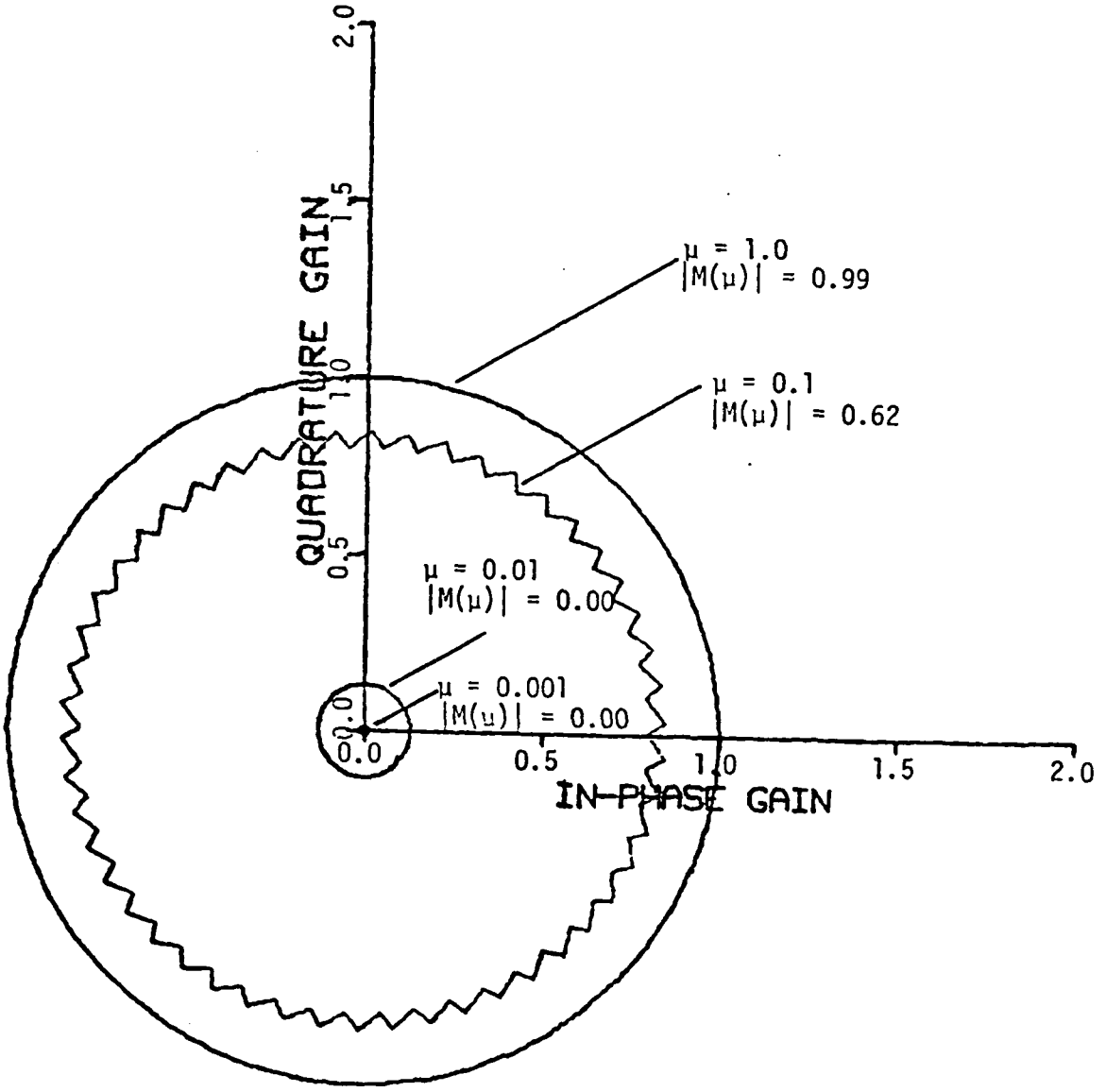

Notes:

a) μ is the adaptation parameter

b) $|M(\mu)|$ is the magnitude of the misadjustment

Figure 12. Solution Loci in the G_I - G_Q Plane.

beyond 1.00 (approximately 1.15). This gives a useful range of μ of about three orders of magnitude over which departure from the Wiener solution is noticeable. This is a rather broad operating region that includes the values of μ for which convergence is most rapid. In many cases it will be very unattractive to sacrifice orders of magnitude in convergence rate in order to obtain a close approximation to the Wiener solution. This is, unfortunately, the nature of the tradeoff that must be addressed when conventional adaptive beamformers are applied.

The loci of Figure 12 have several interesting interpretations. Considered simply as the path traced by the tip of a gain vector, each locus demonstrates the same cyclic weight behavior that was shown earlier in Figure 7. The number of samples required to complete one circuit of a locus is 100; this is the period of the difference frequency between the signal frequency of 0.25 f_{samp} and the jammer frequency of 0.26 f_{samp}.

The radius of each locus may be interpreted as a measure of the peak short-term correlation between the desired signal and the jammer. The time window over which the short-term correlation is computed is governed by the parameter μ: large values of μ lead to rapid adaptation and, consequently, narrow time windows. Peak correlation between the desired signal and the jamming signal can be quite high if only a narrow time window is considered. The peak short-term correlation for $\mu = 1.0$, for example, is almost unity. The weight dynamics serve to create a modified jamming signal in which this short-term correlation is maintained near its peak value. Appendix A considers the dynamic solution from

the viewpoint of short-term correlations and develops a closed-form description of weight behavior when both signal and jammer are sinusoidal.

Another way to view the loci of Figure 12 is to treat them as traces of the minima of dynamic error surfaces. It is well known that, in the stationary case, the Wiener solution defines the minimum of a quadratic error surface. In the case at hand, the error surface may be treated as static only at small values of μ. The minimum of the surface in the stationary case is not at zero error, but is elevated above zero by the power level of the desired signal. At low values of μ the Wiener solution is closely approximated, and the desired signal is delivered essentially without loss at the beamformer output. As μ is increased, the error surface must be treated as dynamic. The minimum of the error surface no longer coincides with the Wiener solution. Instead, for the simple case under consideration, the minimum lies on a circle centered on the Wiener solution. Furthermore, the dynamic minimum does not lie at the same error level as the Wiener solution. The elevation of the minimum is decreased by the amount of signal cancellation attainable at a given value of μ. The decrease, expressed as a fraction of the desired signal power, is related to the quantity termed *misadjustment* [3]

$$\text{misadjustment} = M(\mu) \triangleq \frac{E[y^2(t)] - E[(y^*(t))^2]}{E[(y^*(t))^2]} , \qquad (2\text{-}35)$$

where $y^*(t)$ is the output with the optimal weight vector W^*. Because $E[y^2(t)]$ is less than $E[(y^*(t))^2]$, misadjustment is a negative quantity in the region of

interest. It is, however, the magnitude of misadjustment that is important, not the sign. The contours of Figure 12 have been labelled to show $|M(\mu)|$ levels as well as μ values.

The discussion of the error surface that has just been given differs somewhat from earlier treatments. For a given ABF structure, the error surface has previously been considered simply as a function of the input signals; changes in the error surface were attributable to changes in the input signal description. Here the error surface has been described as a function of the adaptation parameter. In other words, the error surface must be described in terms of the signal environment *perceived by the beamformer,* not simply in terms of some detached statistical characterization of the incident signals.

The view of the solution set that has just been given indicates the nature of the problem at hand. There is a direct coupling between the adaptation parameter that is chosen and the solution that is delivered by the ABF. Low values of the adaptation parameter μ yield a solution that conforms closely to the Wiener solution and satisfies the requirement for signal preservation. These values of μ fail, however, to meet the requirements of responding rapidly and tracking a dynamic signal environment. Higher values of μ provide better tracking of changes in the environment, but the non-Wiener solutions involve sacrifices in the quality of the recovered signal. Given the beamformer under consideration, nothing can be done beyond striking the best compromise between signal quality and tracking capability. A change in the nature of the beamformer

is needed to break away from the limitations imposed by the coupling between the adaptation parameter and the solution generated by the ABF.

III. A COMPOSITE BEAMFORMER THAT ELIMINATES SIGNAL CANCELLATION

Chapter 2 has illustrated the signal cancellation effects that can arise in relatively simple signal/jammer scenarios and has demonstrated that even the most rigid constraints can fail to preserve the desired signal. This chapter turns from a discussion of the problem to the description of a solution and shows how signal cancellation can be avoided at the price of some increase in beamformer complexity.

Chapter 3 consists of three sections. The first section builds upon the background provided by Chapter 2 and reformulates the adaptive beamformer problem in such a way that jammer nulling can be accomplished at high adaptation rates without signal cancellation. The beamformer structure that arises out of the reformulation is termed a *composite beamformer* or CBF. The next section discusses the key issue of signal relationships within the new beamformer. A demonstration of the performance improvement afforded by the new beamformer is given in the third section by revisiting the wideband problem from Chapter 2.

A. Problem Reformulation

Chapter 2 and Appendix A described the differing solutions derived by a hard-constrained beamformer at various adaptation rates. The solutions differ

because, from the beamformer viewpoint, the problem changes. Unfortunately, the viewpoints of the beamformer and the system designer begin to clash as signal cancellation becomes significant. The designer is not interested in the minimization of output power at all costs, and will typically invoke constraints in an attempt to restrict the minimization process. The beamformer, however, is designed to relentlessly pursue minimization. At high adaptation rates the beamformer weights possess the mobility to exploit short-term correlations between signal and jammers and thereby circumvent the constraints. Design objectives are simultaneously bypassed, and system performance is unsatisfactory. A problem reformulation is needed that harmonizes design objectives with the realities of beamformer behavior at high adaptation rates; this section pursues that reformulation.

Two observations can be made at this point that are useful in developing a problem reformulation. One observation is that interaction between the desired signal and the jammer is the root of the cancellation phenomenon. The nature of this interaction was demonstrated in some detail in Chapter 2 for the case involving a signal and a jammer that are narrowband. It was shown experimentally and analytically that the presence of both signal and jammer energy is a prerequisite for signal cancellation. In particular, it was shown that the output signal is the "target" of the cancellation process and that short-term correlation between signal and jammer waveforms is the phenomenon that makes cancellation possible.

A second observation that can be made is that the signal plays no role in the Wiener-solution calculation in a perfectly steered Frost ABF. In other words, it is completely equivalent to write

$$W^* = R_{\bar{N}\bar{N}}^{-1} C [C^T R_{\bar{N}\bar{N}}^{-1} C]\, \mathcal{L} \tag{3-1}$$

rather than the earlier statement

$$W^* = R_{\bar{X}\bar{X}}^{-1} C [C^T R_{\bar{X}\bar{X}}^{-1} C]\, \mathcal{L} \quad , \tag{2-13}$$

where $R_{XX} = R_{SS} + R_{NN}$ as originally assumed. This point can be appreciated intuitively from the fact that the look-direction response is determined exclusively by the hard constraints, not by the desired signal. The equivalence of (3-1) and (2-13) may be rigorously demonstrated by substituting for R_{XX} in (2-13) and simplifying. An appropriate substitution is

$$R_{XX} = R_{SS} + R_{NN} = C^T R_{RR} C + R_{NN} \tag{3-2}$$

where R_{RR} is the autocorrelation matrix for the vector of signal voltages appearing at the taps of any one of the beamformer filters. Appendix B traces the somewhat lengthy proof of the equivalence for both a narrowband processor using a single complex weight per beamformer channel and a wideband processor using tapped-delay-line filters for each beamformer channel. Yet another way to explore the role of the signal is to consider the problem in the context of an equivalent generalized sidelobe canceller; Appendix C discusses this approach to the problem.

Reconsideration of the adaptive beamformer problem has thus far indicated 1) that the signal drives the process of signal cancellation that results in its own demise and 2) that the signal has no role in the determination of a set of weights that optimizes array performance. These two points argue for exclusion of the desired signal from the beamformer. The overlooked consideration is, of course, that the original objective was to recover the signal. The remaining step is to harmonize the objectives of cancellation-free adaptation and successful signal reception by devising a structure that excludes the signal from the adaptive process but allows the signal to pass through to the system output. The problem reformulation thus amounts to more precisely defining the role of the desired signal in an adaptive array.

Figure 13 illustrates a beamformer based upon the problem reformulation. The array has been augmented so that subarrays consisting of multiple elements appear in place of the individual elements of the original array. A preprocessor operates upon the received signals from the augmented array to generate an environment that is free of desired-signal content. A Frost ABF operates in this synthetic environment and derives weights that are copied to a slaved beamformer. The slaved beamformer has the same signal-path structure as the adaptive beamformer, but is connected directly to selected antenna elements.* Desired-signal components are present in the slaved beamformer, and a useful

*It is also possible to connect the slaved beamformer to the subarrays through a preprocessor that makes use of multiple elements of each subarray. The pattern response of the element combination generated by this second preprocessor must have nonzero response in the look direction.

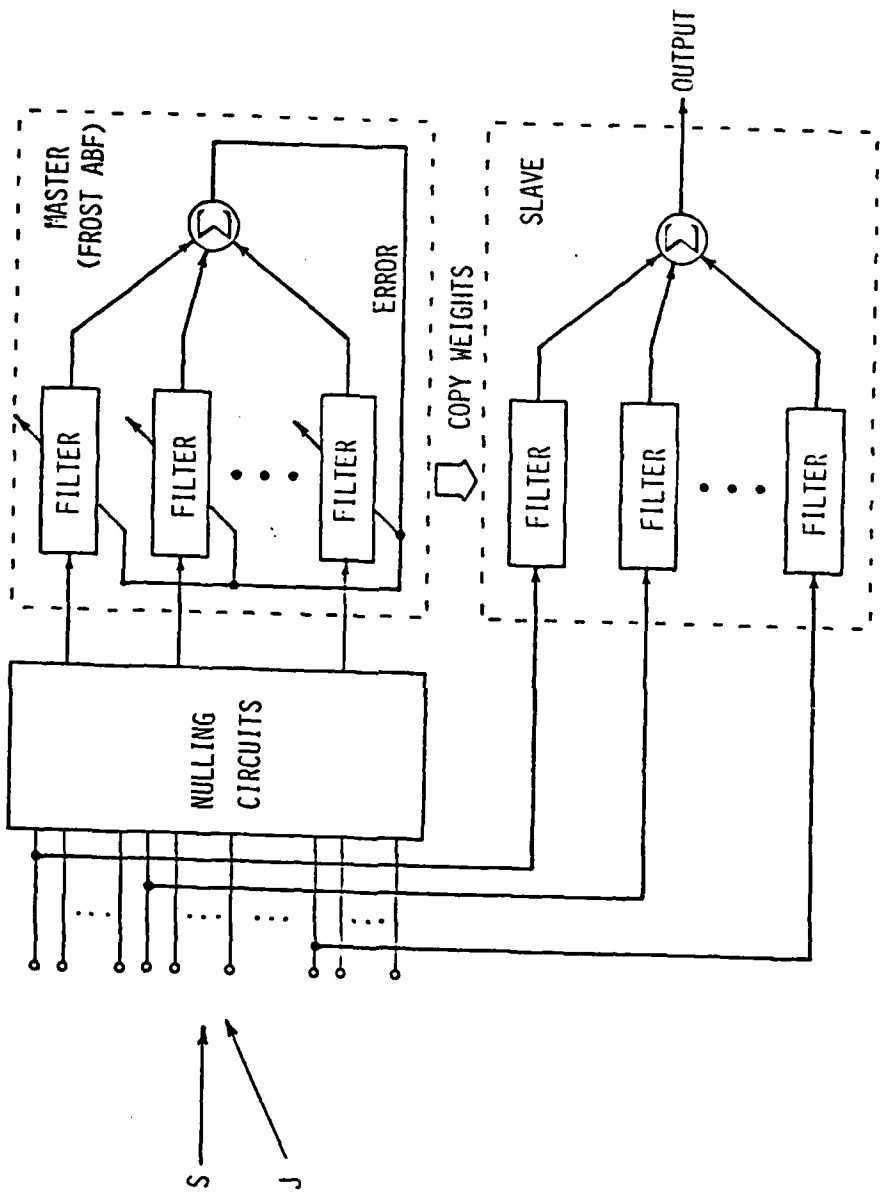

Figure 13. A Frost-based Composite Beamformer

output may be drawn from it.

Taken as a whole, the structure shown in Figure 13 is termed a *composite beamformer* (CBF). The key elements are 1) an augmented array, 2) a preprocessor that excludes the desired signal from the adaptive process, 3) an adaptive beamformer that can be constrained to control look-direction response while nulling jamming signals, and 4) a slaved beamformer that is used to implement the computed solution and recover the desired signal. Three of these elements, the array, the preprocessor and the adaptive beamformer, afford considerable flexibility in that a variety of specific realizations are possible; the slaved beamformer design is inflexible in the sense that it mirrors the adaptive beamformer design. Appendix D describes an alternative CBF realization based upon Widrow's pilot-signal algorithm; other realizations may also be derived.

B. Signal Relationships in the CBF Master and Slave

Because CBF operation involves the derivation of weights in the master beamformer for application in the slave, it is essential that the signal sets in the two beamformers be closely related. Ideally, the two signal sets would be identical, save for the absence of look-direction components in the master. This would assure that weights derived in the master were equally appropriate for and effective in the slave. Unfortunately, it is not possible, in general, to attain the ideal signal relationships between the two beamformers, and compromises must be allowed. This section begins a discussion of the nature of the compromises

that are necessary and of the consequences of those compromises.

The basic difficulty in attaining the ideal signal sets lies in removing the look-direction signal from the master beamformer without perturbing the various noise signals. If an omnidirectional element is used for the slaved beamformer, then the perfect subarray/preprocessor combination serving the master must have the pattern response shown in Figure 14(a). The omnidirectional pattern is perfectly replicated, except for an infinitely deep, vanishingly narrow notch in precisely the look direction. Obviously, a pattern of this nature can neither be realized nor successfully applied; some modification of interference signals arriving near the look direction must be accepted if the desired signal is to be excluded based upon directional information.

A simple means of realizing a look-direction null is to use a two-element subarray, apply any necessary steering delays to cophase the desired signal, and difference the element signals. Figure 14(b) gives the response of such a subarray at the frequency for which the elements are separated by one-half wavelength. The null is steered to broadside in this instance.

The response of the two-element subarray departs significantly from the ideal response. At $\pm$ 90°, the two-element subarray exhibits 6 dB of gain over isotropic; 0 dB is at about $\pm$ 20°; gains within $\pm$ 10° of the look direction fall seriously below 0 dB. The two-element pattern does, however, exhibit the key features of a deep, wideband null in the look direction and reasonable gains at angles removed from the look direction. These features plus the great simplicity

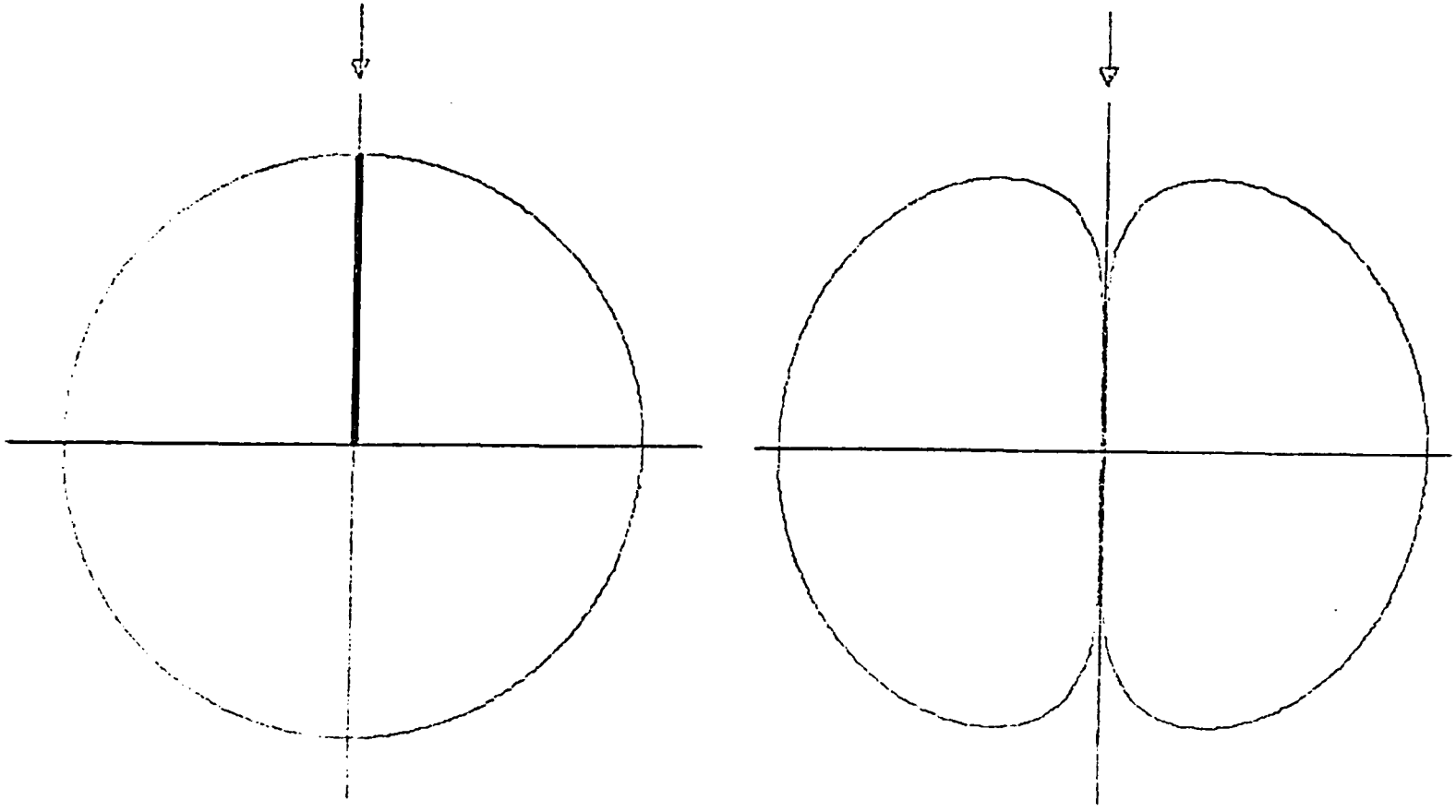

a) Ideal Subarray

b) Two-element Subarray

Figure 14. Nulling - circuit Beampattern Characteristics

of the subarray/preprocessor make the two-element subarray worthy of more detailed consideration.

The general CBF structure of Figure 13 may be specialized to yield the CBF shown in Figure 15. Here the desired signal is assumed to be incident from broadside so beam steering may be neglected. The preprocessor is realized by using two-element subarrays in a simple element-differencing scheme. The sharing of elements between subarrays provides very efficient use of elements; only a single element is needed beyond those ordinarily required for a comparable array.*

A Frost ABF operates upon the preprocessor output to derive a set of weights that minimizes error power subject to a set of look-direct constraints. It should be noted that, in contrast to conventional adaptive beamformers, the error power is distinct from the CBF output signal power. Error power can be driven to zero without endangering the desired signal component in the output. This is, in fact, the ideal state of affairs.

Because weights derived in the Frost ABF will be applied in the slaved beamformer, it is vital that relative signal phases match in the two beamformers. The uniform structure that exists in the preprocessor assures that this phase matching will be obtained. The set of two-element subarrays feeding the Frost ABF echoes the structure of the array of omnidirectional elements serving the

*Element sharing among subarrays does introduce thermal-noise correlations in the master beamformer that are not present in the slave. Generally, however, thermal noise powers will be relatively low, and these spurious correlations will not seriously affect performance.

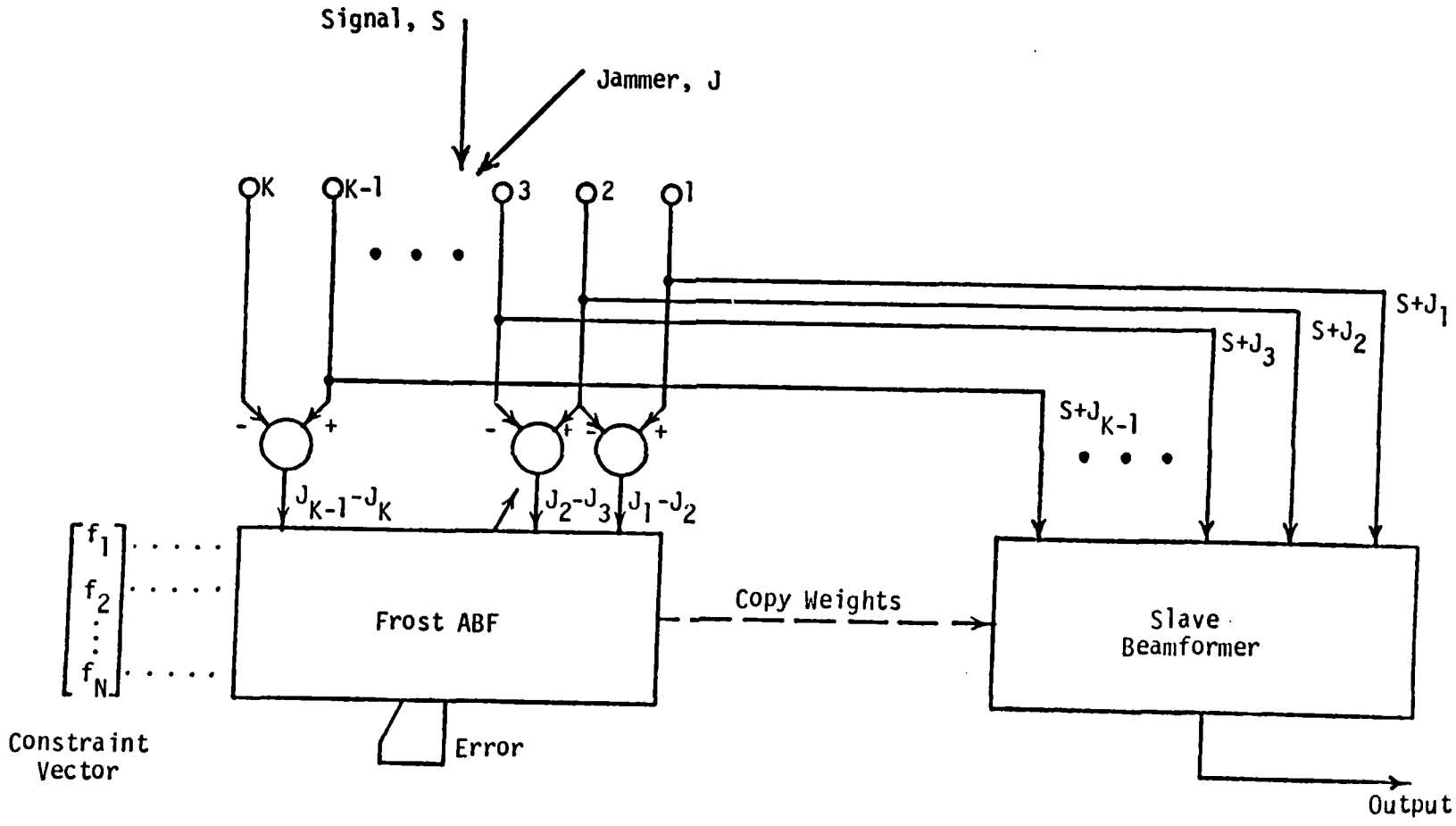

Figure 15. Frost-based CBF with a Subtractive Preprocessor for Signal Nulling

slaved beamformer.

Phase relationships between signals in the ABF and the slaved beamformers are made clearer in Figure 16. The jammer components received by the omnidirectional elements are indicated by a set of equal-amplitude, uniformly spaced phasors J_1, J_2, J_3, ..., J_{K-1}, J_K. The preprocessor operates upon these inputs to produce the phasor outputs J_1–J_2, J_2–J_3, ..., and J_{K-1}–J_K. These phasors are also equal in amplitude and have the same phase-angle separations as the received jammer components. The preservation of relative phase in the preprocessor assures that weights that generate a null in the ABF will also generate a null in the slaved beamformer.

The phasor argument as advanced in Figure 16 applies to a single jammer at a single frequency. Linearity and superposition apply, however, and show that phase relationships are preserved for multiple jammers and for broadband as well as narrowband signals.

The uniform linear array provides an attractive structure for the CBF because there is the option of element sharing between subarrays. A regular array structure is not, however, a prerequisite for the CBF. The fundamental requirement is for phase matching between the master and slave beamformers. Phase matching may be obtained for an arbitrary array geometry by augmenting each original element to form identical subarrays at the element locations. Identical preprocessors may then be used to form subarray responses with nulls in the selected look direction. The preprocessor outputs must be cophased for the

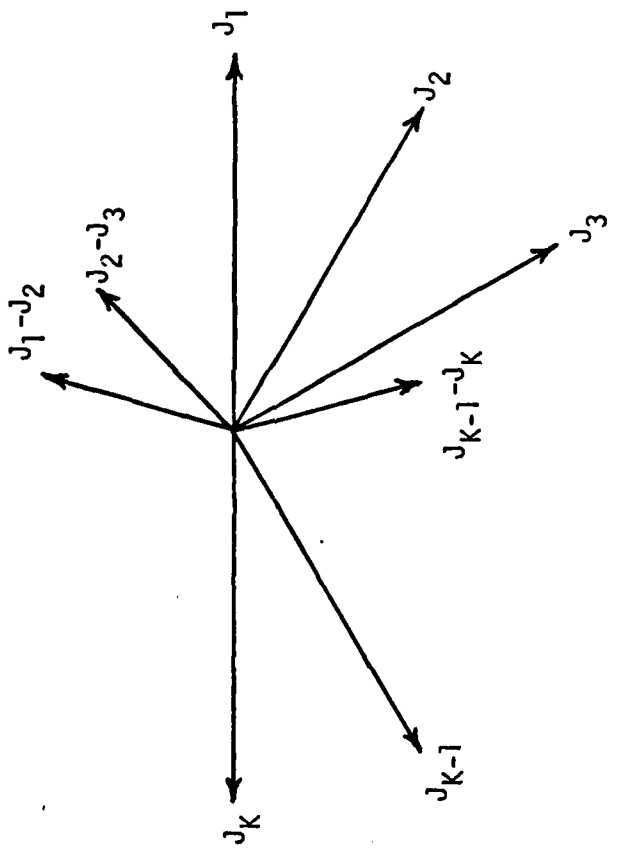

Figure 16. Phasor Diagram for the CBF of Figure 15

look direction and applied to the adaptive beamformer while the original element outputs are cophased and applied to the slave.

C. CBF Performance -- An Example

The CBF described in the previous section is capable of delivering much better performance at high adaptation speeds than, say, a comparable Frost ABF. The performance contrast may be conveniently illustrated by returning to the wideband problem of Chapter 2 for which the Frost ABF performance has already been demonstrated.

Figure 17 diagrams the wideband problem with a Frost-based CBF replacing the original Frost ABF. The signal and jammer descriptions are identical, as are the look-direction constraints. A third antenna element has been added in order to provide appropriate inputs for the subtractive preprocessor. Two of the elements also serve the slaved beamformer, which makes use of weights from and functions in parallel with the adaptive beamformer.

The antenna pattern at the jammer frequency of 0.25 f_{samp} is shown in Part a) of Figure 18. This plot was generated after initial transients had died away and jammer nulling was essentially complete. A deep notch exists at the jammer arrival angle of 30°.

Parts b) and c) of Figure 18 show the frequency response in the jammer direction and look direction. The jammer-direction plot reveals a deep notch at the jammer frequency. The look-direction plot confirms that the unit-gain, all-

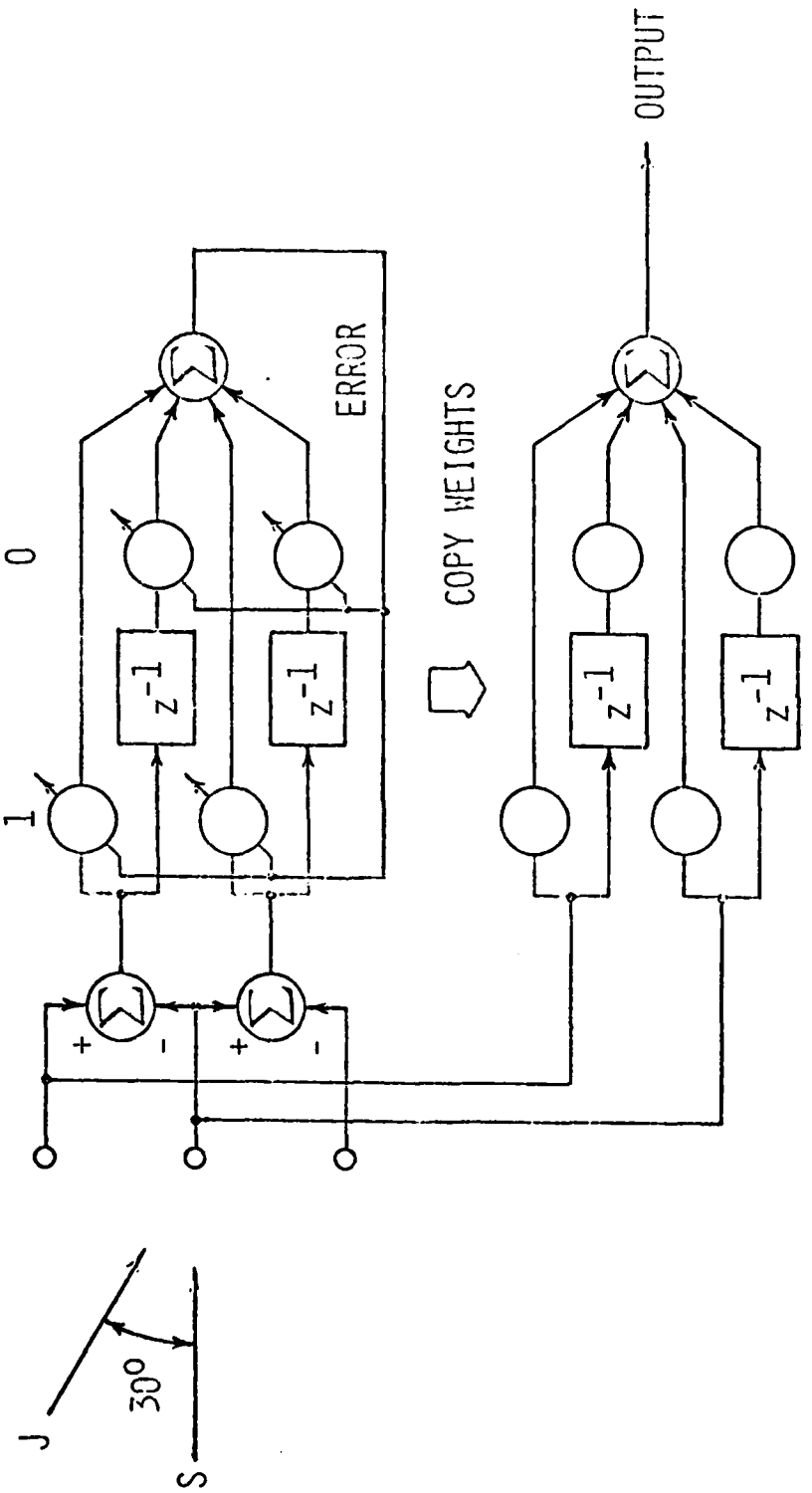

Figure 17. Four-weight CBF in the Single-jammer Case

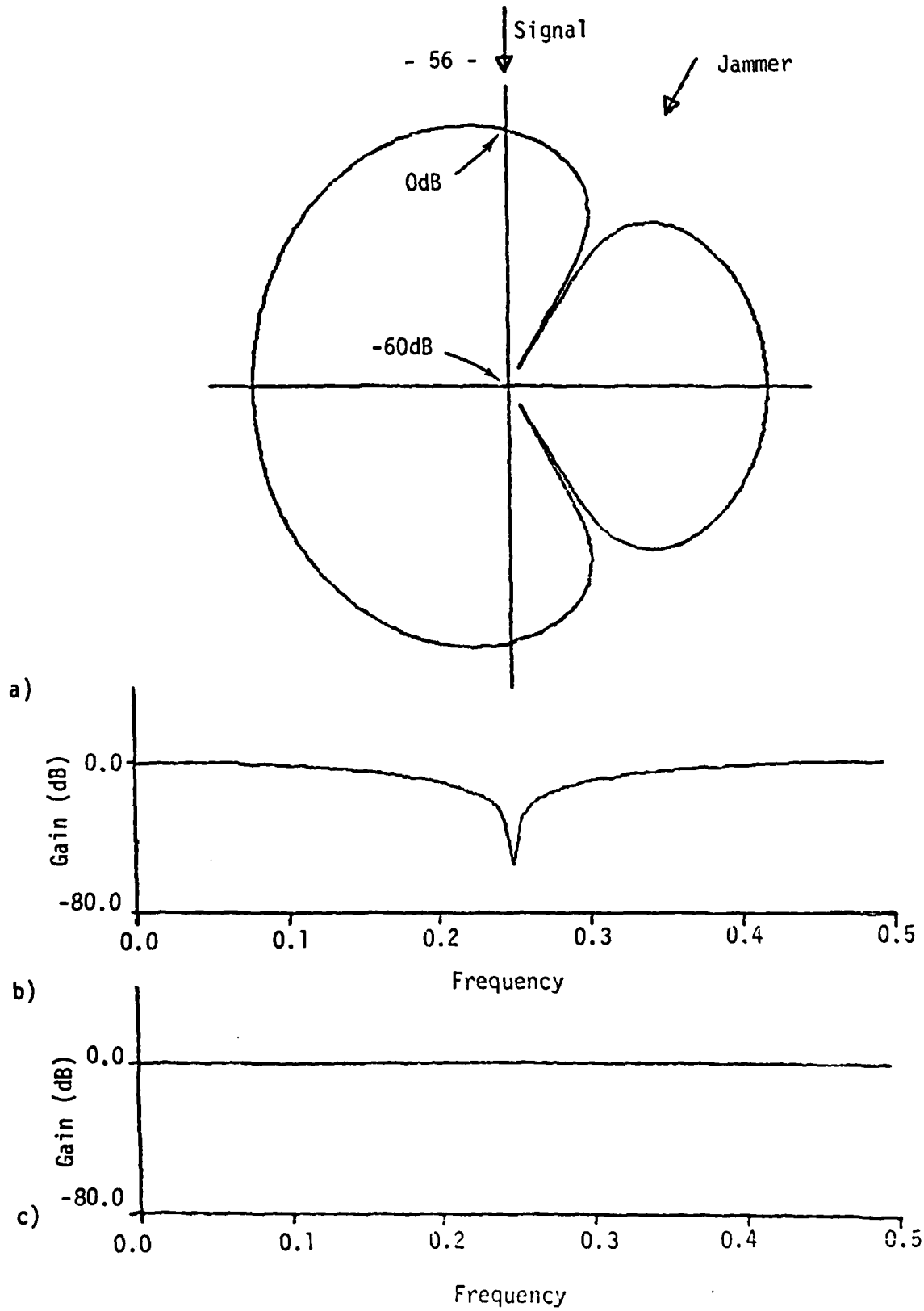

Figure 18. Postconvergence Plots for the Four-element Frost ABF
a) Beampattern
b) Jammer-direction Frequency Response
c) Signal-direction Frequency Response

pass response specified by the constraints has been attained.

Some of the contrasts between Frost ABF and CBF performances may be seen by comparing Figure 3 and Figure 18. The notch depths in both Part a) and Part b) of the figures are greater for the CBF than for the Frost ABF, thus indicating improved jammer rejection.

A more dramatic view of the performance contrasts is provided by the spectral plots of Figure 19. Parts a) and b) of the figure show ensemble averages of the desired signal spectrum and the jammer spectrum. Part c) repeats the ensemble-averaged Frost output spectrum that was shown in Figure 4. Part d) provides the ensemble-averaged CBF output spectrum. The signal-cancellation effects seen in Part c) are not present in the CBF spectrum, and extremely close matching with the desired-signal spectrum is evident.

The differences between Frost ABF and CBF performance may also be clearly seen in the time domain. Figure 20 contains 256-sample segments of time domain data taken from the beginning of the simulation. Part a) illustrates the desired-signal waveform; Part b) the Frost-ABF output; and Part c) the CBF output. Both output waveforms show the transient associated with jammer nulling. Nulling should be complete within 50 samples, and good tracking of the desired signal should be seen. The Frost-ABF output, however, shows considerable distortion due to signal cancellation. CBF tracking, on the other hand, is essentially perfect after jammer nulling.

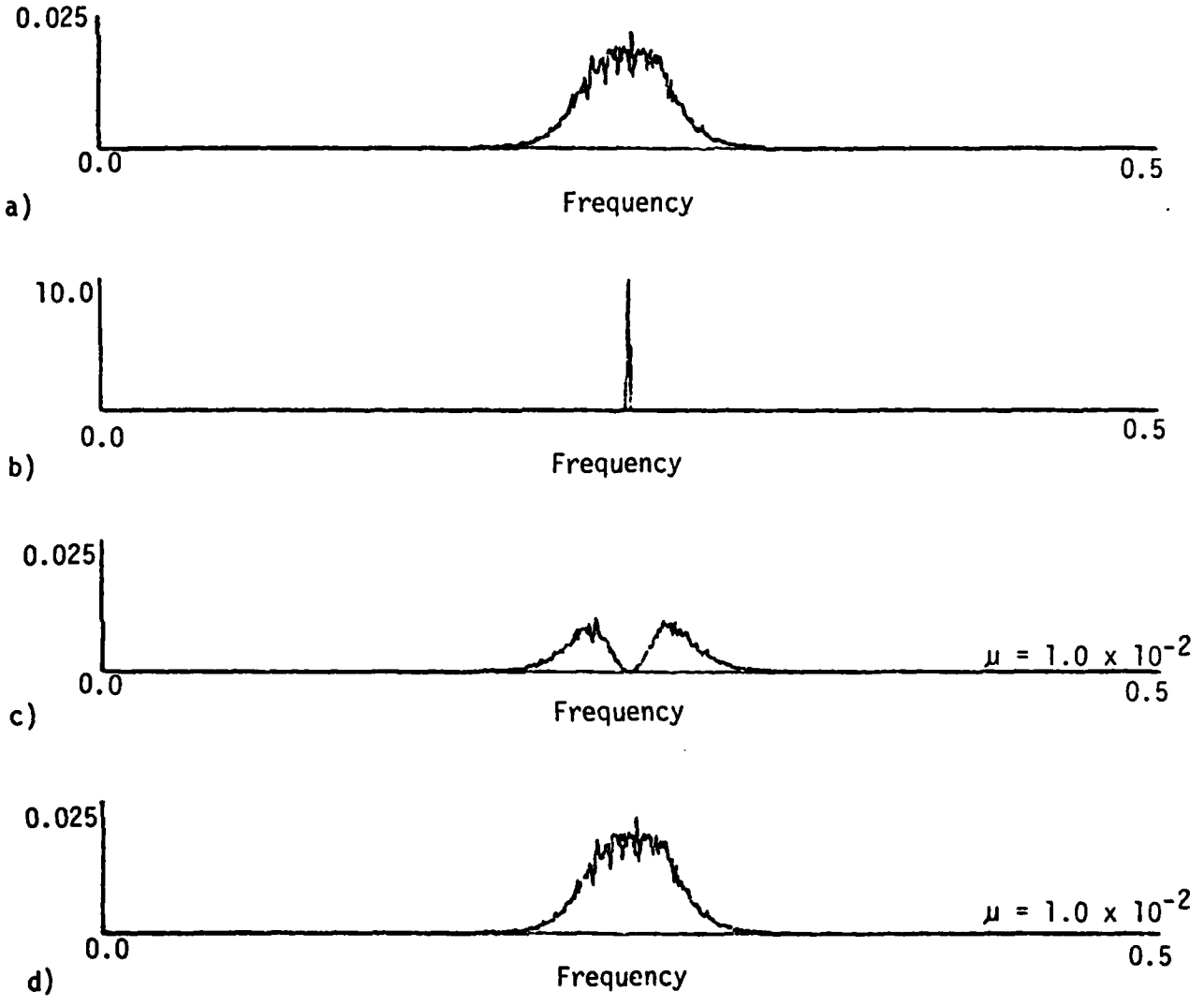

Figure 19. Input and Output Spectra for the Frost ABF and the Frost-based CBF

a) Signal
b) Jammer
c) ABF Output
d) CBF Output

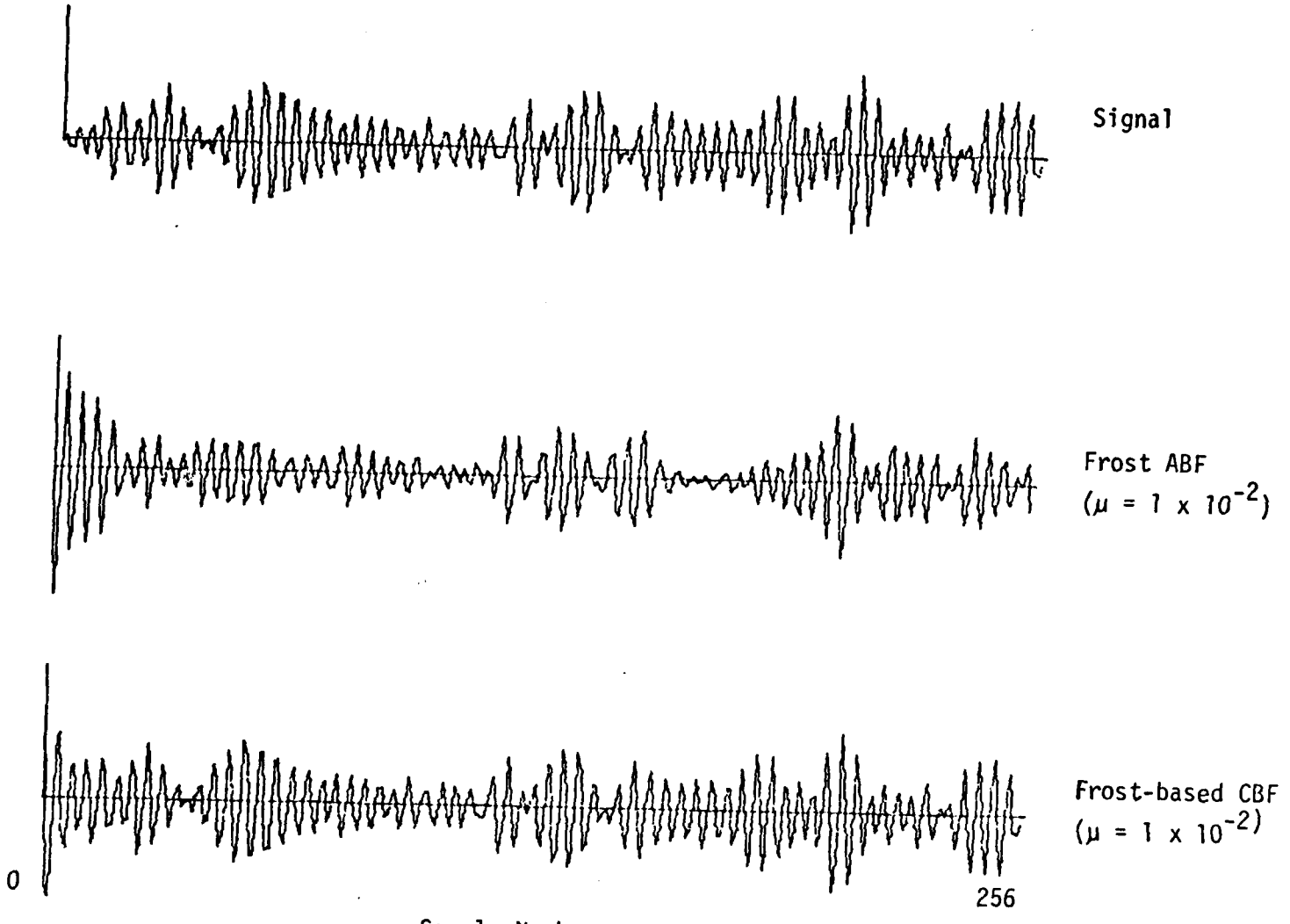

Figure 20. Comparison of ABF and CBF Output Signals

IV. PERFORMANCE OF THE COMPOSITE BEAMFORMER

The preceding chapter introduced the composite beamformer (CBF) and illustrated the performance of a particular CBF realization based upon a simple subtractive preprocessor and Frost's constrained LMS algorithm. An argument was advanced that, due to the deliberate phase matching between the master and slave beamformers, jammer nulling is quite good in the CBF. Additionally, signal cancellation of the type that can be so destructive in a hard-constrained ABF is effectively suppressed. A sample case was shown in which the expected improvements over a Frost ABF were, in fact, realized by a CBF using a simple signal-nulling scheme.

This chapter continues the exploration of CBF performance. The first section examines the issue of CBF optimality in greater depth. The second section then describes further simulation experiments designed explicitly to probe CBF behavior with regard to optimality. A third section considers convergence time constants in the CBF and draws comparisons with the Frost ABF. The fourth section describes CBF weight behavior near convergence and shows contrasts between CBF and ABF behavior in that important region.

A. CBF Optimality in the Narrowband Case

The experiment of the previous chapter has indicated that, at least in a selected case, the performance of the CBF at high adaptation speeds is greatly superior to that of a comparable ABF. Questions remain, however, about the

range of conditions for which optimal performance is approached. In this section the issue of optimality will be investigated in greater depth for the important case in which jammer signals are narrowband.

The discussion in this section will center upon the noise autocorrelation matrix R_{NN}. As was shown in Chapter III, R_{NN}^{-1} governs the optimal solution for the Frost ABF. Ideally, the adaptive (master) processor in the CBF would receive unperturbed noise voltages and would thus tend toward the optimal solution as indicated by R_{NN}^{-1}. In practice, the phases of interference signals are preserved through appropriate preprocessor design, but the interference amplitudes (or, equivalently, the interference-to-thermal-noise ratios) are altered. It is of interest to consider the influence of perturbations in interference-to-thermal-noise ratio upon R_{NN}^{-1}.

The signal vector $\underline{u}_i$ associated with the i^{th} narrowband interference source may be written as

$$\underline{u}_i = f(\theta_i, P_i)\,\underline{v}_i = f(\theta_i, P_i) \begin{bmatrix} e^{j\phi_{1i}} \\ e^{j\phi_{2i}} \\ \vdots \\ e^{j\phi_{Ki}} \end{bmatrix} \tag{4-1}$$

where $f(\theta_i, P_i)$ is the pattern response of the K identical elements (or subarrays) constituting the array, θ_i is the arrival angle of the signal with respect to a reference direction, P_i is the signal power, $\underline{v}_i$ is a propagation vector, and ϕ_{li} is the signal phase at the l^{th} element with respect to a coordinate origin. For the

important case of a uniform linear array with element spacing d, (4-1) may be specialized to

$$\underline{u}_i = f(\theta_i, P_i) \begin{bmatrix} 1 \\ e^{j\phi_i} \\ \vdots \\ e^{j(k-1)\phi_i} \end{bmatrix} , \tag{4-2}$$

where the first element is taken as the phase reference and

$$\phi_i = 2\pi(\frac{d}{\lambda_i}) \sin \theta_i \tag{4-3}$$

is the element-to-element phase shift for an arrival angle θ_i (measured clockwise from array broadside) and an interference wavelength of λ_i.

Pattern responses of two types will be of interest. For an ideal omnidirectional element,

$$f_1(\theta, P_i) = P_i \quad . \tag{4-4}$$

If two such elements are placed a half wavelength apart and their outputs are differenced to form the simple nullformer discussed previously, then

$$f_2(\theta, P_i) = P_i[2 - 2\cos(\pi \sin \theta)] \quad . \tag{4-5}$$

The noise autocorrelation matrix R_{NN} for a K-element narrowband array takes a simple form under the assumptions that the thermal noise voltages from the elements are zero-mean Gaussian and mutually uncorrelated and that the M incident narrowband signals have carrier phases that are uniformly distributed on

$(0,2\pi)$ and statistically independent both of one another and of the thermal noises of the elements. Specifically,

$$R_{NN} = [I + \sum_{i=1}^{M} \rho_i \, \underline{v}_i^* \, \underline{v}_i^T]\sigma^2 \quad , \tag{4-6}$$

where I is the $K \times K$ identity matrix, ρ_i is the power ratio between the i^{th} interference signal and the thermal noise voltage, and σ^2 is the thermal noise variance. The power ratio ρ_i incorporates the pattern response $f(\theta_i,P_i)$ and σ^2:

$$\rho_i = \frac{f(\theta_i,p_i)}{\sigma^2} \quad . \tag{4-7}$$

Gupta and Ksienski [20] have observed that correlation matrices having the structure of (4-6) may be inverted into a convenient form when the matrices are reexpressed in terms of an orthonormal basis for $\{\underline{v}_i\}$. Their method will be used to derive an expression for R_{NN}^{-1}. This expression will then be used to determine conditions under which the CBF solution approaches that of the Frost ABF.

The Gram-Schmidt process may be applied to construct an orthonormal basis $\{\underline{q}_i\}$, $i=1, 2, ..., M$, for the $\{\underline{v}_i\}$, $i=1, 2, ..., M$. As a preliminary step the first basis vector is computed:

$$\underline{q}_1 = \frac{\underline{v}_1}{\underline{v}_1^T \underline{v}_1^*} \quad . \tag{4-8}$$

Then a set of orthogonal vectors $\{\underline{p}_i\}$, $i=1, 2, ..., M$, is determined from

$$\underline{p}_i = \underline{v}_i - \sum_{j=1}^{i-1} (\underline{v}_i^T \underline{q}_j^*)\, \underline{q}_j \tag{4-9}$$

and normalized according to

$$\underline{q}_i = \begin{cases} 0 & \text{if } \underline{p}_i^T \underline{p}_i^* = 0 \\ \dfrac{\underline{p}_i}{\underline{p}_i^T \underline{p}_i^*} & \text{otherwise} \end{cases} . \tag{4-10}$$

The vectors $\{\underline{v}_i\}$ may now be written in terms of the basis vectors. The expression given in (4-9) may be rearranged to yield

$$\underline{v}_i = \sum_{j=1}^{i-1} (\underline{v}_i^T \underline{q}_j^*)\, \underline{q}_j + \underline{p}_i \quad . \tag{4-11}$$

Forming the transpose in (4-11) and postmultiplying by $\underline{q}_i^*$ then gives

$$\underline{v}_i^T \underline{q}_i^* = \underline{p}_i^T \underline{q}_i^* = (\underline{p}_i^T \underline{p}_i^*)\, \underline{q}_i^T \underline{q}_i^* = \underline{p}_i^T \underline{p}_i^* \quad , \tag{4-12}$$

where the orthonormality of $\{\underline{q}_i\}$ has been used to simplify the expressions. By using (4-11) and (4-12) together with the definition

$$\alpha_{ij} \triangleq \underline{v}_i^T \underline{q}_j^* \quad , \tag{4-13}$$

$\underline{v}_i$ may be written as

$$\underline{v}_i = \sum_{j=1}^{i} \alpha_{ij}\, \underline{q}_j \quad . \tag{4-14}$$

The expression (4-6) for R_{NN} now becomes

$$R_{NN} = \left\{ I + \sum_{i=1}^{M} \rho_i \left[\sum_{j=1}^{i} \alpha_{ij} \, g_j \right]^* \left[\sum_{k=1}^{i} \alpha_{ik} \, g_k \right]^T \right\} \sigma^2 \quad . \tag{4-15}$$

Because the optimal weights for both the Frost ABF and the Frost-based CBF depend upon R_{NN}^{-1}, it is necessary to invert the expression on the right-hand side of (4-15). The inversion technique depends upon the matrix inversion lemma* and is most readily applied by first considering the case $M = 1$. In that case (4-15) becomes

$$R_{NN} = \{ I + \rho_1 \, \alpha_{11}^2 \, g_1^* \, 1 \, g_1^T \} \, \sigma^2 \quad . \tag{4-16}$$

Application of the inversion lemma to (4-16) then yields

$$R_{NN}^{-1} = \{ I - \rho_1 \, \alpha_{11}^2 \, g_1^* (1 + g_1^T \, \rho_1 \, \alpha_{11}^2 \, g_1^*)^{-1} \, g_1^T \} \, \frac{1}{\sigma^2} \quad , \tag{4-17}$$

which rearranges to the form

$$R_{NN}^{-1} = \left\{ I - \frac{g_1^* \, g_1^T}{\frac{1}{\rho_1 \alpha_{11}^2} + g_1^T g_1^*} \right\} \frac{1}{\sigma^2} \quad . \tag{4-18}$$

By orthonormality,

$$g_1^T \, g_1^* = 1 \quad . \tag{4-19}$$

Also

---

*The lemma is discussed in Appendix B in another context.

$$\alpha_{11} = \underline{v}_1^T \underline{g}_1^* = \frac{\underline{v}_1^T \underline{v}_1^*}{\underline{v}_1^T \underline{v}_1^*} = 1 \quad . \tag{4-20}$$

The expression for R_{NN}^{-1} in (4-18) therefore becomes simply

$$R_{NN}^{-1} = \left\{ I - \frac{\underline{g}_1^* \underline{g}_1^T}{\frac{1}{\rho_1} + 1} \right\} \frac{1}{\sigma^2} \quad . \tag{4-21}$$

It is now clear that, provided $\rho_1 >> 1$,

$$R_{NN}^{-1} \cong \{ I - \underline{g}_1^* \underline{g}_1^T \} \frac{1}{\sigma^2} \quad . \tag{4-22}$$

That is, if the jammer-to-thermal-noise ratio is large, the inverse of the noise autocorrelation matrix is essentially independent of the precise value of that ratio. Because the optimal solution is governed by R_{NN}^{-1}, the solutions toward which the ABF and CBF tend will be indistinguishable, provided the jammer-to-thermal-noise ratio is large in both adaptive processors.

In the ABF with omnidirectional elements the jammer-to-thermal-noise ratio is independent of jammer angle, and the ratio is thus fixed solely by relative power considerations. In the CBF with element differencing the jammer-to-thermal-noise ratio is dependent upon jammer arrival angle in the manner shown in (4-5). At angles approaching 0° the received jammer power goes toward zero, and the transition from (4-21) to (4-22) becomes questionable. It thus becomes clearer that ABF and CBF equivalence is not universal and that the nullformer becomes the crucial factor in CBF convergence toward the optimal weights.

If consideration is now given to the two-jammer case (4-15) becomes

$$R_{NN} = \{I + \rho_1\alpha_{11}^2 g_1^* g_1^T + \rho_2\alpha_{21}^2 g_1^* g_1^T + \rho_2\alpha_{21}\alpha_{22} g_1^* g_2^T + \rho_2\alpha_{22}\alpha_{21} g_2^* g_2^T + \rho_2\alpha_{22}^2 g_2^* g_2^T \}\sigma^2 \quad . \tag{4-23}$$

Repeated application of the matrix inversion lemma shows that

$$R_{NN}^{-1} \cong \left\{ I - g_1^* g_1^T - \frac{g_2^* g_2^T}{1 + \frac{1}{\rho_2\alpha_{22}^2}} \right\} \frac{1}{\sigma^2} \quad . \tag{4-24}$$

Again, under the assumption that $\rho_2\alpha_{22}^2 >> 1$, i.e., that the power of the second jammer is well above the noise and that the projection of the second jammer's propagation vector onto the second basis vector is nonzero

$$R_{NN}^{-1} \cong \{I - g_1^* g_1^T - g_2^* g_2^T \} \frac{1}{\sigma^2} \quad . \tag{4-25}$$

This expression is, like (4-22), independent of the jammer-to-thermal-noise ratios under the assumptions stated; it follows that the ABF and CBF solutions are again equivalent.

If the methods and assumptions just described for the single-jammer and dual-jammer cases are extended to the case of M jammers, then

$$R_{NN}^{-1} \cong \{I + \sum_{i=1}^{M} g_i^* g_i^T \} \frac{1}{\sigma^2} \quad . \tag{4-26}$$

That is, the ABF and CBF solutions become indistinguishable for the cases where jammer-to-thermal-noise ratios in the adaptive processors remain large.

Two conditions must be satisfied for the jammer-to-thermal-noise ratio in the CBF to be large. In the first place, of course, the jammer signal must arrive at the array elements with appreciable power. This will usually be the case if the jammer constitutes a threat. A second condition is that the nullformer not discard so much jammer energy that the jammer contribution is driven into the thermal noise. In the case of the two-element subarray, this difficulty may arise at angles near the look direction, i.e., within about 10° of the signal azimuth; with other nullformers the regions that seriously attenuate jammer signals may be different.

A third condition must also be satisfied if the CBF weights are to reliably approach optimality. This last condition relates to the number of degrees of freedom available versus the number of jammers that must be nulled. In the narrowband case one complex weight is adequate to null a jammer. If there are K beamformer channels, then the number of jammers must be less than or equal to $K-1$ since one complex weight is lost to the constraints in a narrowband Frost ABF.

B. Further Simulation Experiments with the CBF

Two additional simulation experiments were devised to assess CBF performance under more difficult conditions than the single-jammer scenario of Chapter 3. Particular attention was given to testing the optimality criteria just discussed.

The signal/jammer scenario for one experiment is shown in Figure 21. The CBF configuration is identical to that used in the experiment of Chapter 3, but the jammer environment has been altered. The jammer J_1 is a signal centered at 0.25 f_{samp} with a bandwidth of 1%. The actual power of J_1 is 2.0, and its arrival angle is -10^o. The jammer J_2 is equal in center frequency and bandwidth to J_1, but it is independent of J_1. The power of J_2 is 1.5, and its arrival angle is 80^o.

With the restricted number of weights in the CBF, there were insufficient degrees of freedom to meet the criteria stated in the previous section. Specifically, there were only enough weights to null one jammer after allowing for the loss of degrees of freedom to the constraints. It was of interest to examine performance under these conditions of CBF saturation.

Figure 22 shows the beampattern plot obtained after initial transients had disappeared. A relatively shallow null was placed on J_2, while there was no visible attenuation of the stronger J_1. This behavior reflected the perception of the jamming environment within the master beamformer where the nulling circuits had attenuated J_1 and boosted J_2. The actual solution reached by the beamformer in this case was a dynamic one in which the power of J_2 was reduced to approximate that of J_1. Additionally, the response to J_2 was adjusted dynamically to approximately cancel the contribution from J_1. Unfortunately, the solution was one which mapped poorly to the slaved beamformer because of the vastly different nullformer influences on the two jammers.

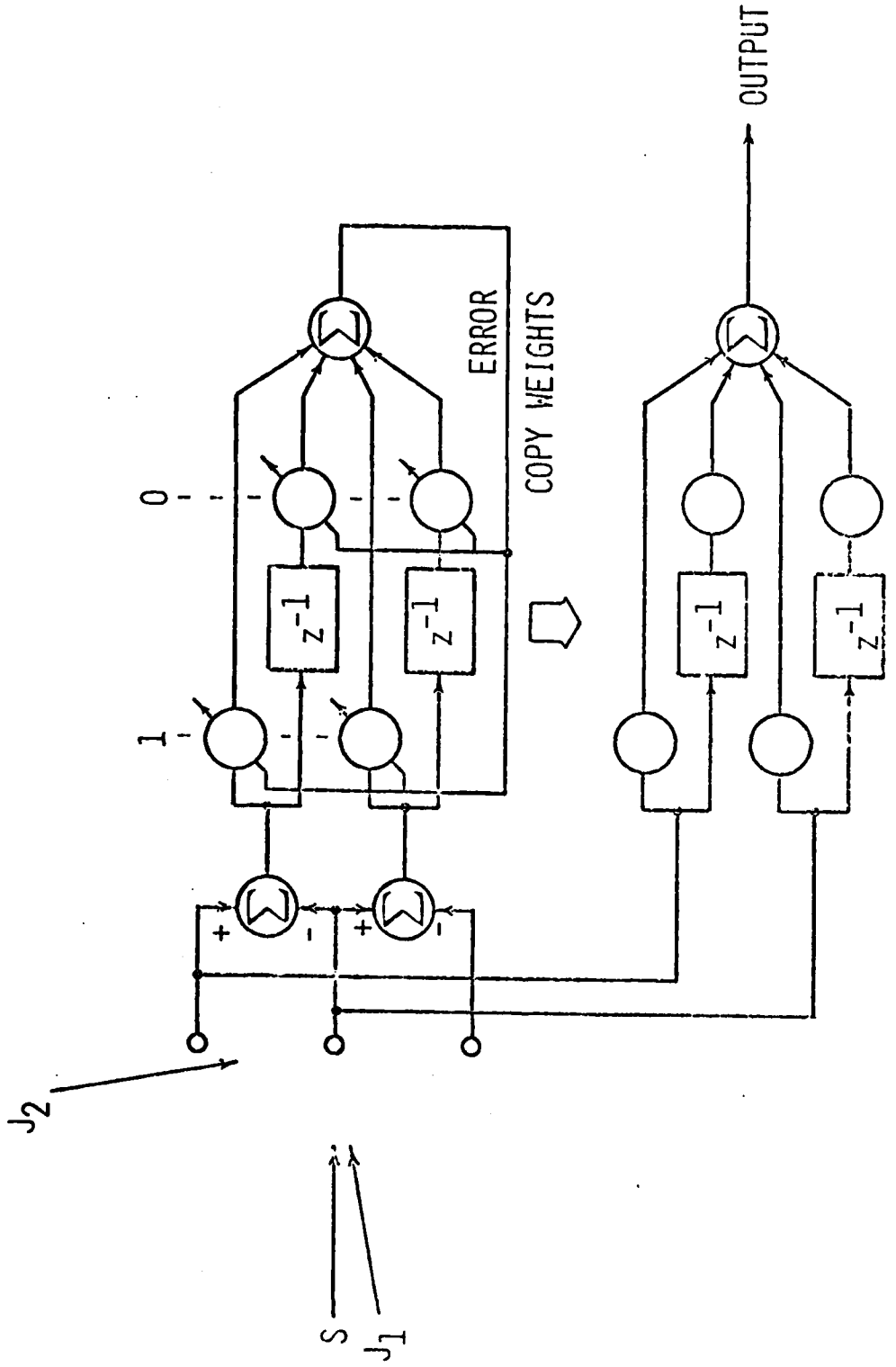

Figure 21. Four-weight CBF in the Two-jammer Case

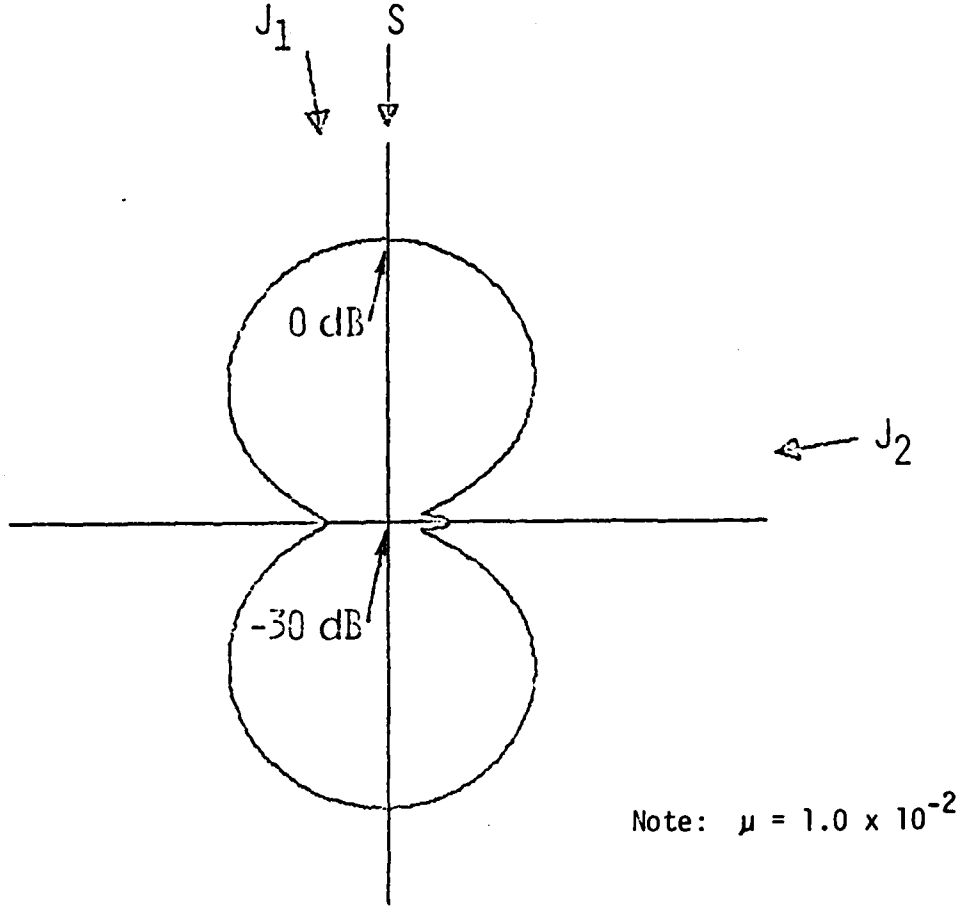

Figure 22. Postconvergence Beampattern for the Four-weight CBF

A second experiment was conducted in which the same signal/jammer scenario was used, but the CBF was extended to provide two additional degrees of freedom in both the master and the slave. Figure 23 shows the configuration of this CBF.

The CBF beampattern after convergence is illustrated in Figure 24. Extremely deep nulls have been placed on both J_1 and J_2, and the beamformer output consists almost exclusively of the desired signal. It is interesting to note that the null depth on J_2 remains somewhat greater than that on J_1. This reflects the relatively greater jammer-to-thermal-noise* ratio of J_2 within the CBF master as a result of nullformer action.

C. Convergence Time Constants

As was stated in Chapter 2, convergence of the constrained LMS algorithm is governed by the eigenvalues of $P\ R_{XX}\ P$. With the aid of

$$P \triangleq I - C(C^T C)^{-1}\ C^T \tag{2-16}$$

and

$$R_{XX} = C\ R_{RR}\ C^T + R_{NN} \quad , \tag{3-2}$$

the matrix $P\ R_{XX}\ P$ may be rewritten as

*Thermal noise per element was set to -40 dB relative to unit power.

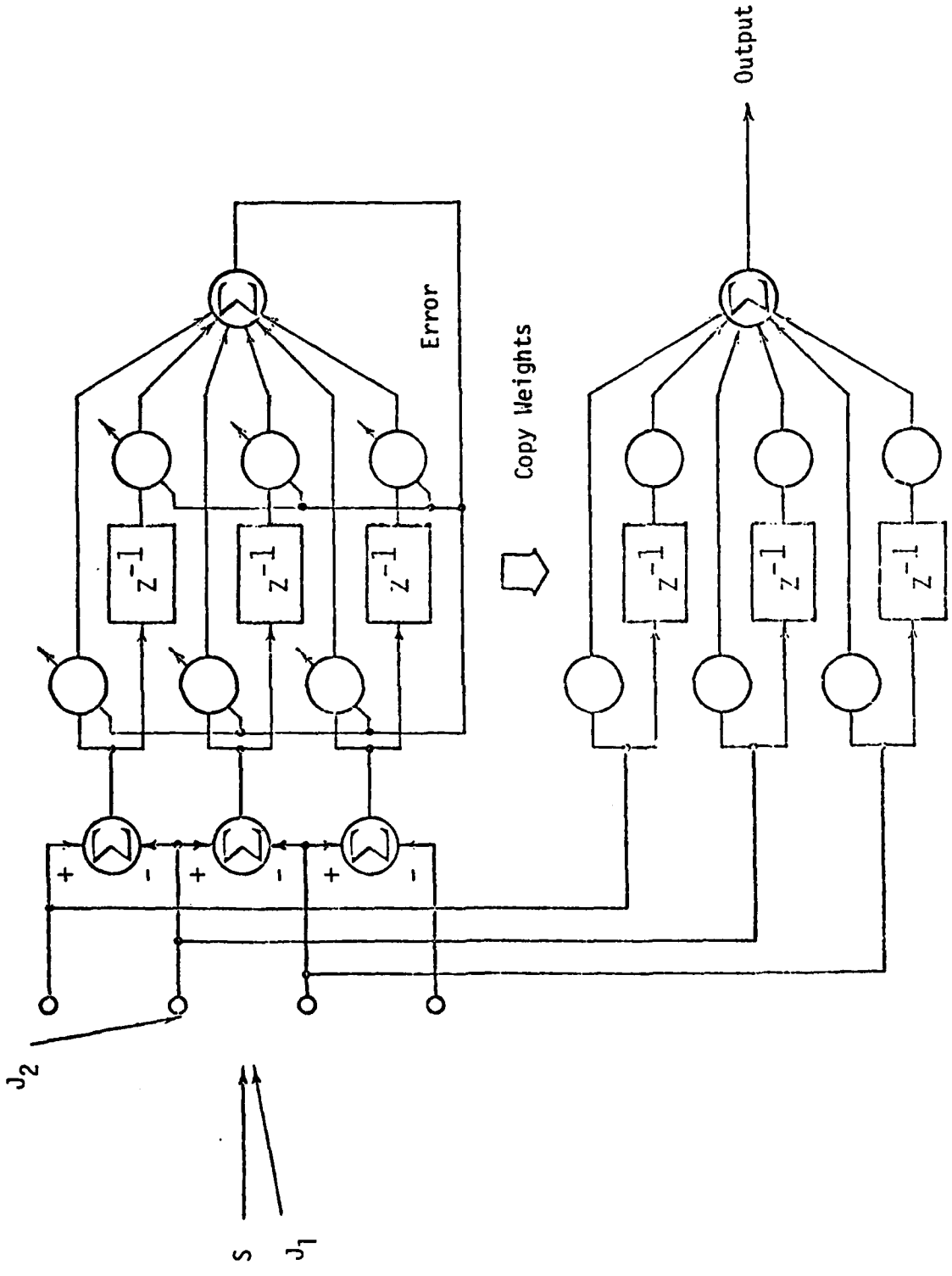

Figure 23. Six-weight CBF in the Two-Jammer Case

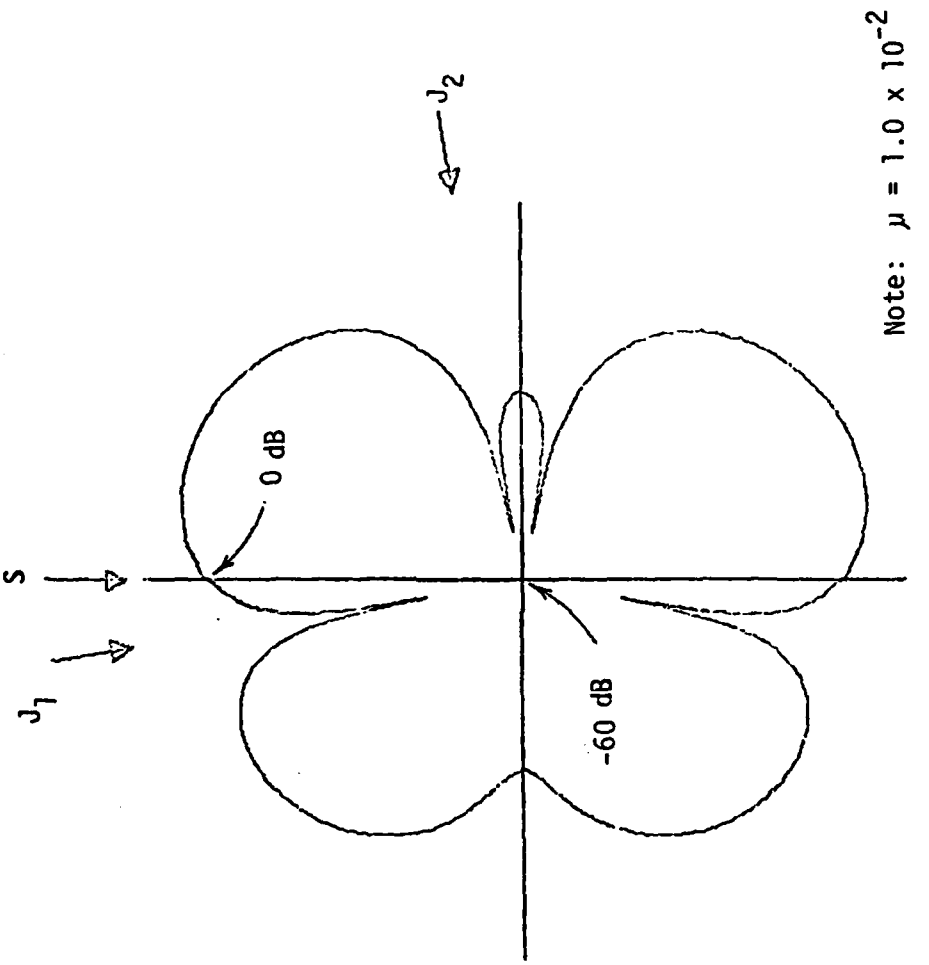

Figure 24. Postconvergence Beampattern Plot for the Six-weight CBF

$$P\,R_{XX}\,P \;=\; [I - C(C^T C)^{-1}\,C^T][C\,R_{RR}\,C^T + R_{NN}]\,P \quad . \qquad (4\text{-}27)$$

which simplifies to

$$P\,R_{XX}\,P \;=\; P\,R_{NN}\,P \quad . \qquad (4\text{-}28)$$

Once again it is seen that the role of the desired signal in the Frost ABF is very limited and that the noise voltages govern convergence. It follows that, if an ideal nulling circuit were realizable, CBF and ABF convergence rates would be identical.

In practice, however, the nulling circuits are imperfect, and the noise voltages in the CBF master only approximate the noise voltages in an equivalent ABF. The actual CBF convergence rates are governed by the noise voltages that are present in the master. These voltages may be expressed as

$$X' \;=\; AX^{(a)} \quad , \qquad (4\text{-}29)$$

where A is a matrix that describes the action of the nulling circuits and $X^{(a)}$ is the vector of voltages from the augmented array that is needed for the CBF. Because the nulling circuits act to remove desired signal components (4-29) may also be written as

$$N' \;=\; A(S^{(a)} + N^{(a)}) \;=\; AN^{(a)} \quad . \qquad (4\text{-}30)$$

The analog of $P\,R_{NN}\,P$ in the Frost ABF then becomes

$$P\,R'_{NN}\,P \;=\; PA\,R^{(a)}_{NN}\,A^T\,P \qquad (4\text{-}31)$$

for the Frost-based CBF.

Nullformer action can either increase or decrease CBF convergence time relative to a equivalent ABF. An experiment was conducted to compare CBF and ABF performance in the case involving a single, sinusoidal jammer. The ABF that was selected was the two-element structure of Figure 6; the CBF was an equivalent structure with three elements and differencing circuits. The two arrays were steered to broadside and constrained to provide an all-pass response in that direction. Signal power was set to zero to avoid the distracting influence of signal cancellation in the ABF. A unit-power jammer signal at a frequency of 0.25 f_{samp} was injected from endfire ($\theta = 90°$), and the two systems were allowed to adapt ($at\ \mu = 1 \times 10^{-2}$) until output power was reduced to $-20dB$ relative to the unit input power. The experiment was repeated to obtain the number of adaptations to convergence at jammer angles ranging from endfire to broadside. The results were plotted in Figure 25, which shows the number of adaptations to convergence versus jammer angle for both the ABF and the CBF.

Figure 25 shows that, depending upon jammer angle, either the ABF or the CBF may provide the more rapid convergence. The CBF yields the better performance in the range from 20° to 90° where the two-element array gain exceeds isotropic. At about 20° the two curves cross, and at angles nearing broadside the ABF provides superior performance. Convergence of both systems becomes very slow at angles approaching the look direction where the requirements of jammer nulling and the requirements of the look-direction constraints begin to conflict. The ABF will be more effective in its response to

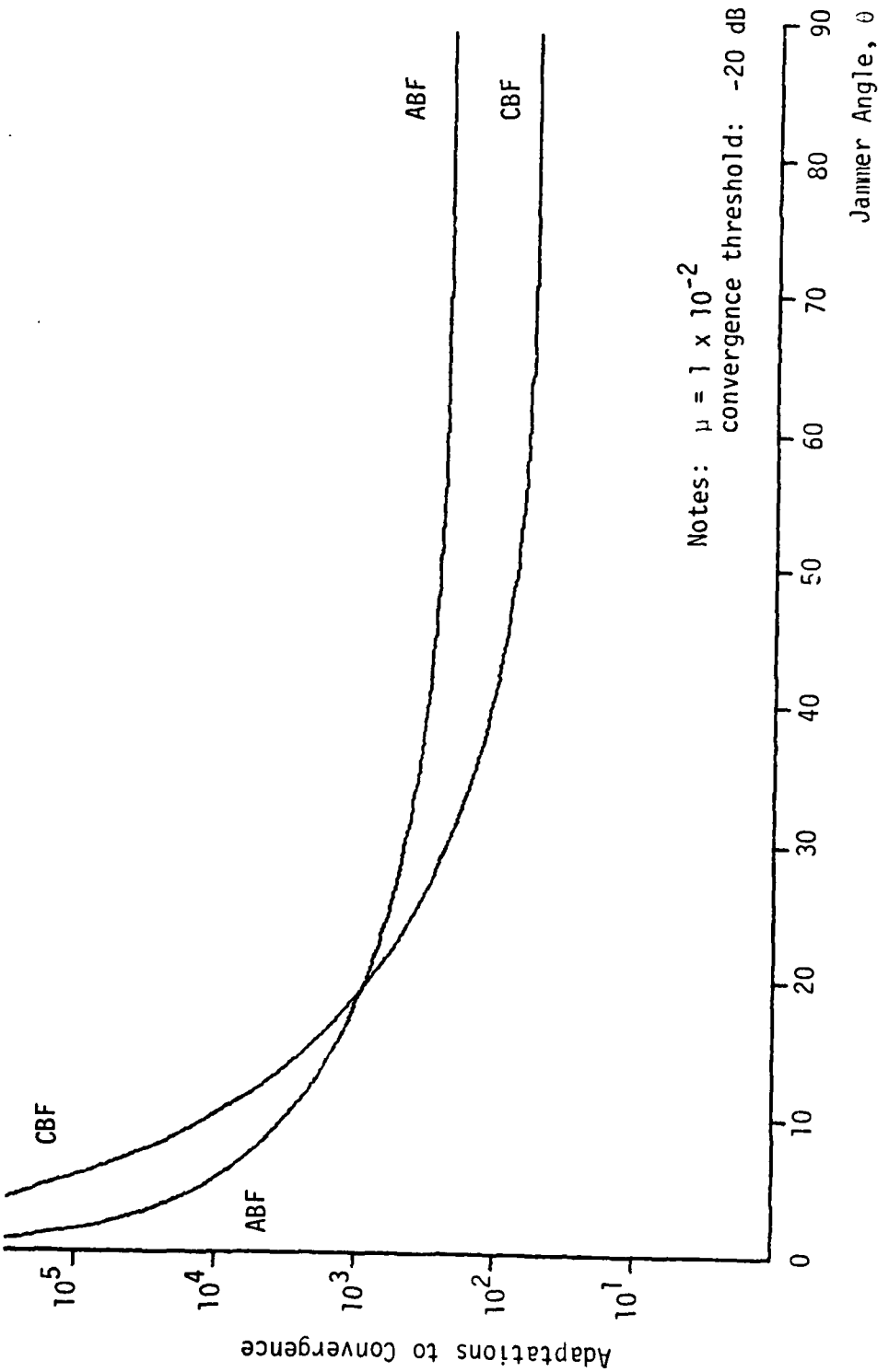

Figure 25. Comparisons of ABF and CBF Convergence Times in the Single-Jammer Case.

jammers arriving near the signal. On the other hand, the CBF will be somewhat more tolerant of small errors in array steering because of its sluggish response at angles near the look direction. It appears likely that, for small steering errors, signal nulling in the CBF will be deferred indefinitely by a reasonably dynamic electromagnetic environment or by the artificial injection of a small amount of noise into the system.

D. Weight Quieting in the CBF

An important aspect of the performance of an adaptive system is its behavior near the optimal solution. Ideally, the weights of an adaptive system should move to the optimal solution, remain at precisely that point in weight space, and displace only in response to a change in the optimal solution, i.e., in response to an actual change in the environment. In practice, a compromise must be reached between the ability of an adaptive system to hold the optimal solution in a stationary environment and to track the optimal solution in a nonstationary environment. The nature of the compromise is not necessarily the same, however, from system to system. This section will compare the performances of the Frost ABF and the Frost-based CBF near the optimal solution and will show from another point of view that the CBF enjoys a performance advantage.

Weight updating in the Frost ABF is accomplished in accordance with the recursion relationships given in (2-14) or (2-17). The same weight updating

technique is used in both the Frost ABF and the Frost-based CBF, but the data samples entering the computations differ significantly as the two systems approach convergence. The contrasts may be seen by examining any of the weights; let the first weight w_1 be selected.

Initially the Frost ABF will be considered. The difference between the values of w_1 at two successive samples may be written from (2-14) as

$$w_1(k+1) - w_1(k) = -\mu y(k)x_1(k) - \frac{1}{K}\sum_{j=1}^{K}[w_j(k) - \mu y(k)x_j(k)] + \frac{f_1}{K} \quad . \tag{4-32}$$

Because the constraint f_1 is, by definition, the sum of the weights in the first column of the beamformer, (4-32) may be simplified to

$$w_1(k+1) - w_1(k) = -\mu y(k)\left[x_1(k) - \frac{1}{K}\sum_{j=1}^{K}x_j(k)\right] \quad . \tag{4-33}$$

Let it be assumed that at the k^{th} sample instant the adaptive system has reached a set of weights that closely approximates the optimal solution. Then

$$w_1(k) \cong w_1^* \quad . \tag{4-34}$$

Additionally, if the constraints are set to provide unity gain and an all-pass response in the look direction, the system output is

$$y(k) \cong s(k) + n_r(k) \quad , \tag{4-35}$$

where $s(k)$ is the signal at the k^{th} sample time at any of the taps in the first

column of the beamformer and $n_r(k)$ is the residual noise that exists at the beamformer output with optimal weights.

The tap voltages in the first beamformer column may also be stated in terms of signal and noise components:

$$x_i(k) = s(k) + n_i(k) , \qquad i = 1, 2, ..., K \quad . \tag{4-36}$$

Note that the cophased signal is the same at taps 1 through K. This allows (4-33) to be simplified to

$$[w_1(k+1) - w_1(k)]_{ABF} = -\mu[s(k) + n_r(k)] \left[n_1 - \frac{1}{K} \sum_{j=1}^{K} n_j\right] \quad . \tag{4-37}$$

The CBF weight recursion will now be considered under like circumstances. Again assume operation near W^*. Further assume that the nulling-circuit performance is nearly ideal so that differences in the noise voltages between the CBF and a comparable ABF may be neglected. Then the CBF tap voltages are

$$x_i(k) = n_i(k) , \qquad i = 1, 2, ..., K \quad . \tag{4-38}$$

The weight difference is obtained from (4-33) as

$$[w_1(k+1) - w_1(k)]_{CBF} = -\mu[n_r(k)] \left[n_1 - \frac{1}{K} \sum_{j=1}^{K} n_j\right] \quad . \tag{4-39}$$

The contrast between ABF and CBF weight behavior near convergence may be seen by comparing (4-37) and (4-39); the difference lies in the inclusion of the signal term in the ABF update expression.

The significance of this contrast is illustrated in Figure 26, which shows a cut along the w_1 axis through the error surfaces of the two systems. Under the assumption of negligibly different noise voltages in the ABF and CBF, the shapes of the two error surfaces are identical. The ABF minimum, however, is substantially elevated above the CBF minimum. If a useful signal is to be delivered by the adaptive system, output signal-to-noise ratios in excess of 10 dB are ordinarily required, and ratios in excess of 20 dB are certainly desirable. These ratios imply that the signal levels will typically be three to ten times the noise levels as the ABF nears convergence. The typical weight adjustment in the ABF will thus be dominated by signal effects as the adaptive system nears convergence. This becomes especially important when it is realized that the signal-times-noise terms amount to short-term estimates of the correlation between the signal and the noise. In other words, the signal influence in the ABF should not be regarded as simply a random weight adjustment, but as a purposeful step toward effecting signal cancellation. Because the CBF weight adjustments are not influenced by the signal, the CBF weights exhibit less variation about the optimal solution than the weights of the comparable ABF. Further, the CBF weight adjustment process cannot cause signal cancellation.

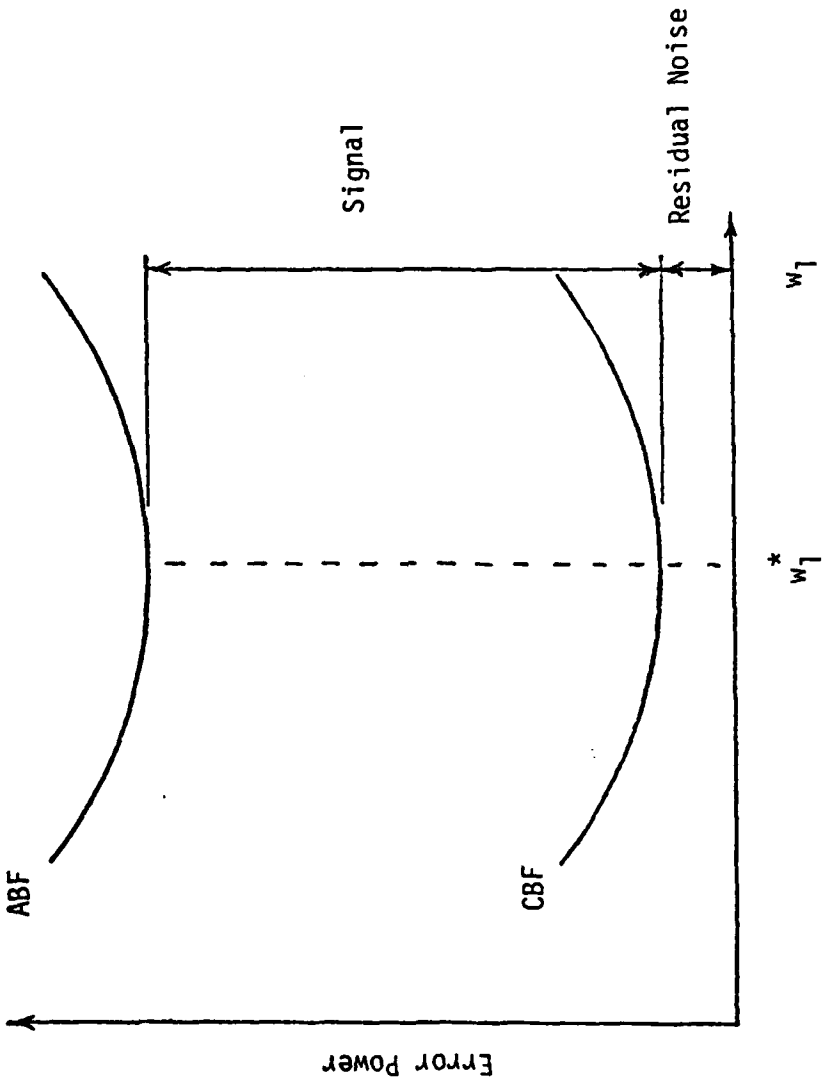

Figure 26. ABF and CBF Error Curves Near the Optimal Weight.

V. SUMMARY AND CONCLUSIONS

It has been shown that interaction between the desired signal and interference signals can lead to partial or total cancellation of the desired signal within an adaptive beamformer (ABF). The signal cancellation phenomenon may arise spontaneously in a multipath environment, or it may be deliberately or accidentally induced by intentional or unintentional jamming. High adaptation rates increase the susceptibility to signal cancellation in beamformers that have not been designed to avoid the effect.

A composite beamformer (CBF) has been described that avoids signal cancellation. The CBF makes use of both an adaptive beamformer and a nonadaptive, slaved beamformer. The inputs to the adaptive beamformer are preprocessed to exclude the desired signal, but retain representation of the interference signals. By restricting the adaptive process in this fashion, a solution (i.e., a set of beamformer weights) is generated that influences only the interference signals. Weights from the adaptive processor are copied to the slaved processor, which is connected directly to the antenna elements and which produces the useful output of the array. The CBF delivers much better performance with regard to signal cancellation than a more conventional ABF. Simulation data have been presented to show the improvement that can be obtained.

The performance of a Frost-based CBF has been compared with that of a Frost ABF. If a narrowband system is assumed, it has been shown that the

Frost-based CBF will tend toward the optimal (i.e., the Wiener) solution provided 1) the preprocessor admits energy from each jammer, 2) energy from each jammer dominates the thermal noise, and 3) there are sufficient degrees of freedom to null each jammer. The properly designed CBF is thus equivalent to the comparable ABF in terms of the ideal solution. The CBF will not, however, exhibit signal-induced weight variations. Performance will therefore be improved in those cases where signal cancellation occurs in the ABF. Convergence toward the optimal solution will, in general, be different for a CBF and an equivalent ABF that are operating in the same environment. The convergence-rate differences are governed by the influence of the preprocessor. In some cases the CBF will attenuate a given interferor more rapidly than the ABF, while in other cases the reverse is true. If the preprocessor is designed to match the basic array element pattern except for a sharp null in the look direction, the convergence rates for the CBF and the ABF are essentially the same. An exception occurs for a jammer incident from very near the look direction. The CBF responds even more sluggishly than the ABF to such an interferor. It is also true, however, that the CBF is less sensitive to small steering errors than the ABF.

The studies of signal cancellation and the CBF have thus far suggested several areas for further investigation. The signal cancellation phenomenon itself is not so well characterized as might be desired. An improved characterization of the phenomenon may provide a better means for analyzing the importance of signal cancellation in various systems and environments. Additionally, this work

may reveal new ways to avoid the effect in adaptive arrays.

Perhaps the most promising area for further CBF improvement is in the preprocessor that nulls the target signal. Work thus far has centered on the element-differencing scheme because of its simplicity. Other preprocessor configurations, though more complex from a hardware viewpoint, are capable of yielding subarray patterns that provide a better match between the patterns seen by the adaptive beamformer and the slaved beamformer. Improved matching will assure that the CBF performance (both dynamic and asymptotic) is approximately that of the equivalent ABF, except for the superior CBF performance with regard to signal cancellation. Steyskal [21] has recently described a procedure for optimal pattern matching subject to null constraints. This procedure appears to be well suited for preprocessor design.

The general procedure of adapting in the absence of signal can sometimes be applied without resorting to the CBF. Systems that make use of low-duty-cycle or frequency-hopped signals can employ other signal-exclusion schemes that arise naturally out of the signaling format. Work is in progress at Stanford on cancellation-free adaptation schemes for systems in these classes. These schemes will trade timing constraints against the spatial-nulling method of the CBF and will almost certainly result in less complex adaptation schemes for systems that do not continuously occupy a channel.

REFERENCES

1. P. W. Howells, "Intermediate Frequency Side-lobe Canceller," U.S. Patent 3,202,990, 24 Aug. 1965 (filed 4 May 1959).

2. P. W. Howells, "Explorations in Fixed and Adaptive Resolution at GE and SURC," IEEE Trans. Ant. and Prop., Vol. AP-24, pp. 575-584, Sept. 1976.

3. B. Widrow, P. E. Mantey, L. J. Griffiths, and B. B. Goode, "Adaptive Antenna Systems," Proc. IEEE, Vol. 55, pp. 2143-2159, Dec. 1967.

4. L. J. Griffiths, "A Simple Adaptive Algorithm for Real-time Processing in Antenna Arrays," Proc. IEEE, Vol. 57, pp. 1696-1704, Oct. 1969.

5. O. L. Frost, III, "Adaptive Least Squares Optimization Subject to Linear Equality Constraints," Ph.D. Dissertation, Stanford University, Stanford, CA, Aug. 1970.

6. O. L. Frost, III, "An Algorithm for Linearly Constrained Adaptive Array Processing," Proc. IEEE, Vol. 60, pp. 926-935, Aug. 1972.

7. C. W. Jim, "A Comparison of Two LMS Constrained Optimal Array Structures," Proc. IEEE, Vol. 65, pp. 1730-1731, Dec. 1977.

8. L. J. Griffiths and C. W. Jim, "An Alternative Approach to Linearly Constrained Adaptive Beamforming," IEEE Trans. Ant. and Prop., Vol. AP-30, pp. 27-34, Jan. 1982.

9. R. A. Chestek, "The Addition of Soft Constraints to the LMS Algorithm," Ph.D. Dissertation, Stanford University, Stanford, CA, May 1979.

10. B. Widrow et al., "Adaptive Noise Cancelling: Principles and Applications," Proc. IEEE, Vol. 63, pp. 1692-1716, Dec. 1975.

11. J. R. Glover, Jr., "Adaptive Noise Cancelling of Sinusoidal Interference," Ph.D. Dissertation, Stanford University, Stanford, CA, Dec. 1975.

12. J. R. Glover, Jr., "Adaptive Noise Cancelling Applied to Sinusoidal Interferences," IEEE Trans. on Acoustics, Speech, and Signal Proc., Vol. ASSP-25, pp. 484-491, Dec. 1977.

13. M. J. Shensa, "Performance of the Adaptive Noise Canceller with a Noisy Reference -- Non-Wiener Solutions," NOSC Tech. Report 381, Naval Ocean Systems Center, San Diego, CA, 15 March 1979.

14. M. J. Shensa, "Non-Wiener Solutions of the Adaptive Noise Canceller with a Noisy Reference," IEEE Trans. on Acoustics, Speech, and Signal Proc., Vol. ASSP-28, Aug. 1980.

15. B. Widrow, K. Duvall, R. Gooch, and W. Newman, "Jamming of Adaptive Arrays by Signal Cancellation: the Phenomenon and Two Remedies," Proceedings of the 1980 Adaptive Antenna Symposium, RADC-TR-80-378, Vol. 1, pp. 270-292, Dec. 1980.

16. B. Widrow, K. Duvall, R. Gooch, and W. Newman, "Signal Cancellation Phenomena in Adaptive Antennas: Causes and Cures," IEEE Trans. on Ant. and Prop., Vol. AP-30, pp. 469-478, May 1982.

17. R. T. Compton, Jr., Letter to B. Widrow referencing Figure 19 of Reference 18, 23 May 1980.

18. T. Miller, R. Caldecott, and R. Huff, "A Satellite Simulator with a TDMA-System-Compatible Adaptive Array," Report 3364-4, Electroscience Laboratory, Ohio State University, Columbus, Ohio, Jan. 1976.

19. P. M. Hansen and J. P. Loughlin, "Adaptive Array for Elimination of Multipath Interference at HF," IEEE Trans. on Ant. and Prop., Vol. AP-29, No. 6, Nov. 1981.

20. I. J. Gupta and A. A. Ksienski, "Dependence of Adaptive Array Performance on Conventional Array Design," IEEE Trans. on Ant. and Prop., Vol. AP-30, No. 4, July 1982.

21. H. Steyskal, "Synthesis of Antenna Patterns with Prescribed Nulls," IEEE Trans. on Ant. and Prop., Vol. AP-30, No. 2, March 1982.

APPENDIX A

ANALYSIS OF THE DYNAMIC SOLUTION FOR THE SINUSOIDAL CASE

Chapter 2 discussed the dynamic solution that is tracked by an ABF when large values of the adaptation parameter μ are used. A computer simulation formed the basis of that discussion, and certain claims were made without a supporting analysis. In this appendix the dynamic error-surface minimum is examined analytically, and a mathematical model is developed that supports the discussion in Chapter 2.

In Chapter 2 the Frost ABF under study was mapped into an equivalent adaptive noise canceller (ANC) in order to reduce the problem dimensionality and simplify the analysis. This same mapping will be used here; Figure A-1 reviews the ANC structure that will be analyzed.

The ANC structure assumes separate availability of the desired signal and the single jammer signal, both of which are sinusoids in the case under consideration. The desired signal is taken directly to the output summing junction in conformance with a unit-gain, all-pass constraint in the look direction. The jammer signal is processed through a two-channel (in-phase and quadrature) filter with one weight per channel and is subtracted from the desired signal at the output summing junction. The ANC output is also the error signal that is fed back to control adaptation of the filter weights. In the notation

AD-A133 676 RESEARCH ON ADAPTIVE ANTENNA TECHNIQUES V(U) STANFORD UNIV CA INFORMATION SYSTEMS LAB K M DUVALL ET AL. SEP 83 N00019-82-C-0189 2/2

UNCLASSIFIED F/G 17/4 NL

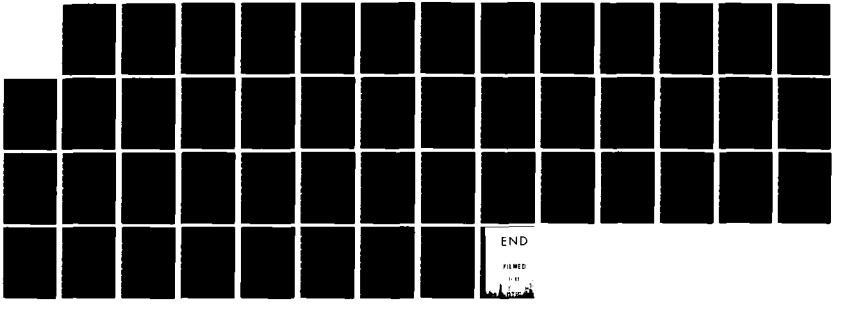

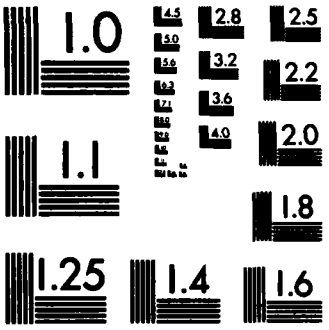

MICROCOPY RESOLUTION TEST CHART
NATIONAL BUREAU OF STANDARDS-1963-A

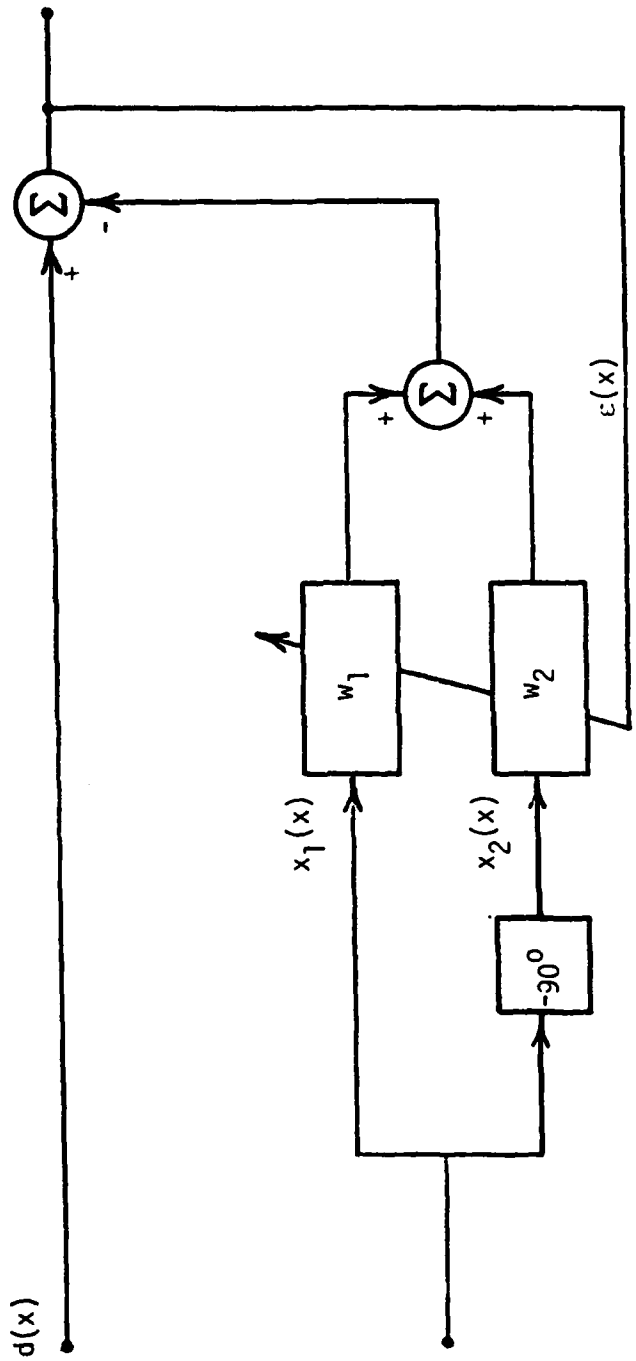

Figure A-1. Equivalent Adaptive-Noise-Canceller Representation.

indicated in the figure, the error is

$$\epsilon(x) = d(x) - [w_1 x_1(x) + w_2 x_2(x)] \quad . \tag{A-1}$$

The task of the adaptation algorithm is to minimize some function of $\epsilon(x)$ by selecting appropriate values for w_1 and w_2. Under the assumptions of stationarity and slow adaptation, the effectiveness of an adaptation algorithm is often established by comparing performance with a minimum-mean-square-error solution that is derived analytically. It has been established that the Widrow-Hoff LMS algorithm delivers asymptotically optimal performance in the stationary case, i.e., the LMS solution tends to the Wiener solution as μ tends to zero.

Here, however, interest centers upon an ABF that is adapting rapidly and is therefore operating on the basis of short-term estimates of the environment. At high adaptation rates it is unrealistic to expect close conformance with the Wiener solution, which is derived under a very different view of the data. Instead, an objective function is needed that more accurately reflects the use of a finite time window and allows the solution to evolve over time. An alternative objective function $\hat{\xi}$ will be taken as the average square error over the interval Δ:

$$\hat{\xi}(t,\Delta) \triangleq \frac{1}{\Delta} \int_{t-\Delta}^{t} \epsilon^2(x)\, dx \quad . \tag{A-2}$$

This objective function has the desirable property of extending to mean-square error as t and Δ increase without bound. Nebat, et al, [1] have made use of a similar finite-time integration in exploring the effect of record length on the

correlation of complex exponentials.

Combining (A-1) and (A-2) gives

$$\hat{\xi}(t,\Delta) = \frac{1}{\Delta}\int_{t-\Delta}^{t} d^2(x)dx - \frac{2w_1}{\Delta}\int_{t-\Delta}^{t} d(x)x_1(x)dx - \frac{2w_2}{\Delta}\int_{t-\Delta}^{t} d(x)x_2(x)dx + \frac{w_1^2}{\Delta}\int_{t-\Delta}^{t} x_1^2(x)dx + \frac{2w_1w_2}{\Delta}\int_{t-\Delta}^{t} x_1(x)x_2(x)dx + \frac{w_2^2}{\Delta}\int_{t-\Delta}^{t} x_2^2(x)dx \quad . \tag{A-3}$$

To provide a more compact notation, let

$$r_{ij}(t,\Delta) \triangleq \frac{1}{\Delta}\int_{t-\Delta}^{t} x_i(x)x_j(x)dx \qquad i, j = 1, 2$$

$$\rho_i(t,\Delta) \triangleq \frac{1}{\Delta}\int_{t-\Delta}^{t} d(x)x_i(x)dx \qquad i = 1, 2 \quad . \tag{A-4}$$

Equation (A-3) may now be rewritten as

$$\hat{\xi}(t,\Delta) = \frac{1}{\Delta}\int_{t-\Delta}^{t} d^2(x)dx - 2w_1\,p_1(t,\Delta) - 2w_2\,p_2(t,\Delta) + w_1^2\,r_{11}(t,\Delta) + 2w_1w_2\,r_{12}(t,\Delta) + w_2^2\,r_{22}(t,\Delta) \tag{A-5}$$

Minimization of $\hat{\xi}(t,\Delta)$ is accomplished by taking the gradient with respect to the weights, setting the gradient to zero, and solving for w_1 and w_2. The first two steps of this procedure yield

$$\nabla\hat{\xi}(t,\Delta) = \begin{bmatrix} -2\,p_1(t,\Delta) + 2w_1\,r_{11}(t,\Delta) + 2w_2\,r_{12}(t,\Delta) \\ -2\,p_2(t,\Delta) + 2w_1\,r_{12}(t,\Delta) + 2w_2\,r_{22}(t,\Delta) \end{bmatrix} = \begin{bmatrix} 0 \\ 0 \end{bmatrix} \tag{A-6}$$

The solution of (A-6) may be written as

$$\begin{bmatrix} w_{1m} \\ w_{2m} \end{bmatrix} = \begin{bmatrix} r_{11}(t,\Delta) & r_{12}(t,\Delta) \\ r_{21}(t,\Delta) & r_{22}(t,\Delta) \end{bmatrix}^{-1} \begin{bmatrix} p_1(t,\Delta) \\ p_2(t,\Delta) \end{bmatrix} , \qquad \text{(A-7)}$$

where w_{1m} and w_{2m} are the values of the weights that minimize the objective function during a given time window and where existence of the matrix inverse is assumed. The equivalent matrix equation for (A-7) is

$$W_m = R^{-1}(t,\Delta)\, P(t,\Delta) \qquad \text{(A-8)}$$

Equations (A-7) and (A-8) are finite-time-window versions of the familiar Wiener-Hopf equation.

Since the dimension of (A-7) is only two, it is simple to expand the matrix inverse and obtain expressions for the weights:

$$\begin{aligned} w_{1m} &= \left\{ \frac{1}{det\,[R(t,\Delta)]} \right\} \left\{ r_{22}(t,\Delta)\, p_1(t,\Delta) - r_{12}(t,\Delta)\, p_2(t,\Delta) \right\} \\ w_{2m} &= \left\{ \frac{1}{det\,[R(t,\Delta)]} \right\} \left\{ -r_{21}(t,\Delta)\, p_1(t,\Delta) + r_{11}(t,\Delta)\, p_2(t,\Delta) \right\} . \end{aligned} \qquad \text{(A-9)}$$

Equations (A-9) describe the optimal weights for the two-weight adaptive noise canceller at time t when averaging is over a window of duration Δ.

In order to obtain a direct comparison with the sinusoidal case considered in Chapter 2, let

$$\begin{aligned} d(x) &= \cos \omega_1 x \\ x_1(x) &= \cos (\omega_2 x + \phi) \\ x_2(x) &= \sin (\omega_2 x + \phi) . \end{aligned} \qquad \text{(A-10)}$$

These signal definitions lead to the following values for components of the $R(t,\Delta)$ matrix and the $P(t,\Delta)$ vector:

$$r_{11}(t,\Delta) = \frac{1}{2} + \frac{1}{2}\,\mathrm{sinc}\left(\frac{\omega_2\Delta}{\pi}\right)\cos\left[2\left(\omega_2 + \phi + \frac{\omega_2\Delta}{2}\right)\right]$$

$$r_{12}(t,\Delta) = r_{21}(t,\Delta) = \frac{1}{2}\,\mathrm{sinc}\left(\frac{\omega_2\Delta}{\pi}\right)\sin\left[2\left(\omega_2 t + \phi + \frac{\omega_2\Delta}{2}\right)\right]$$

$$r_{22}(t,\Delta) = \frac{1}{2} - \frac{1}{2}\,\mathrm{sinc}\left(\frac{\omega_2\Delta}{\pi}\right)\cos\left[2\left(\omega_2 t + \phi + \frac{\omega_2\Delta}{2}\right)\right]$$

$$p_1(t,\Delta) = \frac{1}{2}\,\mathrm{sinc}\left[\frac{(\omega_1-\omega_2)\Delta}{2\pi}\right]\cos\left[(\omega_1-\omega_2)t - \phi + \frac{(\omega_1-\omega_2)\Delta}{2}\right]$$
$$+ \frac{1}{2}\,\mathrm{sinc}\left[\frac{(\omega_1+\omega_2)\Delta}{2\pi}\right]\cos\left[(\omega_1+\omega_2)t + \phi + \frac{(\omega_1+\omega_2)\Delta}{2}\right]$$

$$p_2(t,\Delta) = -\frac{1}{2}\,\mathrm{sinc}\left[\frac{(\omega_1-\omega_2)\Delta}{2\pi}\right]\sin\left[(\omega_1-\omega_2)t - \phi + \frac{(\omega_1-\omega_2)\Delta}{2}\right]$$
$$+ \frac{1}{2}\,\mathrm{sinc}\left[\frac{(\omega_1+\omega_2)\Delta}{2\pi}\right]\sin\left[(\omega_1+\omega_2)t + \phi + \frac{(\omega_1+\omega_2)\Delta}{2}\right] \quad . \tag{A-11}$$

Equations (A-9) and (A-11) provide a complete specification of ideal weight behavior in the ANC problem being considered. It would be possible at this point to utilize these equations to write expressions for w_{1m} and w_{2m}. It is apparent, however, that the combined complexities of (A-9) and (A-11) would lead to a rather unwieldly pair of equations for the weights. A more satisfactory approach is to continue with the existing equations and examine some particular aspects of weight behavior that bear upon the discussion in Chapter 2.

Initial attention will be directed toward Equations (A-11). Sinc functions appear prominently in the expressions for all of the components of the $R(t,\Delta)$

matrix and the $P(t,\Delta)$ vector. These sinc functions govern the peak amplitudes of most terms in the correlation expressions and thus play a key role in determining weight behavior. The arguments of the sinc functions involve only the time window Δ and some function of ω_1 and ω_2. This latter quantity is fixed for a given problem statement, but the equivalent time window can be governed in an adaptive system by choice of the adaptation parameter μ. The observation that weight amplitudes can be influenced by the choice of adaptation parameter harmonizes well with the behavior observed in the experiments of Chapter 2.

A better understanding of the relative importance of the terms in (A-11) can be obtained from a closer study of the sinc functions. Figure A-2 is a plot of sinc function magnitude as a function of the argument. An upper bound for the sinc function is also plotted to reflect the inverse dependency on argument that dominates the sinc function behavior. It is clear from the figure that a small argument is necessary if the sinc function is to contribute significant amplitude to a term. Conversely, it is easy to see that, unless ω_1 and ω_2 are equal, large values of Δ will lead to large arguments and vanishing amplitude contributions from the terms involving sinc functions, i.e.,

$$\lim_{\Delta\to\infty} r_{11}(t,\Delta) = \frac{1}{2}$$

$$\lim_{\Delta\to\infty} r_{12}(t,\Delta) = \lim_{\Delta\to\infty} r_{21}(t,\Delta) = 0$$

$$\lim_{\Delta\to\infty} r_{22}(t,\Delta) = \frac{1}{2}$$

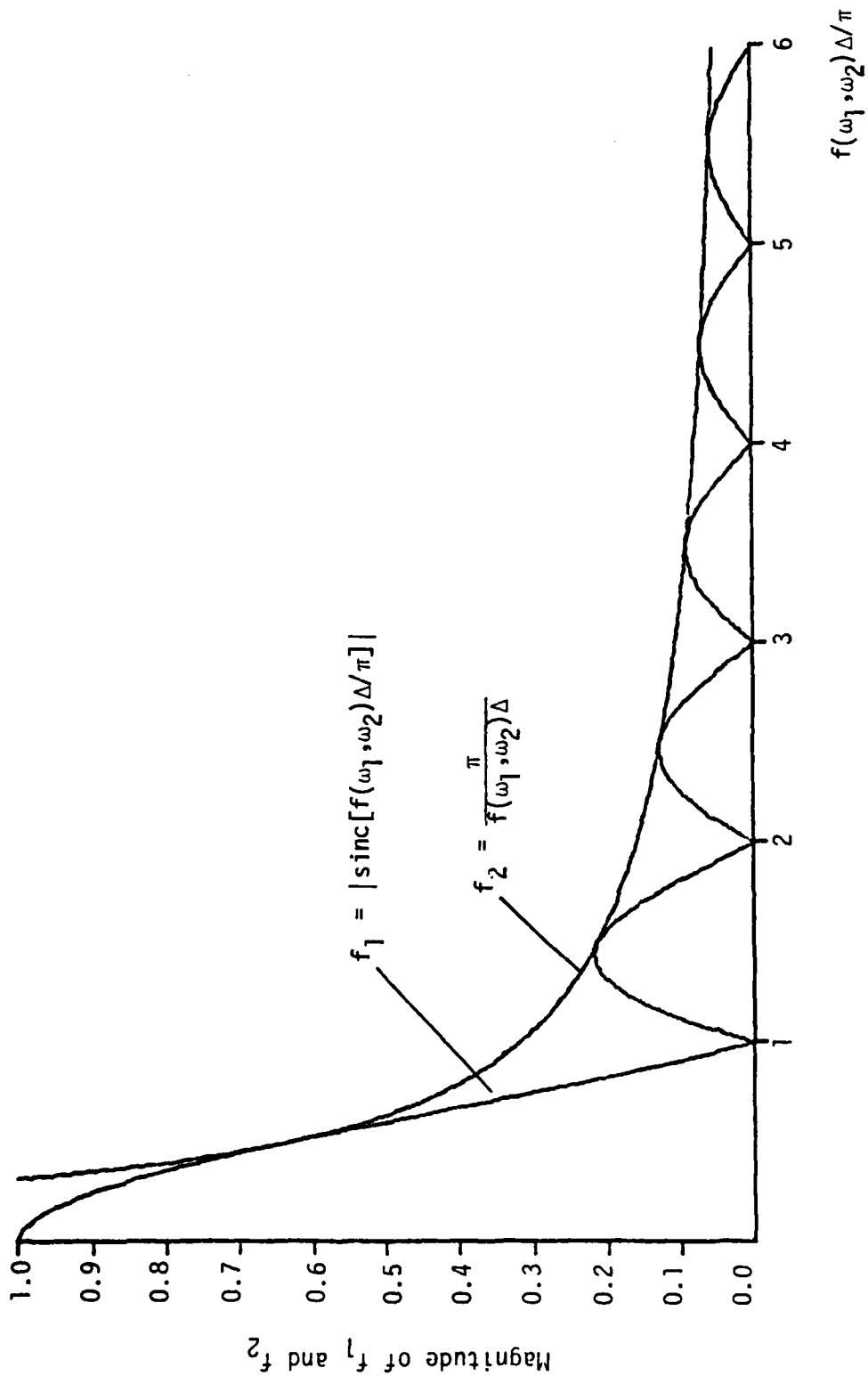

Figure A-2. Plot of Sinc Function Magnitude and an Upper Bound.

$$\lim_{\Delta\to\infty} p_1(t,\Delta) = 0$$
$$\lim_{\Delta\to\infty} p_2(t,\Delta) = 0 \quad . \tag{A-12}$$

These are the same values of the correlation functions that would have been obtained from the traditional calculations involving expected values. The values in (A-12) may be used in (A-9) to compute the Wiener weights:

$$w_1^* = 0$$
$$w_2^* = 0 \quad . \tag{A-13}$$

The vector components $p_1(t,\Delta)$ and $p_2(t,\Delta)$ each involve sinc functions with arguments containing the sum $\omega_1 + \omega_2$ and difference $\omega_1 - \omega_2$ of the signal and jammer frequencies. Since ω_1 and ω_2 will be taken as non-negative numbers in this context,

$$\omega_1 + \omega_2 \geq \omega_1 - \omega_2 \tag{A-14}$$

for all allowed choices of ω_1 and ω_2. When appreciable levels of cancellation are occurring, the argument $\Delta(\omega_1-\omega_2)/2\pi$ will be small so that the leading terms in $p_1(t,\Delta)$ and $p_2(t,\Delta)$ will have magnitudes approaching unity. The argument $\Delta(\omega_1+\omega_2)/2\pi$ can be no smaller than $\Delta(\omega_1-\omega_2)/2\pi$, and can be much larger. In the case considered in Chapter 2, for example, $\omega_1 + \omega_2$ was approximately 50 times larger than $\omega_1 - \omega_2$. This difference was sufficiently large to assure that difference-frequency terms dominated weight behavior over the entire adaptation-parameter range that yielded measurable deviation from the Wiener solution. Sum-frequency influence was visible in the weight loci for some values

of the adaptation parameter, but never caused deviations of more than a few percent from the basically circular loci.

It is useful to look more closely at weight behavior when difference-frequency terms are dominant. Assume that ω_1 and ω_2 are nearly equal and are sufficiently different from zero so that

$$\frac{(\omega_1-\omega_2)\Delta}{2\pi} < 0.5 \qquad \text{(A-15)}$$

and

$$\omega_1 + \omega_2 >> \omega_1 - \omega_2 \quad . \qquad \text{(A-16)}$$

Under these circumstances, the difference-frequency terms in $p_1(t,\Delta)$ and $p_2(t,\Delta)$ are dominant and

$$p_1(t,\Delta) \approx \frac{1}{2}\, sinc\left[\frac{(\omega_1-\omega_2)\Delta}{2\pi}\right] \cos\left[(\omega_1-\omega_2)t - \phi + \frac{(\omega_1-\omega_2)\Delta}{2}\right]$$

$$p_2(t,\Delta) \approx \frac{1}{2}\, sinc\left[\frac{(\omega_1-\omega_2)\Delta}{2\pi}\right] \sin\left[(\omega_1-\omega_2)t - \phi + \frac{(\omega_1-\omega_2)\Delta}{2}\right] \quad . \qquad \text{(A-17)}$$

Further, if $\text{sinc}\left[\frac{(\omega_1+\omega_2)\Delta}{2\pi}\right]$ is negligible, then so is $\text{sinc}\left[\frac{\omega_2\Delta}{\pi}\right]$. This observation allows the approximations

$$r_{11}(t,\Delta) \approx \frac{1}{2}$$

$$r_{12}(t,\Delta) = r_{21}(t,\Delta) \approx 0$$

$$r_{22}(t,\Delta) \overset{\approx}{=} \frac{1}{2} \quad . \tag{A-18}$$

Now, from (A-9)

$$w_{1m} \overset{\approx}{=} sinc\left[\frac{(\omega_1-\omega_2)\Delta}{2\pi}\right] \cos\left[(\omega_1-\omega_2)t - \phi + \frac{(\omega_1-\omega_2)\Delta}{2}\right]$$

$$w_{2m} \overset{\approx}{=} sinc\left[\frac{(\omega_1-\omega_2)\Delta}{2\pi}\right] \sin\left[(\omega_1-\omega_2)t - \phi + \frac{(\omega_1-\omega_2)\Delta}{2}\right] \quad . \tag{A-19}$$

Equations (A-19) describe a phasor rotating in the $w_1 - w_2$ plane at the difference frequency $(\omega_1-\omega_2)$. The magnitude of the phasor is proportional to the magnitude of the cross-correlation functions $p_1(t,\Delta)$ and $p_2(t,\Delta)$.

For a given time window Δ and a specified time t, the phasor given by Equations (A-19) defines the weight pair that minimizes the ANC output. Equivalently, the phasor marks the projection of the dynamic error surface minimum onto the $w_1 - w_2$ plane. As time evolves, the tip of the phasor traces out the circular locus of the projection of the minimum. This is the behavior that was exhibited in Figure 12 of Chapter 2.

APPENDIX A Reference

1. J. Nebat et al., "Effect of Record Length on the Correlation of Complex Exponentials," IEEE Trans. on Ant. and Prop., Vol. AP-30, No. 3, March 1982.

APPENDIX B

AN ALTERNATIVE EXPRESSION FOR THE OPTIMAL WEIGHTS IN A FROST ABF

Frost [1,2] derived an expression for the optimal weight vector in a hard-constrained adaptive beamformer:

$$W^*_{ABF} = R_{XX}^{-1}\, C[C^T R_{XX}^{-1} C]^{-1}\, \boldsymbol{f} \quad , \tag{B-1}$$

where $R_{XX} \triangleq E[XX^T]$ is the correlation matrix for the tap voltages, $\boldsymbol{f} \triangleq [f_1, f_2, \ldots, f_J]^T$ is a constraint vector, and

$$C \triangleq \overbrace{\begin{bmatrix} 1 & 0 & & 0 \\ 1 & 0 & & 0 \\ \vdots & \vdots & & \vdots \\ 1 & 0 & & 0 \\ 0 & 1 & & 0 \\ 0 & 1 & & 0 \\ \vdots & \vdots & & \vdots \\ 0 & 1 & \cdots & 0 \\ 0 & 0 & & 0 \\ \vdots & \vdots & & \vdots \\ 0 & 0 & & 0 \\ 0 & 0 & & 1 \\ 0 & 0 & & 1 \\ \vdots & \vdots & & \vdots \\ 0 & 0 & & 1 \end{bmatrix}}^{J} \begin{matrix} \left.\begin{matrix} \\ \\ \\ \\ \end{matrix}\right\} K \\ \left.\begin{matrix} \\ \\ \\ \\ \end{matrix}\right\} K \\ \\ \\ \\ \left.\begin{matrix} \\ \\ \\ \\ \end{matrix}\right\} K \end{matrix} \quad KJ \tag{B-2}$$

is a constraint matrix. In this expression for W^*_{ABF}, the dependency on the signal environment is given in terms of the tap voltages, i.e., in term of R_{XX}, which may be estimated from X.

In this appendix it will be shown that an equivalent formulation for the optimal weight vector may be given in terms of the vector N where

$$N = X - S \tag{B-3}$$

is the vector of tap noise voltages that is obtained by deleting the desired-signal component S. In particular, it will be shown that the equivalent expression is

$$W^*_{ABF} = R^{-1}_{NN} C [C^T R^{-1}_{NN} C]^{-1} \mathcal{L} \quad , \tag{B-4}$$

where $R_{NN} \triangleq E[NN^T]$ is the correlation matrix for the tap noise voltages.

The balance of this appendix is broken into two sections. In the first section the validity of (B-4) will be demonstrated for the narrowband case. The second section will then examine the somewhat more complicated wideband case.

A. The Narrowband Case

In the narrowband case it is assumed that signal bandwidths are small enough to allow incident signals to be characterized as sinusoids with amplitude and phase variations that are slow with respect to the carrier frequency. Under these circumstances a single complex weight is adequate to adjust the gain and phase of each beamformer channel. That is, the tapped-delay-line filter constituting each beamformer channel is replaced by an in-phase weight and a

quadrature weight. For the narrowband Frost ABF, the constraint vector becomes simply

$$\underline{f} = f_1 \quad , \tag{B-5}$$

with f_1 a complex number giving the in-phase constraint as its real part and the quadrature constraint as its imaginary part. Additionally, the constraint matrix takes a simple form:

$$C = [1\ 1\ \cdots\ 1]^T \triangleq \underline{1} \quad . \tag{B-6}$$

The correlation matrix R_{XX} must be decomposed into its desired-signal component and its noise component in order to proceed further. This may be accomplished by rewriting (B-3) in the form

$$X = N + S \tag{B-7}$$

and then making use of the cophased nature of the signal to obtain

$$X = N + \sqrt{s}\,\underline{1} \quad , \tag{B-8}$$

where the signal amplitude is taken as $\sqrt{s}$. Now, (B-8) may be used to obtain

$$\begin{aligned} R_{XX} = E[XX^T] &= E[NN^T] + s\,\underline{1}\,\underline{1}^T \\ &= R_{NN} + s\underline{1}\,\underline{1}^T \quad , \end{aligned} \tag{B-9}$$

where Frost's assumption [1] of a lack of correlation between signal and noise voltages has been used to simplify the expression for R_{XX}.

It will be useful at this point to focus attention on the factor $R_{XX}^{-1}\,C$ that

appears twice in (B-1) and to make use of an observation by Baird and Zahm [3] regarding the utility of the matrix inversion lemma in a closely related problem. The lemma may be drawn from [4] in the following form:

If a nonsingular matrix H of order n can be written in the form

$$H = A + BDE \quad , \tag{B-10}$$

where B, D, and E are $n \times p$, $p \times p$, and $p \times n$, respectively, and A and D are nonsingular, then

$$H^{-1} = A^{-1} - A^{-1}B(D^{-1} + EA^{-1}B)^{-1}\, EA^{-1} \quad . \tag{B-11}$$

The lemma given in (B-11) may be used to invert R_{XX} in

$$R_{XX}^{-1}C = [R_{NN} + s\mathbf{1}\mathbf{1}^T]^{-1}\,\mathbf{1} \quad . \tag{B-12}$$

As a preliminary step it is noted that R_{NN}, which is analogous to the A matrix in (B-10), is invertible because it is assumed to be positive definite. The vectors $s\mathbf{1}$ and $\mathbf{1}^T$, which correspond to B and E in (10), are K x 1 and 1 x K, respectively. The D matrix in (B-10) degenerates to the scalar 1 in (B-12) and is clearly invertible. With the applicability of the inversion lemma established, (B-12) may be written as

$$R_{XX}^{-1}C = \left[R_{NN}^{-1} - \frac{s\, R_{NN}^{-1}\,\mathbf{1}\mathbf{1}^T\, R_{NN}^{-1}}{(1 + s\,\mathbf{1}^T\, R_{NN}^{-1}\,\mathbf{1})} \right]\mathbf{1} \quad . \tag{B-13}$$

Expanding gives

$$R_{\bar{X}\bar{X}}^{-1} C = \frac{R_{\bar{N}\bar{N}}^{-1} 1 + s R_{\bar{N}\bar{N}}^{-1}(1^T R_{\bar{N}\bar{N}}^{-1} 1) 1 - s R_{\bar{N}\bar{N}}^{-1} 1(1^T R_{\bar{N}\bar{N}}^{-1} 1)}{\varsigma} , \quad \text{(B-14)}$$

where

$$\varsigma \triangleq (1 + s 1^T R_{\bar{N}\bar{N}}^{-1} 1) . \quad \text{(B-15)}$$

Because $(1^T R_{\bar{N}\bar{N}}^{-1} 1)$ is a scalar, the rightmost two terms of (B-14) can be written in the same form and cancelled to yield

$$R_{\bar{X}\bar{X}}^{-1} C = \frac{R_{\bar{N}\bar{N}}^{-1} 1}{\varsigma} = \frac{R_{\bar{N}\bar{N}}^{-1} C}{\varsigma} . \quad \text{(B-16)}$$

The expression in (B-16) may be substituted in (B-1) to obtain the desired result:

$$W_{ABF}^{*} = \frac{R_{\bar{N}\bar{N}}^{-1} C}{\varsigma} \left[\frac{C^T R_{\bar{N}\bar{N}}^{-1} C}{\varsigma} \right]^{-1} f = R_{\bar{N}\bar{N}}^{-1} C [C^T R_{\bar{N}\bar{N}}^{-1} C]^{-1} f . \quad \text{(B-17)}$$

B. The Wideband Case

The beamformer in the wideband case is assumed to contain K filters, each with J taps. The KJ-element vector X of tap voltages may again be written as

$$X = N + S , \quad \text{(B-18)}$$

where N is the vector of tap voltages attributable to noise and interference and S is the desired-signal vector. In general, the components of N will each be different due to independent noise in each channel and due to the fact that interference signals will typically not be aligned across the array. The signal, on

the other hand, is aligned across the array and is therefore identical down any column of taps within the beamformer. The special structure of S may be expressed by the relationship

$$S = CR \quad , \tag{B-19}$$

where C is defined by (B-2) and

$$R \triangleq [s(k)\ s(k-\tau)\ s(k-2\tau)\ \cdots\ s(k-(J-1)\tau)\ ]^T \tag{B-20}$$

is the vector of desired-signal voltages at the taps of any beamformer delay line. Combining (B-18) and (B-19) yields

$$X = N + CR \quad . \tag{B-21}$$

The correlation matrix for the wide band case may be computed based upon (B-21):

$$R_{XX} = E[(N + CR)(N^T + R^T C^T)] \tag{B-22}$$

$$R_{XX} = E[NN^T] + CE[RR^T]\ C^T \quad . \tag{B-23}$$

The transition from (B-22) to (B-23) has made use of the assumed lack of correlation between signal and noise. Alternative forms for (B-23) are

$$R_{XX} = R_{NN} + C\ R_{RR}\ C^T \tag{B-24}$$

and

$$R_{XX} = R_{NN} + R_{SS} \quad . \tag{B-25}$$

It should be noted that R_{NN} and R_{SS} are dimensioned KJ x KJ, while R_{RR} is

dimensioned J x J. The difference in dimension between R_{SS} and R_{RR} reflects, of course, the redundancy in R_{SS}.

The matrix inversion lemma that was used in the narrowband case will again be used to invert the matrix R_{XX} as expressed in (B-24):

$$R_{XX}^{-1} = R_{NN}^{-1} - R_{NN}^{-1}C[R_{RR}^{-1} + C^T R_{NN}^{-1}C]^{-1} C^T R_{NN}^{-1} \quad . \qquad \text{(B-26)}$$

Both R_{NN} and R_{RR} are assumed to be positive definite and therefore invertible.

The relationship given in (B-26) will now be used to structure components of the expression for W_{ABF}^{*} given in (B-1). The leading factor is easily constructed by postmultiplying (B-26) by C:

$$R_{XX}^{-1}C = R_{NN}^{-1}C - R_{NN}^{-1}C[R_{RR}^{-1} + C^T R_{NN}^{-1}C]^{-1} C^T R_{NN}^{-1}C \quad . \qquad \text{(B-27)}$$

The central factor is obtained in two steps. First, (B-27) is premultiplied by C^T:

$$C^T R_{XX}^{-1}C = [C^T R_{NN}^{-1}C] + [-C^T R_{NN}^{-1}C]\,[R_{RR}^{-1} + C^T R_{NN}^{-1}C]^{-1}\,[C^T R_{NN}^{-1}C] \quad . \qquad \text{(B-28)}$$

The matrix inversion lemma is then applied once again to obtain:

$$[C^T R_{XX}^{-1}C]^{-1} = [C^T R_{NN}^{-1}C]^{-1} + [C^T R_{NN}^{-1}C]^{-1}\,[C^T R_{NN}^{-1}C]\,\{\,[R_{RR}^{-1} + C^T R_{NN}^{-1}C] - [C^T R_{NN}^{-1}C][C^T R_{NN}^{-1}C]^{-1}\,[C^T R_{NN}^{-1}C]\}^{-1} [C^T R_{NN}^{-1}C][C^T R_{NN}^{-1}C]^{-1}$$

$$[C^T R_{XX}^{-1}C]^{-1} = [C^T R_{NN}^{-1}C]^{-1} + R_{RR} \quad . \qquad \text{(B-29)}$$

Equations (B-27) and (B-29) may now be used to synthesize

$$R_{XX}^{-1}C[C^T R_{XX}^{-1}C]^{-1} = \{R_{NN}^{-1}C - R_{NN}^{-1}C[R_{RR}^{-1} + C^T R_{NN}^{-1}C]^{-1} C^T R_{NN}^{-1}C\}$$
$$\{[C^T R_{NN}^{-1}C] + R_{RR}\} \quad . \tag{B-30}$$

Performing the indicated multiplication on the righthand side of (B-30) and simplifying yields

$$R_{XX}^{-1}C[C^T R_{XX}^{-1}C]^{-1} = R_{NN}^{-1} C[C^T R_{NN}^{-1}C]^{-1} + R_{NN}^{-1}C\, R_{RR}$$
$$- R_{NN}^{-1}C[R_{RR}^{-1} + C^T R_{NN}^{-1}C]^{-1} I_J$$
$$- R_{NN}^{-1}C[R_{RR}^{-1} + C^T R_{NN}^{-1}C]^{-1} C^T R_{NN}^{-1}C\, R_{RR} \quad . \tag{B-31}$$

After it is recognized that the J x J identity matrix I_J may be factored as

$$I_J = R_{RR}^{-1}\, R_{RR} \quad , \tag{B-32}$$

(B-31) may be rewritten as

$$R_{XX}^{-1}C[C^T R_{XX}^{-1}C]^{-1} = R_{NN}^{-1}C[C^T R_{NN}^{-1}C]^{-1} + R_{NN}^{-1}C\, R_{RR}$$
$$- R_{NN}^{-1}C[R_{RR}^{-1} + C^T R_{NN}^{-1}C]^{-1} [R_{RR}^{-1} + C^T R_{NN}^{-1}C]\, R_{RR} \quad . \tag{B-33}$$

This last equation readily simplifies to

$$R_{XX}^{-1}C[C^T R_{XX}^{-1}C]^{-1} = R_{NN}^{-1}C[C^T R_{NN}^{-1}C]^{-1} \quad . \tag{B-34}$$

Postmultiplying (B-34) by the constraint vector $\mathcal{L}$ leads to the desired result:

$$W_{ABF}^{*} = R_{XX}^{-1}C[C^T R_{XX}{}^{-1}C]^{-1}\mathcal{L} = R_{NN}^{-1}C[C^T R_{NN}^{-1}C]^{-1}\mathcal{L} \quad .$$

APPENDIX B References

1. O. L. Frost III, "An Algorithm for Linearly Constrained Adaptive Array Processing," Proc. IEEE, Vol. 60, No. 8, Aug. 1972.

2. O. L. Frost III, *Adaptive Least Squares Optimization Subject to Linear Equality Constraints,* Stanford Electronics Lab, Stanford, CA, Doc. SEL-70-055, Technical Report 6796-2, Aug. 1970.

3. C. A. Baird, Jr., and C. L. Zahm, "Performance Criteria for Narrowband Array Processing," Proc. 1971 IEEE Conference on Decision and Control, Miami Beach, FL, 15-17, Dec. 1971.

4. B. Noble, *Applied Linear Algebra,* Prentice-Hall, Englewood Cliffs, N. J., 1969.

APPENDIX C

AN ANALYSIS OF SIGNAL INFLUENCE BASED UPON THE GENERALIZED SIDELOBE CANCELLER

Another vehicle for analyzing the role of the desired or look-direction signal is provided by the Griffiths-Jim generalized sidelobe canceller [1,2], a form of which is diagrammed in Figure C-1. In this beamformer there is a fixed processor (shown at the right side of the figure) that operates directly upon the signals from the array and implements the look-direction constraints as stated by $\{f_i\}$, $i = 1, 2, ..., N$. Note that the look direction is perpendicular to the array in the case shown; steering delays are needed for other look-direction choices. There is also a second, adaptive processor that operates upon the difference signals between adjacent elements and therefore is not exposed to look direction signals *through the signal vector* X'.* The output of the adaptive processor is subtracted from the output of the fixed processor to obtain a useful signal. This signal also constitutes the error signal that is used in an LMS update algorithm as opposed the more complicated constrained LMS algorithm that would otherwise be needed to implement hard constraints. It has been shown [2], that the Frost ABF and the generalized sidelobe canceller generate equivalent solutions when the sidelobe canceller takes the particular form shown in

*There is, however, exposure to the look-direction signal through the error signal that is fed back to direct adaptation; the generalized sidelobe canceller is subject to signal cancellation.

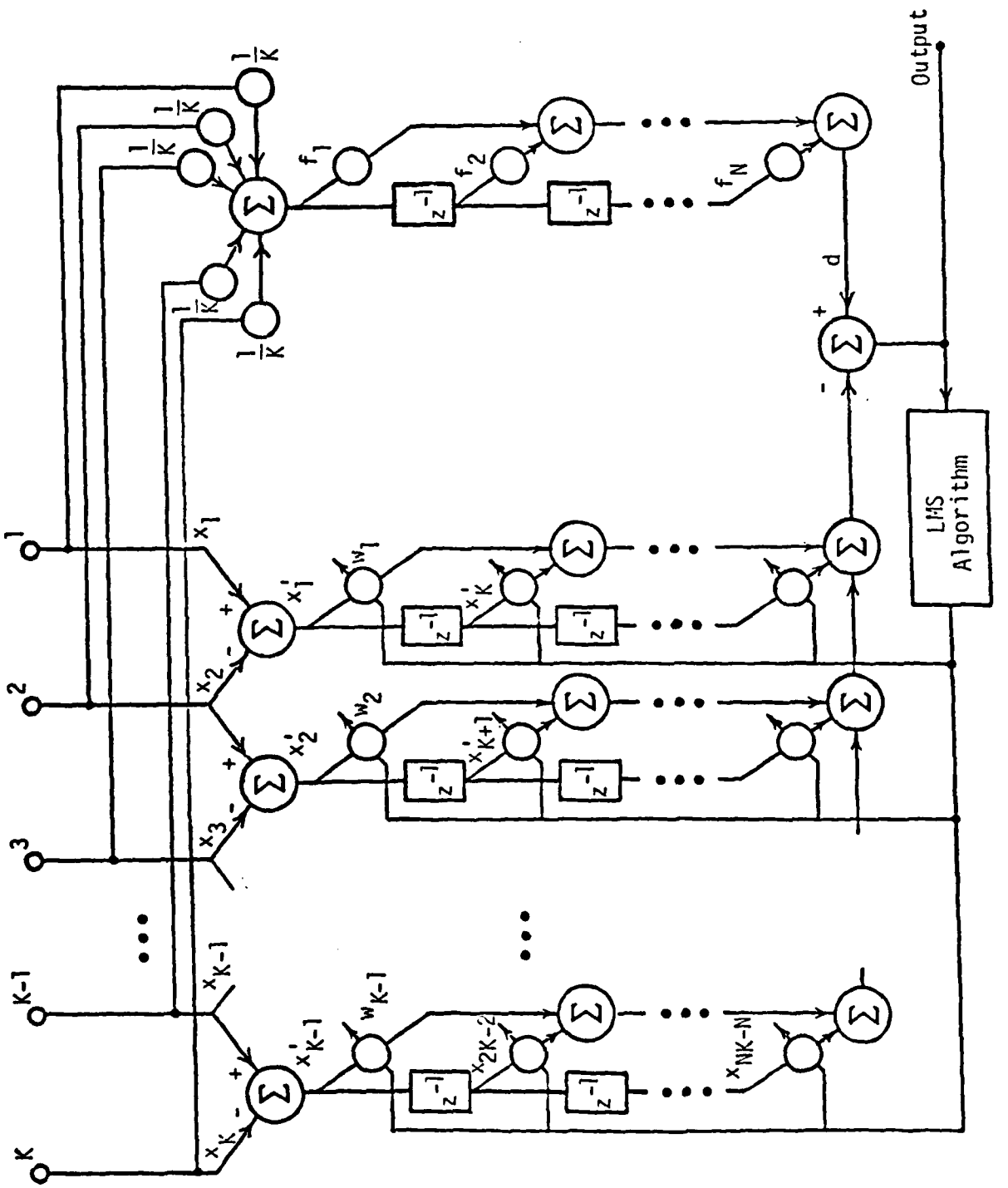

Figure C-1. Block Diagram of a Griffiths-Jim Sidelobe Canceller.

Figure C-1.

In terms of the difference signal vector X' and the signal d, the Wiener weight vector for the generalized sidelobe canceller may be written as

$$W_{GSC}^{*} = R_{X'X'}^{-1} P_{dX'} \quad . \tag{C-1}$$

where

$$\begin{aligned} X' &\triangleq [x_1', x_2', \ldots, x_{KN-N}']^T \\ R_{X'X'} &\triangleq E[X' X'^T] \\ P_{X'd} &\triangleq E[dX'] \quad . \end{aligned} \tag{C-2}$$

A representative element x_i', $1 \leq i \leq K-1$, of the difference signal vector X' is obtained from the received signals according to

$$x_i' = x_i - x_{i-1} \quad . \tag{C-3}$$

(The remaining elements of X' were derived in the same manner at an earlier point in time.) Each received signal is taken to consist of a signal component plus noise components. Because the array is assumed to consist of identical elements and to be perfectly steered, the signal components are identical across the array. Therefore

$$x_i' = x_i - x_{i-1} = (s + n_i) - (s + n_{i-1}) = n_i - n_{i-1} \quad . \tag{C-4}$$

It is evident from the lack of signal components in the difference signal vector that the factor $R_{X'X'}^{-1}$ can bring no signal influence to the Wiener solution.

The output d of the fixed beamformer in the generalized sidelobe canceller is

given by

$$d = \sum_{i=1}^{K} \frac{1}{K} z_i = \frac{1}{K} \sum_{i=1}^{K} (s + n_i) = s + \frac{1}{K} \sum_{i=1}^{K} n_i \quad . \qquad \text{(C-5)}$$

The crosscorrelation may be calculated from X' and d as follows:

$$\begin{aligned} P'_{dX} &\triangleq E[dX'] \\ &= E[(s + \frac{1}{K} \sum_{i=1}^{K} n_i)X'] \\ &= E[sX'] + E[(\frac{1}{K} \sum_{i=1}^{K} n_i)X'] \\ &= E[(\frac{1}{K} \sum_{i=1}^{K} n_i)X'] \quad . \end{aligned} \qquad \text{(C-6)}$$

It is now seen that the second factor of Equation (C-1) is also free of signal influence and therefore that the Wiener solution for a hard-constrained ABF is uninfluenced by the desired signal.

APPENDIX C References

1. C. W. Jim, "A Comparison of Two LMS Constrained Optimal Array Structures," Proc. IEEE, Vol. 65, pp. 1730-1731, Dec. 1977.

2. L. J. Griffiths and C. W. Jim, "An Alternative Approach to Linearly Constrained Adaptive Beamforming," IEEE Trans. Ant. and Prop., Vol. AP-30, pp. 27-34, Jan. 1982.

APPENDIX D

A COMPOSITE BEAMFORMER BASED UPON WIDROW'S PILOT-SIGNAL ALGORITHM

The composite-beamformer discussions in the body of this report centered upon the use of Frost's algorithm for weight adaptation. Frost's algorithm is designed to operate in a signal-aligned environment, i.e., the array must be steered either mechanically or electrically so that signals from the look direction are cophased across the array. Once the array has been properly steered, the Frost algorithm provides excellent control over the response in the chosen look direction. The Frost-based CBF is an appropriate choice when a single look direction can be established with reasonable accuracy.

In many cases, however, it is not possible or desirable to specify a single direction of arrival for desired signals. These situations arise, for example, when communications must be maintained with multiple stations, when the location of a station is imprecisely known, or when motion of the receiving platform makes it difficult to maintain high pointing accuracies. An alternative to the single, hard-constrained look direction is needed in these cases.

There are two requirements that must be met in order to realize a CBF that provides multiple look directions. The first requirement is to eliminate signal energy incident from the various look directions. It is difficult and expensive to generate wideband nulls in multiple directions. On the other hand, it is relatively

simple to create multiple narrowband nulls by using a structure such as a nulling tree. The second requirement is to adaptively eliminate jammer signals while sustaining useful responses in the look directions. Widrow's pilot-signal algorithm provides a convenient method for nulling jammers while maintaining soft-constrained responses in multiple look directions. Taken together, the nulling-tree preprocessor and the pilot-signal algorithm form the building blocks for a CBF that can serve multiple, narrowband signals.

The balance of this appendix describes the pilot-signal CBF and draws some comparisons with the basic pilot-signal beamformer. The first section discusses the nulling-tree preprocessor and illustrates the use of the nulling tree to generate multiple notches and broadened notches. The next section then explains the CBF structure, which essentially consists of a nulling-tree preprocessor plus a pilot-signal beamformer. The final section shows that, in contrast with the basic pilot-signal ABF, the pilot-signal CBF is capable of generating an unbiased solution for the narrowband case.

A. The Nulling Tree

The nulling tree was described by Davies [1] and is also termed the Davies cascade or Davies null-steering network. As has been noted by Steinberg [2], the nulling tree does not necessarily constitute the most efficient means of realizing multiple nulls. The great virtue of the nulling tree lies in its ability to provide independent control over multiple nulls. In that sense the nulling tree is well

matched to Widrow's pilot-signal algorithm, which provides independent control through the separate pilot signal established for each look direction.

The structure of the nulling tree is shown in Figure D-1. The tree consists of a number of stages equal to the number of nulls to be generated. Each stage is formed from a set of identical sections. The sections operate upon two outputs from the preceding stage and perform a phase-shift-and-add process that nulls signals arriving from a selected direction. In particular, a null is generated in the i^{th} stage for signals arriving from an angle θ by choosing the phase shift ϕ_i given by

$$\phi_i = \frac{2\pi\, d \sin\theta}{\lambda} + \pi \quad \text{radians} \quad , \tag{D-1}$$

where d is the interelement distance in the uniform linear array and λ is the wavelength at the frequency for which nulling is desired.

A computer program was written to design nulling trees and plot the beampatterns resulting from the designs. Various test cases were examined to determine the characteristics of the nulling-tree preprocessor.

Figure D-2 shows a series of beampattern pilots that result from adding successive nulls at separate arrival angles. The initial null is established for signals arriving from broadside; the second stage nulls signals from $+45°$; and the third stage is set for $-30°$ arrivals. This preprocessor can accommodate an environment in which there are multiple signals sources at well-defined look directions.

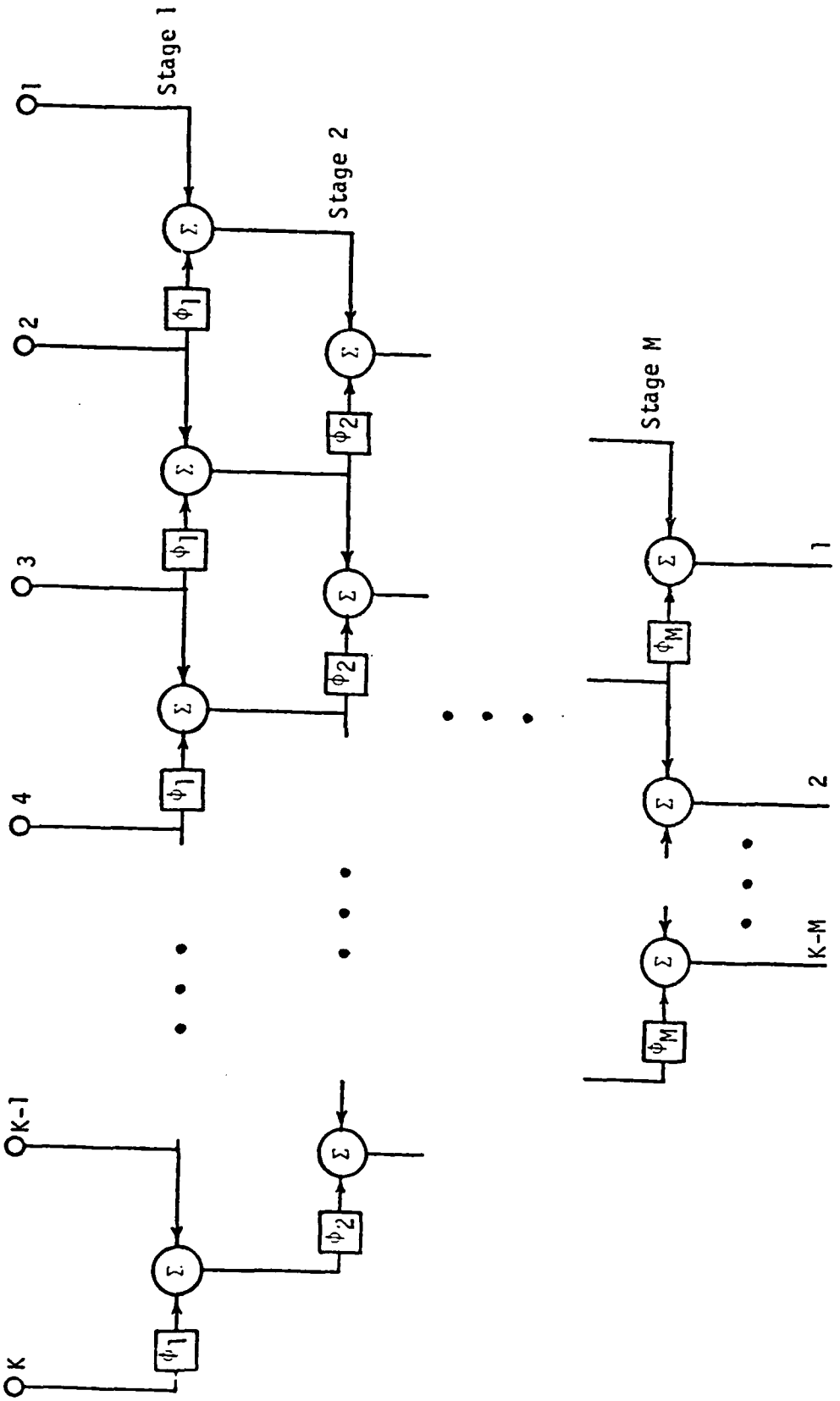

Figure D-1. Diagram of an M-Stage Nulling Tree.

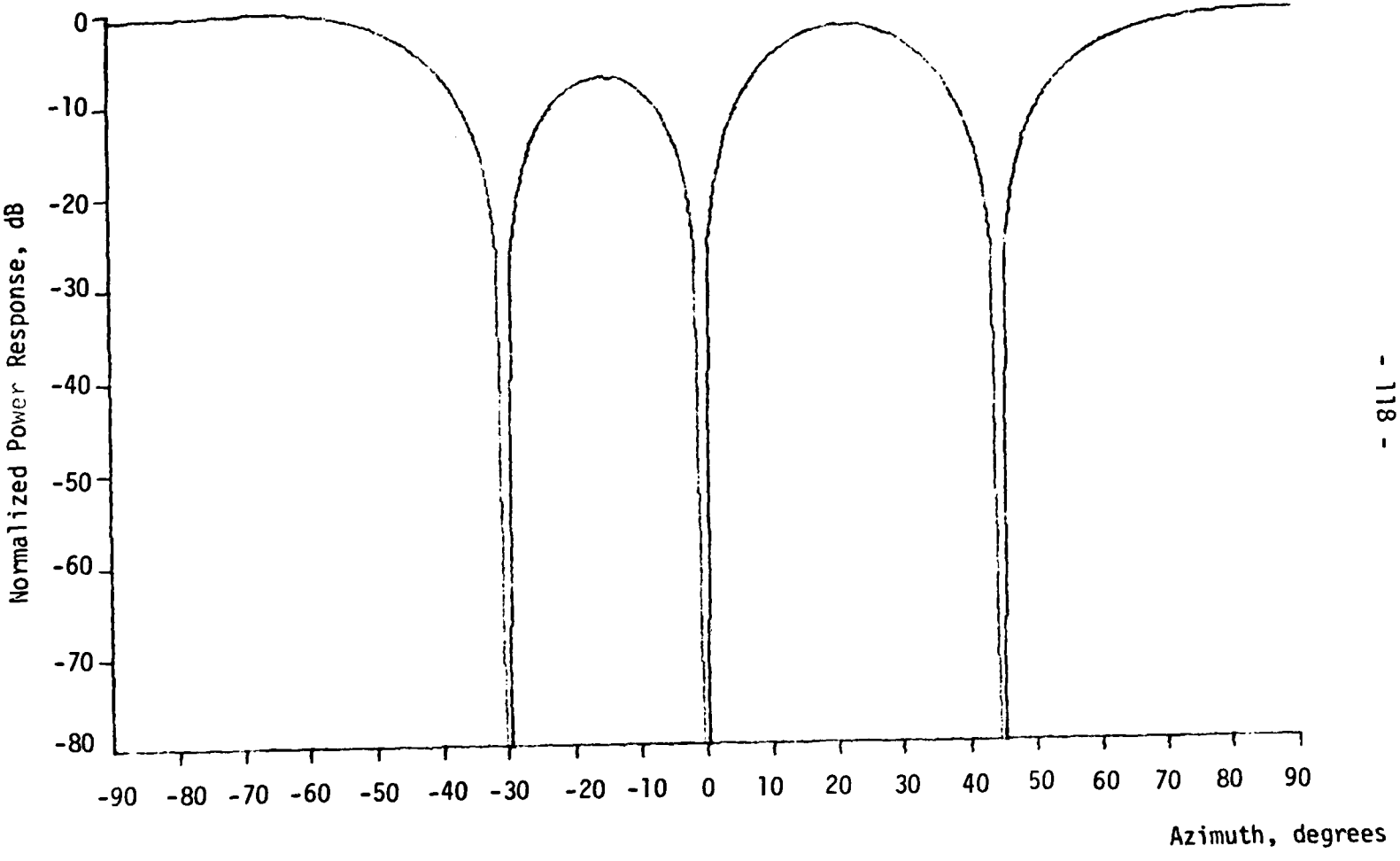

Figure D-2. Nulling-tree Beampattern Plot with Nulls at -30^{o}, 0^{o}, and 45^{o}.

Another type of requirement is considered in Figure D-3. Here it is assumed that only one emitter is of interest, but the look direction is imprecisely known. An initial null is established in the estimated look direction, and successive stages are used to broaden the null by creating additional spatial notches on each side of the estimated direction.

B. Structure of the Pilot-Signal CBF

Figure D-4 is a block diagram of the pilot-signal CBF. A uniform linear array of K elements provides the input signals to the CBF. All of the elements are connected to the nulling-tree preprocessor, which consists of M stages that create M nulls in the various directions from which desired signals may arrive. The $K-M$ outputs from the nulling tree constitute a signal-free environment in which adaptation can proceed without concern about cancellation effects. The slaved beamformer is connected directly to the first $K-M$ elements of the array and is used to derive a useful output signal for the receivers.

The pilot-signal algorithm is used to provide a prespecified, soft-constrained response in each potential look direction. A separate pilot signal is generated for each look direction and, after appropriate phasing, is added to the ABF inputs. The pilots are also filtered and summed to form a synthetic "desired" signal against which the ABF output is compared. The difference between the summed pilots and the ABF output is the error signal that is used to guide adaptation.

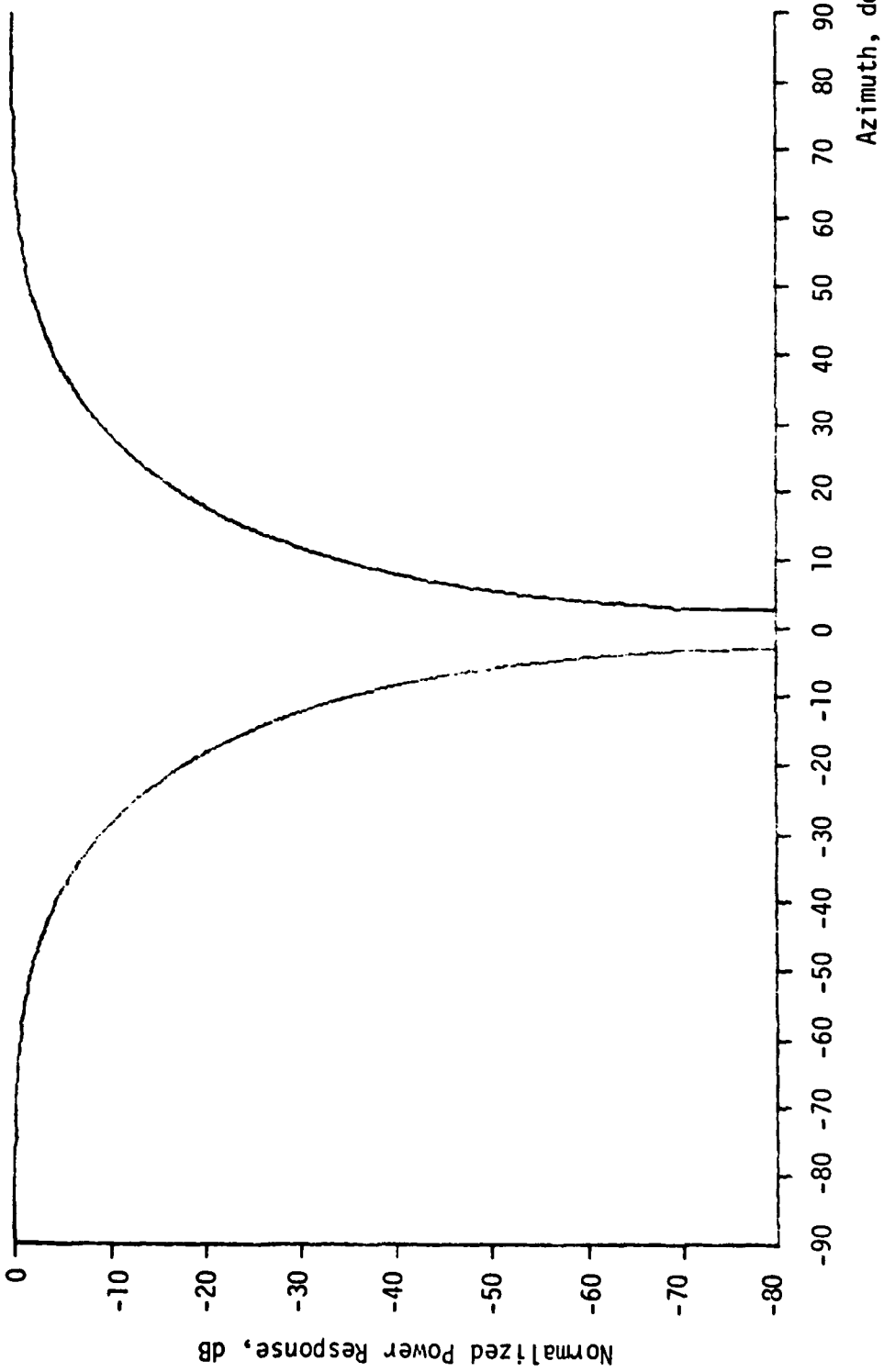

Figure D-3. Nulling-tree Beampattern Plot with Broadened Null at 0^{o}.

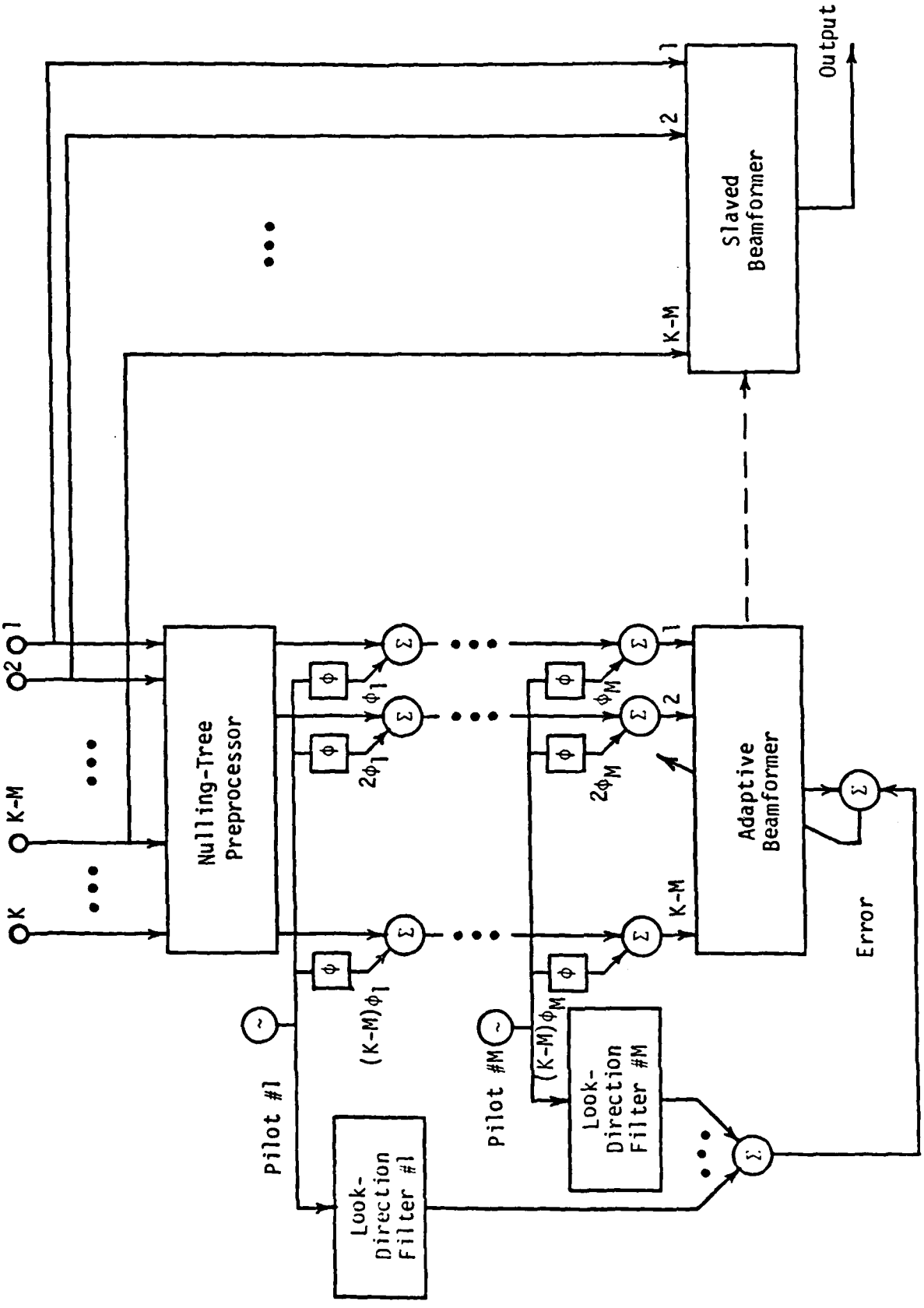

Figure D-4. Block Diagram of the Pilot-signal CBF.

Weight adaptation can be accomplished with a variety of different algorithms. The Widrow-Hoff LMS algorithm [3] was initially proposed for use in a digital implementation of the pilot-signal ABF. Applebaum [4] described an analog implementation that makes use of correlation loops.

It is interesting to note that very few changes are needed to transform the basic pilot-signal ABF into a pilot-signal CBF. The slaved beamformer is already present in the pilot-signal scheme and therefore need not be introduced. The only new components are the null-forming preprocessor and the extra antenna elements entailed by the nulling process.

C. Bias Removal by the CBF

Soon after the development of the pilot-signal algorithm, it was recognized that the solution it generates in the presence of signal is biased from the Wiener solution. Griffiths [5] investigated the source of bias in some detail and succeeded both in explaining the phenomenon and devising an alternative beamformer that avoided the problem. Griffiths' beamformer, however, is subject to signal cancellation. The paragraphs that follow will demonstrate that, in addition to solving the signal-cancellation problem, the CBF solves the bias problem, thus eliminating both disadvantages normally encountered with pilot-signal beamformers.

Griffiths investigated the bias issue in the context of a pilot-signal ABF with a single look direction and, consequently, a single pilot signal. The same approach will be followed here because the use of multiple pilot signals complicates matters without contributing anything of substance.

The pilot signal in Griffiths' model is taken to be some multiple β of the estimated desired signal $\hat{g}(k)$, i.e.,

$$d(k) = \beta\hat{g}(k) \quad . \tag{D-2}$$

After phase shifting to allow for propagation effects, the pilot is added to the beamformer inputs. This injected signal vector is identified as $\beta\hat{S}(k)$, where $\hat{S}(k)$ is the estimated desired-signal vector across the inputs.

Weight updating is accomplished using the LMS algorithm:

$$W(k+1) = W(k) + 2\mu\{\beta\hat{g}(k) - [X^T(k) + \beta\hat{S}^T(k)]\ W(k)\}\ \{X(k) + \beta\hat{S}(k)\} \quad , \tag{D-3}$$

where

$X(k)$ is the input signal vector,
$W(k)$ is the beamformer weight vector, and
μ is the adaptation parameter.

Griffiths showed that the limiting value of the expectation of the weight vector is given by

$$\bar{M}_W = \left[\frac{R_{XX}}{\beta^2} + \hat{R}_{SS}\right]^{-1} \hat{P}_g \quad . \tag{D-4}$$

where

$$R_{XX} \triangleq E[X(k)X^T(k)]$$
$$\hat{R}_{SS} \triangleq E[\hat{S}(k)\hat{S}^T(k)]$$
$$\hat{P}_g \triangleq E[\hat{g}(k)\hat{S}(k)] \quad .$$

The equation for $\bar{M}_W$ differs from the Wiener solution

$$W^* = R_{ss}^{-1} P_g \tag{D-5}$$

even if the pilot happens to be a perfect replica of the desired signal. This effect occurs because the actual incoming signal contributes to the beamformer inputs, and the combination of actual signal and pilot signal enter the adaptation process. Bias in the pilot-signal solution is undesirable and can only be eliminated in the original design by limiting adaptation to periods when the desired signal is known to be absent. This is, under most circumstances, an unworkable operational constraint.

In the pilot-signal CBF, adaptation is always conducted in the absence of signal due to the action of the preprocessor. It might therefore be expected that superior performance can be obtained. This is, in fact, the case.

Some further examination of the signal environment is needed to demonstrate the superiority of the CBF with regard to bias. The signal vector $X(k)$ that appears at the beamformer weights is taken to consist of two

components:

$$X(k) = S(k) + N(k) \quad . \tag{D-6}$$

The vector $S(k)$ is comprised solely of desired-signal components arriving via the direct path. The noise vector $N(k)$ is the sum of all interfering signals (including desired-signal multipath) and element noise. The autocorrelation matrix for $X(k)$ can now be calculated:

$$\begin{aligned} R_{XX} &\triangleq E[X(k)X^T(k)] \\ &= E\{[S(k) + N(k)][S^T(k) + N^T(k)]\} \\ &= E[S(k)S^T(k)] + E[S(k)N^T(k)] + E[N(k)S^T(k)] + E[N(k)N^T(k)] \\ &= R_{SS} + R_{SN} + R_{NS} + R_{NN} \quad . \end{aligned} \tag{D-7}$$

Several different sets of assumptions concerning the signal environment and the CBF realization will now be considered:

Case 1: Assume that signal and noise processes are uncorrelated, i.e., that multipath and repeater jamming are not present. For this environment

$$R_{XX} = R_{SS} + R_{NN} \quad . \tag{D-8}$$

Further assume perfect implementation of the CBF. A perfect preprocessor excises the desired signal without affecting noise components and generates a modified beamformer input given by

$$X'(k) = N(k) \quad . \tag{D-9}$$

The autocorrelation matrix for $X'(k)$ is

$$R_{X'X'} = R_{NN} \quad . \tag{D-10}$$

For a perfect choice of pilot-signal amplitude and statistics

$$\begin{aligned} \beta &= 1 \\ \hat{R}_{SS} &= R_{SS} \\ \hat{P}_{\ell} &= P_{\ell} \quad . \end{aligned} \tag{D-11}$$

The limiting value $\overline{M}_W$ for Case 1 may now be written as

$$\begin{aligned} \overline{M}_W &= \left[\frac{R_{X'X'}}{\beta} + \hat{R}_{SS}\right]^{-1} \hat{P}_{\ell} \\ &= [R_{NN} + R_{SS}]^{-1} P_{\ell} \\ &= R_{XX}^{-1} P_{\ell} \quad . \end{aligned} \tag{D-12}$$

This last equation indicates that, unlike perfect realization of the basic pilot-signal ABF, perfect realization of the pilot-signal CBF yields the Wiener solution.

Case 2: Repeat the assumptions of Case 1, except for the assumption of perfect preprocessing. Instead allow perfect removal of the desired signal, but assume incidental modification of the noise field. Under these conditions

$$\overline{M}_W = [A\, R_{NN}\, A^T + R_{SS}]^{-1} P_{\ell} \quad , \tag{D-13}$$

where the A matrix describes the preprocessor influence on the noise vector. The right-hand side of this equation is not necessarily equal to the Wiener solution.

Under the set of assumptions discussed in Chapter 4 (i.e., narrowband interference, sufficient degrees of freedom, high jammer-to-noise ratios element spacing less than half-wave), the right-hand side does reduce to the Wiener solution.

Case 3: Repeat the assumptions of Case 1, except for the assumption that the signal and noise processes are uncorrelated. When correlation is allowed

$$R_{XX} = R_{SS} + R_{SN} + R_{NS} + R_{NN} \quad . \tag{D-14}$$

Preprocessing now produces a much simpler environment within the adaptive beamformer:

$$X'(k) = N(k)$$
$$R_{X'X'} = R_{NN} \quad .$$

The limiting value of the weight mean is

$$\bar{M}_W = [R_{NN} + R_{SS}]^{-1} P_g \quad . \tag{D-16}$$

In other words, the pilot-signal CBF treats the correlated signal as though it were uncorrelated. This is not the Wiener solution, but it is the desired solution in this important case.

APPENDIX D References

1. D. V. N. Davies, "Independent Angular Steering of Each Zero of the Directional Pattern for a Linear Array," IEEE Trans. Ant. and Prop., AP-15, pp. 296-298, March 1967.

2. B. Steinberg, *Principles of Aperture and Array System Design,* John Wiley and Sons, New York, 1976.

3. B. Widrow, P. E. Mantey, L. J. Griffiths, and B. B. Goode, "Adaptive Antenna Systems," Proc. IEEE, Vol. 55, pp. 2143-2159, Dec. 1967.

4. S. P. Applebaum and D. J. Chapman, "Adaptive Arrays with Main Beam Constraints," IEEE Trans. Ant. and Prop., Vol. AP-24, pp. 650-662, Sept. 1976.

5. L. J. Griffiths, "Signal Extraction Using Real-time Adaptation of a Linear Multichannel Filter," Ph.D. Dissertation, Stanford University, Stanford, CA, Jan. 1968.

APPENDIX E

SIMULATION METHODS

Computer simulations of the Frost ABF and the Frost-based CBF were used to illustrate signal-cancellation effects and to demonstrate the performance contrasts between the two beamformers. This appendix outlines the simulation methods that were employed.

A. Simulation Facility

The adaptive-antenna simulations for this research were performed on an HP 1000F minicomputer facility at Stanford University. The simulation software was, for the most part, an existing Fortran package that was written by a team of students* during 1979-1980 under the joint sponsorship of the U. S. Air Force's Rome Air Development Center and the Naval Air Development Center. The software package is organized as a set of programs that run under the control of a driver program and exchange data through disk files. This arrangement allows multiple simulation functions to be performed in parallel (albeit on a time-shared basis) and facilitates research by allowing time-consuming adaptation experiments to proceed in the background while experiment preparation and data analysis are being performed by the user. The software package is capable of simulating several different beamformer types and

*Principal contributors were R. Gooch, W. Manning, F. McCarthy, W. Newman, and P. Titchener.

is sufficiently flexible to support most of the basic investigations that might be required for a specified adaptive antenna and signal/jammer scenario.

B. Simulation of an Adaptive Antenna

The program flow for adaptive antenna simulation is shown in Figure E-1. The initial step in preparing a simulation experiment is to thoroughly specify the problem that is to be considered. The driver program organizes this process by prompting for the inputs that are needed to specify the following:

A. Antenna configuration

   1. Number of elements

   2. Location of each element

B. Beamformer structure

   1. Number of taps per beamformer filter

   2. Adaptive algorithm

   3. Constraints (if applicable)

   4. Initial weight values

C. Signal/jammer scenario

   1. Number of signals/jammers

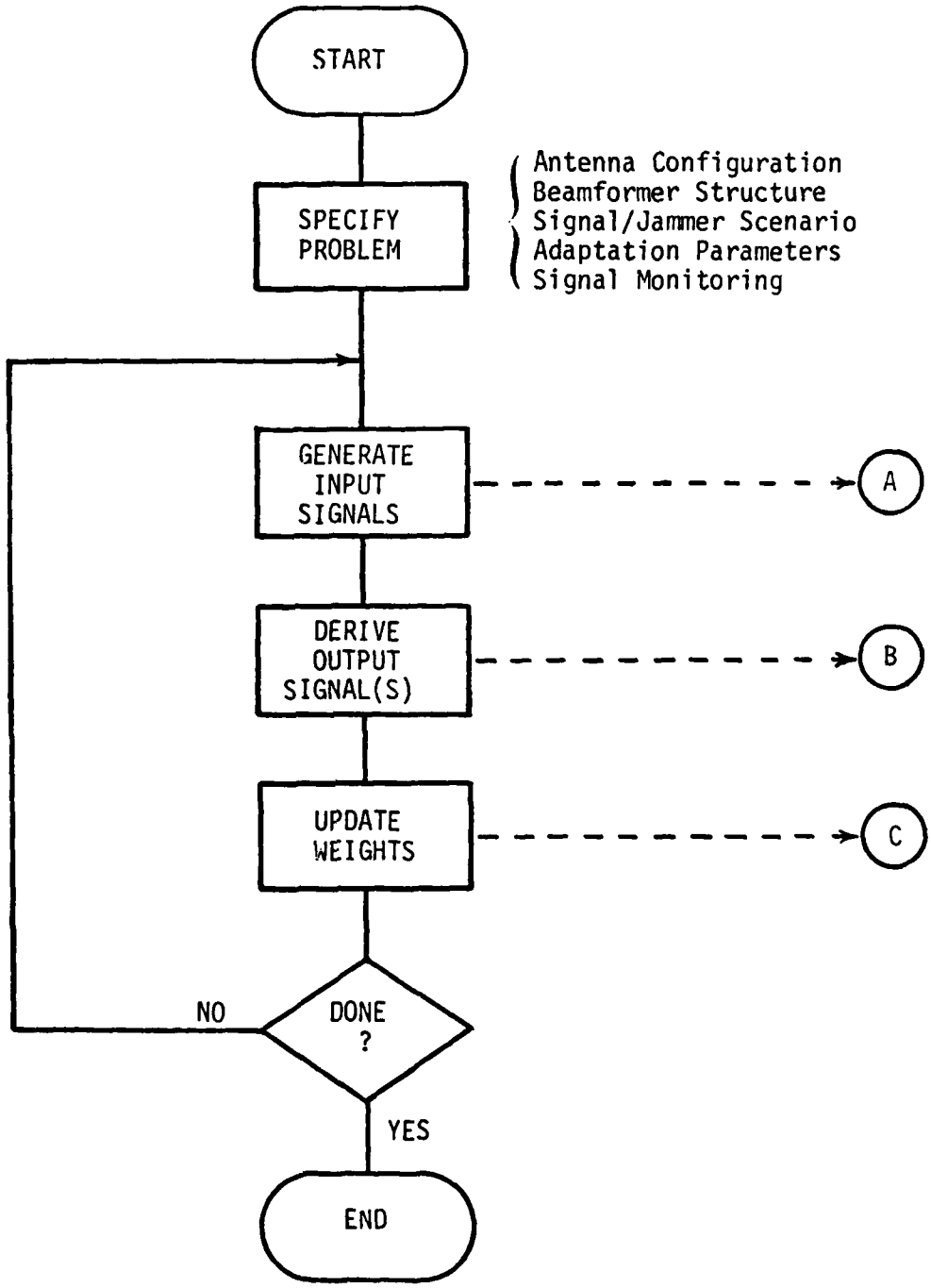

Figure E-1. Flowchart for Adaptive Antenna Simulation.

2. Signal/jammer arrival angle

3. Signal/jammer power

4. Signal/jammer center frequency and bandwidth

D. Adaptation parameters

1. Number of adaptation cycles

2. Adaptation constant

E. Signal (e.g. input, master output, slave output) to be stored for later analysis.

All of these data are organized into disk files and thus made available for use by various programs during the simulation or for reuse in subsequent runs.

The first step in the actual simulation is generation of the initial samples of the input signals. This can be accomplished by a direct computation for sinusoidal signals since amplitude is known from the power specification and the phase at any tap is known from the antenna/beamformer specifications, the signal frequency, and the initial (or prior-sample) phase. The process is more difficult for wideband signals. These signals are derived by first generating a white-noise sequence and then digitally bandpass filtering to obtain the desired center frequency and bandwidth. In general, the sample values derived in this fashion will not correspond exactly to the sample values needed at the antenna elements since fractional-sample-interval delays are often encountered. A sinc

interpolation is used to correct for this effect and provide accurate input samples in the wideband case. The aggregate signal sample at each tap is just the sum of the various signal and jammer samples derived for the tap. Separate signal vectors are maintained for master and slave beamformers.

Once the signal vectors have been obtained for some sample instant, it is straightforward to calculate the output signal or signals by forming the inner product of a signal vector with the current weight vector. In the case of the composite beamformer, both the master beamformer output and the slaved beamformer output are required.

Weight updating is accomplished based upon the current signal vector and the current adaptive array output. The weight recursion for the Frost ABF was given in Eq. (2-17).

After the new weight vector has been obtained, the next adaptation cycle can begin. A check is made at this point to determine whether the prespecified number of cycles has been completed. If so, the adaptation routine halts. If not, the process of computing input samples, outputs, and new weight values continues.

As the simulation progresses, data of interest are saved by transcribing to disk files. The use of disk files allows large amounts of data to be saved and thus supports lengthy adaptation experiments involving tens of thousands of adaptation cycles. Additionally, the disk files provide convenient interfaces between the simulation program and various data analysis programs.

C. Plotting of Antenna Responses

Two types of plots are typically used to characterize the response of an adaptive antenna with some specified set of beamformer weights. One plot shows the response to a unit-power test signal of specified frequency as the test-signal angle of arrival is varied through, say, 360°. This plot is usually termed a "beampattern" and is useful in determining the relative response of the system to jammers and desired signals. The second plot shows the response to a unit-power test signal from a specified direction as the test-signal frequency is varied over some range, generally from zero to half the sampling frequency. This plot is a frequency-response characterization for the selected direction and is useful in checking the effectiveness of jammer nulling and confirming the maintenance of look-direction constraints. Both plot types are used most frequently to study antenna response after the beamformer weights have converged (in the mean) to the optimal solution for the environment under consideration. The plots may, however, be plotted for any specified set of weights. A series of plots may be generated to study, for example, the evolution of the antenna response as adaptation occurs or the dynamics of the antenna response after convergence.

A flowchart of the procedure for generating and plotting antenna responses is given in Figure E-2. The response plots are specified from the driver program, which then starts the appropriate program for either a beampattern plot or a frequency-response plot. Either program must first read the driver-specified weight file and plot-parameter files from disk. The response for a given arrival

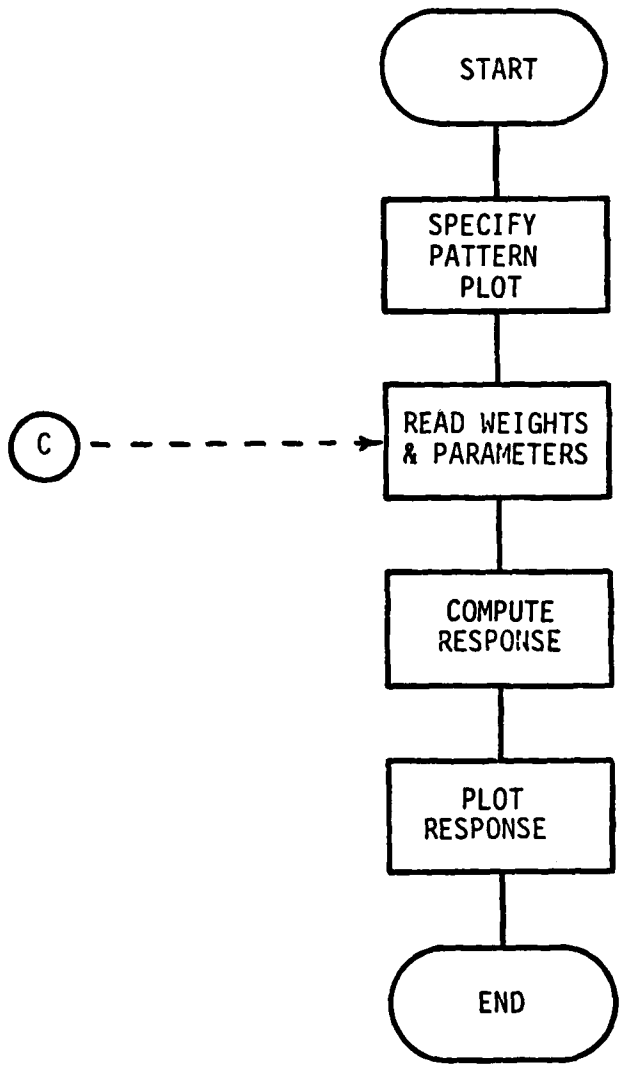

Figure E-2. Flowchart for Generation and Plotting of Antenna Responses.

direction and frequency is then found by forming the phasor sum of the weighted tap voltages and computing the beamformer output power from the amplitude of the sum. Repeated computations of this type give the response at enough directions or frequencies to accurately characterize the antenna response. The response is then plotted for study. A polar plot with a logarithmic (dB) radial scale is usually preferred for beampattern plots, but a semilogarithmic cartesian presentation sometimes serves well. A cartesian plot is used for the frequency-response data, with frequency as the abscissa and power (in dB) as the ordinate.

D. Plotting of Input/Output Signals

Plots of input and output signals and their spectra are important in the study of adaptive antenna performance. These plots are especially valuable in investigations of signal cancellation. Cancellation effects that are difficult to recognize in beampattern or frequency-response plots can be easily detected by comparing input and output waveforms or spectra.

Input and output data are gathered during the course of simulation experiments and written to disk files for later analysis and display. A number of different signals (e.g. the desired signal, jammer signals, master beamformer output, slaved beamformer output) may be collected to thoroughly characterize beamformer behavior during various simulations. Plots of these data allow comparisons to be drawn between different beamformers, different operating conditions, etc.

Figure E-3 diagrams the event flow for production of input/output plots. If spectral plots are elected, a DFT routine is entered to generate power spectra for the selected signals. The DFT routine allows selection of transform size and supports the computation of an average power spectrum over some specified range of data samples. The power spectra are written to disk upon completion of this computation. The plot program allows several signals or spectra to be presented simultaneously for comparison. Waveform or spectral data are read from specified disk files and plotted on separate axes with a common scale for easy comparison.

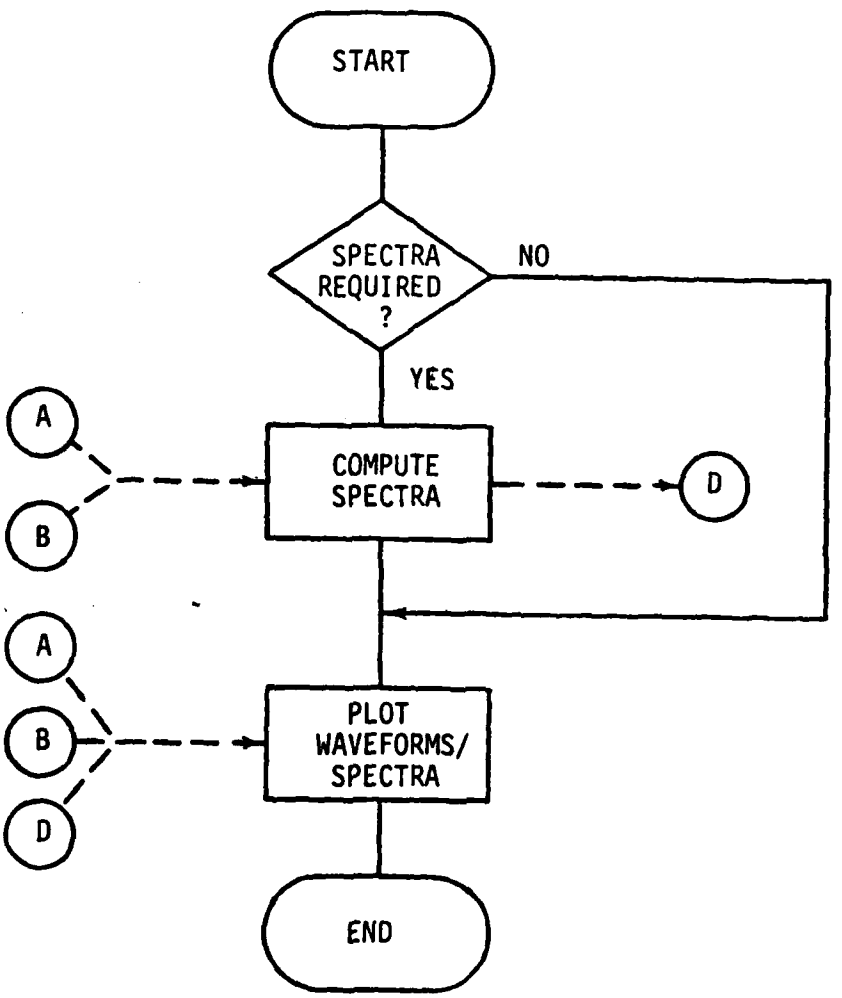

Figure E-3. Flowchart for Generating and Plotting Input/Output Signals.

END

FILMED

11-83

DTIC